BLEJSKE DELAVNICE IZ FIZIKE LETNIK 16, ŠT. 1
BLED WORKSHOPS IN PHYSICS VOL. 16, NO. 1

ISSN 1580-4992

Proceedings of the Mini-Workshop

Exploring Hadron Resonances

Bled, Slovenia, July 5 – 11, 2015

Edited by

Bojan Golli
Mitja Rosina
Simon Širca

University of Ljubljana and Jožef Stefan Institute

DMFA – ZALOŽNIŠTVO
LJUBLJANA, NOVEMBER 2015

The Mini-Workshop *Exploring Hadron Resonances*

was organized by

Society of Mathematicians, Physicists and Astronomers of Slovenia
Department of Physics, Faculty of Mathematics and Physics, University of Ljubljana

and sponsored by

Department of Physics, Faculty of Mathematics and Physics, University of Ljubljana
Jožef Stefan Institute, Ljubljana
Society of Mathematicians, Physicists and Astronomers of Slovenia

Organizing Committee

Mitja Rosina, Bojan Golli, Simon Širca

List of participants

Marko Bračko, Ljubljana, marko.bracko@ijs.si
Ido Gilary, Haifa, chgilary@tx.technion.ac.il
Bojan Golli, Ljubljana, bojan.golli@ijs.si
Ju-Hyun Jung, Graz, ju.jung@uni-graz.at
Viktor Kashevarov, Mainz, kashev@kph.uni-mainz.de
Dubravko Klabučar, Zagreb, klabucar@oberon.phy.hr
Luka Leskovec, Ljubljana, luka.leskovec@ijs.si
Felipe Llanes-Estrada, Madrid, fllanes@ucm.es
Willi Plessas, Graz, willibald.plessas@uni-graz.at
Mitja Rosina, Ljubljana, mitja.rosina@ijs.si
George Rupp, Lisboa, george@ist.utl.pt
Wolfgang Schweiger, Graz, wolfgang.schweiger@uni-graz.at
Simon Širca, Ljubljana, simon.sirca@fmf.uni-lj.si
Jugoslav Stahov, Tuzla, jugoslav.stahov@untz.ba
Igor Strakovsky, Washington, igor@gwu.edu
Alfred Švarc, Zagreb, svarc@irb.hr
Lothar Tiator, Mainz, tiator@kph.uni-mainz.de
Yannick Wunderlich, Bonn, wunderlich@hiskp.uni-bonn.de

Electronic edition

http://www-f1.ijs.si/BledPub/

Contents

Preface V

Predgovor VII

Resonance states and branching ratios from a time-dependent perspective.
Ido Gilary 1

In-medium properties of the nucleon within a π-ρ-ω model
Ju-Hyun Jung, Ulugbek Yakhshiev, Hyun-Chul Kim 4

η MAID-2015: update with new data and new resonances
V. L. Kashevarov, L. Tiator, M. Ostrick 9

Analytic structure of nonperturbative quark propagators and meson processes
Dalibor Kekez and Dubravko Klabučar 16

Comparing mesons and $W_L W_L$ TeV-resonances
Felipe J. Llanes-Estrada et al. 20

Resonances in the Constituent-Quark Model
R. Kleinhappel and W. Plessas 27

Unquenched quark-model calculation of excited ρ resonances and P-wave $\pi\pi$ phase shifts
Susana Coito, George Rupp, Eef van Beveren 30

The pion-cloud contribution to the electromagnetic nucleon structure
D. Kupelwieser and W. Schweiger 36

Partial wave analysis of η photoproduction data with analyticity constraints
J. Stahov et al. 40

Progress in Neutron Couplings
W. J. Briscoe and I. Strakovsky 49

Exciting Baryon Resonances with Meson Photoproduction
L. Tiator, A. Svarc 59

Complete experiments in pseudoscalar meson photoproduction
Y. Wunderlich 68

Recent Spectroscopy Results from Belle
M. Bračko 75

Eta and kaon production in a chiral quark model
B. Golli 81

Vector and scalar charmonium resonances with lattice QCD
Luka Leskovec, C.B. Lang, Daniel Mohler, Saša Prelovsek 87

Resonances in the Nambu–Jona-Lasinio model
Mitja Rosina 91

The Roper resonance — Ignoramus ignorabimus?
S. Širca 96

Povzetki v slovenščini 101

Preface

At the end of the day, it looked like a resonance. We came together, exchanged news and ideas, and separated. The decay time seemed to be one week, but the ideas kept on boiling until the tail (the Proceedings) has been reached after four months. We hope that this final state shall trigger new resonances or echoes in the next years at Bled again.

The emphasis has been on the interpretation of experimental data and on the development of new theoretical and computational techniques for resonances. The prevailing experiments to generate and study low-energy hadronic resonances have been the photoproduction and electroproduction of mesons. The prevailing theoretical advance has been in exploiting analytic properties of scattering and production amplitudes.

Light hadron spectroscopy remains an exciting field in nuclear and particle physics. The Roper resonance is still an elusive entity, however, new experiments at MAMI, Jefferson Lab and other laboratories have elucidated several attempts at explaining it within models involving quark+meson and baryon+meson degrees of freedom. The progress beyond the Roper has required very elaborate partial-wave analyses, strongly based on recently measured polarization observables, and disentanglement of the isoscalar and isovector electromagnetic couplings. Theoretical studies took account of analytical constraints and of the final-state interactions which play a critical role. The photoproduction and electroproduction of η, η' mesons and kaons has opened an avenue to a detailed study of several non-strange and strange resonances.

Nucleon structure is still a motivating topic, for example, the question of the pion-cloud contribution to the electromagnetic properties, or, the issue of medium modifications of the structure of nucleons bound in a nuclear medium.

In the meson sector, radial recurrences of the $\rho(770)$ vector resonance have been studied in terms of $\pi\pi$ P-wave phase shifts, including all relevant decay channels. The resonances X(3872) and $Z^{\pm}$(4430, 4200, 4050,4250) are now better understood. Charmonium resonances in D-D scattering, including $\psi(3770)$, have been studied in Lattice QCD, suggesting a narrow resonance below 4 GeV. A $W_L W_L$ TeV-resonance has been speculated about, based on the analogy with meson-meson resonances and hints from LHC.

We would like to thank all participants for coming and for making, once more, the Mini-Workshop so friendly, lively and fruitful. The aim of the Proceedings is to prevent the vivid impressions of talks and discussions from fading away. The problems that have been opened are now documented in order to stimulate our further mutual interactions.

Ljubljana, November 2015 B. Golli, M. Rosina, S. Širca

Predgovor

Doživeli smo resonanco! Zbrali smo se, izmenjali novice in ideje, in se spet razšli. Razpadni čas naj bi bil en teden, toda nove ideje so vrele še več mesecev in rep (Zbornik) so dosegle po štirih mesecih. Upamo, da bo ta resonanca sprožila nove resonance ali odmeve v prihodnjih letih na Bledu.

Poudarek je bil na tolmačenju eksperimentalnih podatkov in na razvoju novih teoretičnih in računskih veščin za resonance. Prevladujoči eksperimenti za tvorbo in raziskavo nizkoenergijskih hadronskih resonanc so bili fotoprodukcija in elektroprodukcija mezonov. Prevladujoč napredek v teoriji pa je bil v izkoriščanju analitičnih lastnosti amplitud za sipanje in procese.

Spektroskopija lahkih hadronov je še vedno vzpodbudno področje fizike jedra in delcev. Roperjeva resonanca je še vedno izmuzljiva, vendar so novi eksperimenti v laboratorijih MAMI, Jefferson Lab in drugih osvetlili razlage s prostostnimi stopnjami kvark-mezon in barion-mezon. Napredek iznad Roperja je zahteval zelo prefinjeno analizo delnih valov, tudi za nedavno merjene polarizacijske količine, ter razločitev izoskalarnih in izovektorskih elektromagnetnih sklopitev. Teoretične obravnave pa so upoštevale analitične omejitve ter zelo pomembno interakcijo v končnem stanju. Fotoprodukcija in elektroprodukcija mezonov η, η' in kaonov je odprla pot podrobnim raziskavam številnih navadnih in čudnih resonanc.

Zgradba nukleona se gradi naprej. Zanimiv je prispevek pionskega oblaka k elektromagnetnim lastnostim nukleona. Posebno področje je raziskava vpliva okolice na zgradbo nukleona potopljenega v jedrsko snov.

V mezonskem področju je bil uspešen študij radialnih ponovitev vektorske resonance $\rho(770)$ v okviru faznih premikov za sipanje mezonov $\pi + \pi$ v valu P in z vključitvijo vseh važnih kanalov. Napredek je tudi pri razumevanju resonanc X(3872) in $Z^{\pm}$(4430, 4200, 4050,4250). S kromodinamiko na mreži so raziskovali čarmonijske resonance v sipanju mezonov D-D (zlasti $\psi(3770)$) in napovedali ozko resonanco nekoliko pod 4 GeV. Z nekaj domišljije (in namigom z Velikega hadronskega trkalnika) bi lahko napovedali resonanco $W_L W_L$ pri eneriji več TeV po analogiji z resonancami mezon-mezon.

Radi bi se zahvalili vsem udeležencem, da so napravili našo mini-delavnico tako prijazno, živahno in plodno. Namen pričujočega Zbornika je, naj živi vtisi predavanj in razprav ne splahnijo. Problemi, ki smo jih odprli, so zabeleženi z namenom, da vzpodbujajo nadaljnje sodelovanje med nami.

Ljubljana, november 2015 B. Golli, M. Rosina, S. Širca

Workshops organized at Bled

- *What Comes beyond the Standard Model*
  (June 29–July 9, 1998), Vol. **0** (1999) No. 1
  (July 22–31, 1999)
  (July 17–31, 2000)
  (July 16–28, 2001), Vol. **2** (2001) No. 2
  (July 14–25, 2002), Vol. **3** (2002) No. 4
  (July 18–28, 2003) Vol. **4** (2003) Nos. 2-3
  (July 19–31, 2004), Vol. **5** (2004) No. 2
  (July 19–29, 2005) , Vol. **6** (2005) No. 2
  (September 16–26, 2006), Vol. **7** (2006) No. 2
  (July 17–27, 2007), Vol. **8** (2007) No. 2
  (July 15–25, 2008), Vol. **9** (2008) No. 2
  (July 14–24, 2009), Vol. **10** (2009) No. 2
  (July 12–22, 2010), Vol. **11** (2010) No. 2
  (July 11–21, 2011), Vol. **12** (2011) No. 2
  (July 9–19, 2012), Vol. **13** (2012) No. 2
  (July 14–21, 2013), Vol. **14** (2013) No. 2
  (July 20–28, 2014), Vol. **15** (2014) No. 2
  (July 11–20, 2015), Vol. **16** (2015) No. 2
- *Hadrons as Solitons* (July 6–17, 1999)
- *Few-Quark Problems* (July 8–15, 2000), Vol. **1** (2000) No. 1
- *Statistical Mechanics of Complex Systems* (August 27–September 2, 2000)
- *Selected Few-Body Problems in Hadronic and Atomic Physics* (July 7–14, 2001), Vol. **2** (2001) No. 1
- *Studies of Elementary Steps of Radical Reactions in Atmospheric Chemistry* (August 25–28, 2001)
- *Quarks and Hadrons* (July 6–13, 2002), Vol. **3** (2002) No. 3
- *Effective Quark-Quark Interaction* (July 7–14, 2003), Vol. **4** (2003) No. 1
- *Quark Dynamics* (July 12–19, 2004), Vol. **5** (2004) No. 1
- *Exciting Hadrons* (July 11–18, 2005), Vol. **6** (2005) No. 1
- *Progress in Quark Models* (July 10–17, 2006), Vol. **7** (2006) No. 1
- *Hadron Structure and Lattice QCD* (July 9–16, 2007), Vol. **8** (2007) No. 1
- *Few-Quark States and the Continuum* (September 15–22, 2008), Vol. **9** (2008) No. 1
- *Problems in Multi-Quark States* (June 29–July 6, 2009), Vol. **10** (2009) No. 1
- *Dressing Hadrons* (July 4–11, 2010), Vol. **11** (2010) No. 1
- *Understanding hadronic spectra* (July 3–10, 2011), Vol. **12** (2011) No. 1
- *Hadronic Resonances* (July 1–8, 2012), Vol. **13** (2012) No. 1
- *Looking into Hadrons* (July 7–14, 2013), Vol. **14** (2013) No. 1
- *Quark Masses and Hadron Spectra* (July 6–13, 2014), Vol. **15** (2014) No. 1
- *Exploring Hadron Resonances* (July 5–11, 2015), Vol. **16** (2015) No. 1

Satellite view (top) and the GPS track (bottom) of the two-boat rowing excursion on Lake Bled on July 11, 2015.

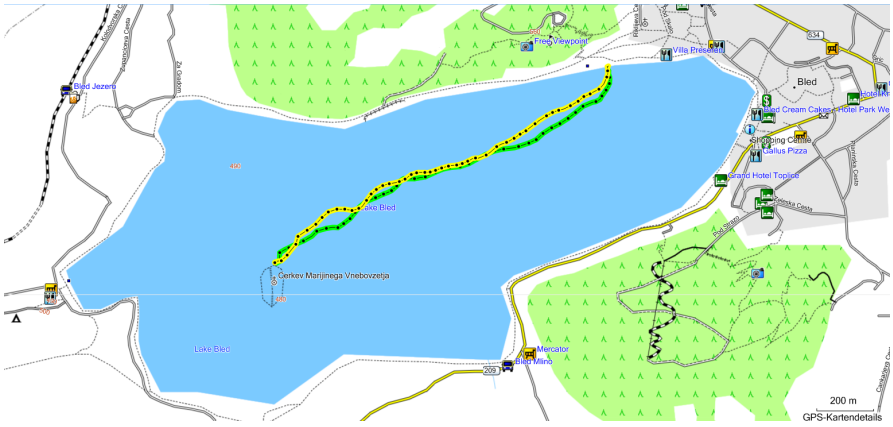

Bled Workshops
in Physics
Vol. 16, No. 1
p. 1

Proceedings of the Mini-Workshop
Exploring Hadron Resonances
Bled, Slovenia, July 5 - 11, 2015

Resonance states and branching ratios from a time-dependent perspective.

Ido Gilary

Shulich Faculty of Chemistry, Technion, Haifa, 3200003, Israel

The spectrum of a given Hermitian quantum mechanical system can be generally separated into a discrete part containing the bound states and a continuous part of scattering states above the threshold. These states are solutions to the time-independent Schrödinger equation (TISE) with the corresponding boundary conditions. The discrete nature of the bound spectrum enables the characterization of the stable part of the studied system along with its physical properties based on its energy levels. The continuum can be used to characterize the system by probing it through scattering experiments. In this context instead of discrete energy levels the discussion is usually shifted to resonances in the scattering profile of the studied system. These appear as sharp features in the energy profile of the interaction.

Wavepacket dynamics in the continuum of meta-stable open quantum systems reveals that in the interaction region the evolution resembles that of bound states. There is, however, one difference where a bound system preserves probability in a meta-stable one when we observe decay in time. When the decay from the interaction region tends to follow an exponential form then the energy content of the localized part of the wavepacket assumes a constant value. This value is complex where the real part represents the energy of a resonance of the system and the imaginary part is related to the width of this resonance. The dynamics outside the interaction region exhibit a spatial exponential increase which drops off at the edge of the escaping wavefront. The velocity of the escaping part of the wavepacket has the momentum corresponding to the average energy inside. Similar dynamics is observed when scattering a wavepacket off a potential at a resonant energy. Initially the arriving wavepacket populates a resonant bound-like state inside the interaction region and consequently the formed meta-stable state decays.

The time-dependent dynamics observed in meta-stable systems demonstrates the properties of both stationary bound and scattering states. This type of dynamics usually occurs due to either the shape of the potential of interaction where the variation can lead to confinement of finite time or due the coupling of a bound state in an closed channel with the continuum of an open channel. The first type of states is often termed shape-type resonance whereas the second type is usually called Feshbach-type resonances. The above discussion suggests that the essence of the dynamics can be captured by solving a time independent equation with appropriate boundary conditions. Such boundary conditions allow only outgo-

ing flux. Solving the TISE with outgoing boundary conditions leads to solutions with complex momentum. This makes the energies of these states complex just as the portrayed dynamics and it also displays the asymptotic divergence which was observed.

In order to be able to calculate the energies of the resonance states one needs to be able to fix the asymptotic divergence. This can be achieved in various ways which all lead to a non-Hermitian Hamiltonian. Some of the techniques used are: (1) scaling of the coordinate by a complex factor (complex scaling); (2) addition of a complex absorbing potential at the asymptotes far from the interaction region; (3) Feshabch projection formalism which separates between the spaces of localized and scattering states; (4) Siegert pseudo states which satisfy the required boundary condition on a given surface but lead to a quadratic eiegnvalue problem.

The use of Non-Hermitian Hamiltonians readily yields the information regarding the lifetime of a given meta-stable state in addition to its energy. On the other hand, it leads to some complications due the non-Hermiticity. First of all, the resonance states are not orthogonal with respect to the conventional scalar Dirac product. Instead one needs to find and additional set of states which are orthogonal to them. These are the eigenstates of the Hermitian conjugate Hamiltonian which physically are their time-reversed counterparts. The two bi-orthogonal states form together the resolution of the identity. Another aspect is the loss of the probabilistic interpretation due to the non-Hermiticty. This can be amended by redefining the inner product based on the bi-orthogonal set of states. By doing so the probabilistic interpretation is retained along with the non-unitary evolution resulting from the decay of the system. This allows to describe very complicated dynamics in the continuum based on dynamics of several resonance states alone.

In decaying few-body systems there are often several channels open to decay. In such case the decay rate of the resonance contains contributions due to the flux in each of the open channels. When considering the above mentioned outgoing boundary conditions one finds that the momentum of the outgoing flux in each channel depends on the resonance energy and the threshold energy of the given channel. When following the wavepacket dynamics in such systems one observes that at every channel the wavepacket leaks at the velocity given by the momentum in that channel. Consequently all the information regarding the partial widths to the different channels and their branching ratios can be extracted from the stationary resonance wavefunction. All that is needed in order to evaluate the branching ratios is the complex amplitude of the resonance wavefunction at the asymptotes and the momentum at every given channel which is obtained from the difference between the resonance energy and the channel's threshold energy.

References

1. Shachar Klaiman and Ido Gilary, "On Resonance: A First Glance into the Behavior of Unstable States." In: Advances in Quantum Chemistry, **63**. "Unstable States in the Continuous Spectra, Part II: Interpretation, Theory and Applications", Edited by Cleanthes A. Nicolaides and Erkki Brändas. San Diego: Academic Press, pp. 131 (2012).
2. Tamar Goldzak, Ido Gilary and Nimrod Moiseyev, "Evaluation of partial widths and branching ratios from resonance wave functions." Physical Review A. **82**, 052105 (2010).

BLED WORKSHOPS
IN PHYSICS
VOL. 16, NO. 1
p. 4

Proceedings of the Mini-Workshop
Exploring Hadron Resonances
Bled, Slovenia, July 5 - 11, 2015

In-medium properties of the nucleon within a π-ρ-ω model*

Ju-Hyun Jung[a], Ulugbek Yakhshiev[b], Hyun-Chul Kim[b]

[a]Theoretical Physics, Institute of Physics, University of Graz, Universitatsplatz 5, A-8010 Graz, Austria
[b]Department of Physics, Inha University, Incheon 402-751, Republic of Korea

Abstract. In this talk, we report on a recent investigation of the transverse charge and energy-momentum densities of the nucleon in the nuclear medium, based on an in-medium modified π-ρ-ω soliton model. The results allow us to establish general features of medium modifications of the structure of nucleons bound in a nuclear medium. We briefly discuss the results of the transverse charge and energy-momentum densities.

1 Introduction

The generalized parton distributions (GPDs) provide a new aspect of the structure of the nucleon, since they contain essential information on how the constituents of the nucleon behave inside a nucleon. The energy-momentum tensor (EMT) form factors (FFs) are given by Mellin moments of certain GPDs and characterize how mass, spin, and internal forces are distributed inside a nucleon. The EMT FFs are essential quantities in understanding the internal structure of the nucleon [1–3]. Furthermore the transverse charge which is defined by a Fourier transform in the transverse plane provides a tomographic picture of how the charge densities of quarks are distributed transversely [4,5].

2 Lagrangian of the model

We start from the in-medium modified effective chiral Lagrangian with the π, ρ, and ω meson degrees of freedom, where the nucleon arises as a topological soliton. Using the asteriks to indicate medium modified quantities, the Lagrangian has the form

$$\mathcal{L}^* = \mathcal{L}^*_\pi + \mathcal{L}^*_{\rm V} + \mathcal{L}^*_{\rm kin} + \mathcal{L}^*_{\rm WZ}, \tag{1}$$

* Talk delivered by Ju-Hyun Jung

where the corresponding terms are expressed as

$$\mathcal{L}^*_\pi = \frac{f_\pi^2}{4}\,\mathrm{Tr}\left(\partial_0 U \partial_0 U^\dagger\right) - \alpha_p \frac{f_\pi^2}{4}\,\mathrm{Tr}\left(\partial_i U \partial_i U^\dagger\right) + \alpha_s \frac{f_\pi^2 m_\pi^2}{2}\,\mathrm{Tr}\left(U-1\right), \quad (2)$$

$$\mathcal{L}^*_V = \frac{f_\pi^2}{2}\,\mathrm{Tr}\left[D_\mu \xi\cdot\xi^\dagger + D_\mu \xi^\dagger\cdot\xi\right]^2, \quad (3)$$

$$\mathcal{L}^*_{kin} = -\frac{1}{2g_V^2\zeta_V}\,\mathrm{Tr}\left(F_{\mu\nu}^2\right), \quad (4)$$

$$\mathcal{L}^*_{WZ} = \left(\frac{N_c}{2} g_\omega \sqrt{\zeta_\omega}\right)\omega_\mu \frac{\epsilon^{\mu\nu\alpha\beta}}{24\pi^2}\,\mathrm{Tr}\left\{\left(U^\dagger\partial_\nu U\right)\left(U^\dagger\partial_\alpha U\right)\left(U^\dagger\partial_\beta U\right)\right\}. \quad (5)$$

Here, the SU(2) chiral field is written as $U = \xi_L^\dagger\,\xi_R$ in unitary gauge, and the field-strength tensor and the covariant derivative are defined, respectively, as

$$F_{\mu\nu} = \partial_\mu V_\nu - \partial_\nu V_\mu - i[V_\mu, V_\nu], \quad (6)$$

$$D_\mu\,\xi_{L(R)} = \partial_\mu\,\xi_{L(R)} - i\,V_\mu\,\xi_{L(R)}. \quad (7)$$

We assume the following ansätze for the pseudoscalar and vector mesons

$$U = \exp\left\{\frac{i\boldsymbol{\tau}\cdot\mathbf{r}}{r}F(r)\right\}, \quad V_\mu = \frac{g}{2}\left(\boldsymbol{\tau}\cdot\boldsymbol{\rho}_\mu + \omega_\mu\right),$$
$$\rho_0^a = 0, \quad \rho_i^a = \frac{\epsilon_{ika}r_k}{g\sqrt{\zeta}r^2}\,G(r), \quad \omega_\mu = \omega(r)\delta_{\mu 0} \quad (8)$$

with the Pauli matrices $\boldsymbol{\tau}$ in isospin space. One can minimize the static mass functional related to the Lagrangian in Eq. (1) and find the solitonic solutions corresponding to a unit baryon number ($B = 1$). The integrand of the static mass functional corresponds to T^{00} component of the energy momentum tensor presented below. The details of the minimization procedure can be found in Ref. [6].

Using the Lagrangian in Eq. (1), one can calculate each component of the EMT as follows:

$$\begin{aligned} T^{00*}(r) = {} & \alpha_p \frac{f_\pi^2}{2}\left(2\frac{\sin^2 F}{r^2} + F'^2\right) + \alpha_s f_\pi^2 m_\pi^2 (1-\cos F) \\ & + \frac{2f_\pi^2}{r^2}(1-\cos F+G)^2 - \zeta g^2 f_\pi^2 \omega^2 \\ & + \frac{1}{2g^2\zeta r^2}\left\{2r^2G'^2 + G^2(G+2)^2\right\} - \frac{1}{2}\omega'^2 \\ & + \left(\frac{3}{2}g\sqrt{\zeta}\right)\frac{1}{2\pi^2 r^2}\omega\sin^2 F F', \end{aligned} \quad (9)$$

$$T^{0i*}(\mathbf{r},\mathbf{s}) = \frac{\epsilon^{ilm}r^l s^m}{(\mathbf{s}\times\mathbf{r})^2}\rho_J(r), \quad (10)$$

$$T^{ij*}(r) = s(r)\left(\frac{r^i r^j}{r^2} - \frac{1}{3}\delta^{ij}\right) + p(r)\,\delta^{ij}, \quad (11)$$

where

$$\rho_J^*(r) = \frac{f_\pi^2}{3\lambda}\left[\sin^2 F + 8\sin^4\frac{F}{2} - 4\sin^2\frac{F}{2}\xi_1\right] + \frac{1}{3g^2r^2\zeta\lambda}\left[(2-2\xi_1-\xi_2)\,G^2\right] + \frac{g\sqrt{\zeta}}{8\pi^2\lambda}\Phi\sin^2 F F' \tag{12}$$

is the angular momentum density and

$$p^*(r) = -\frac{1}{6}\alpha_p f_\pi^2\left(F'^2 + 2\frac{\sin^2 F}{r^2}\right) - \alpha_s f_\pi^2 m_\pi^2(1-\cos F) - \frac{2}{3r^2}f_\pi^2(1-\cos F+G)^2 + f_\pi^2 g^2\zeta\omega^2 + \frac{1}{6g^2\zeta r^2}\left\{2r^2G'^2 + G^2(G+2)^2\right\} + \frac{1}{6}\omega'^2, \tag{13}$$

$$s^*(r) = \alpha_p f_\pi^2\left(F'^2 - \frac{\sin^2 F}{r^2}\right) - \frac{2f_\pi^2}{r^2}(1-\cos F+G)^2 + \frac{1}{g^2r^2\zeta}\left\{r^2G'^2 - G^2(G+2)^2\right\} - \omega'^2 \tag{14}$$

are the pressure and the shear force distributions inside the nucleon. The moment of inertia of the rotating soliton including $1/N_c$ corrections is given by the expression

$$\lambda^* = 4\pi\int dr\left[\frac{2f_\pi^2}{3}\left(\sin^2 F + 8\sin^4\frac{F}{2} - 4\sin^2\frac{F}{2}\xi_1\right) + \frac{2}{3g^2r^2\zeta}\left\{(2-2\xi_1-\xi_2)\,G^2\right\} + \frac{g\sqrt{\zeta}}{4\pi^2}\Phi\sin^2 F F'\right]. \tag{15}$$

As we mentioned above, the integral of T_{00} gives the soliton mass at zero momentum transfer $t = 0$. Therefore, the $M_2(t)$ form factor is normalized by the nucleon mass as

$$M_2(0) = \frac{1}{M_N}\int_0^\infty d^3r\, T_{00}(r) = 1 \tag{16}$$

to leading order in M_N, which is equals to the soliton mass [7]. For details, we refer to Refs. [8,9]

The EMT FFs of the nucleon parametrize the nucleon matrix elements of the symmetric EMT operator as follows [2,3]:

$$\langle p'|\hat{T}_{\mu\nu}(0)|p\rangle = \bar{u}(p',s')\left[M_2(q^2)\frac{P_\mu P_\nu}{M_N} + J(q^2)\frac{i(P_\mu\sigma_{\nu\rho}+P_\nu\sigma_{\mu\rho})q^\rho}{2M_N}\right. \tag{17}$$

$$\left. + d_1(q^2)\frac{q_\mu q_\nu - g_{\mu\nu}q^2}{5M_N}\right]u(p,s), \tag{18}$$

where $P = (p+p')/2$.

One can be related GPDs. In the specific case, $\xi = 0$, one has

$$A_{20}(t) = M_2(t) = \int_{-1}^{1} dx x H(x, 0, t) , \tag{19}$$

$$B_{20}(t) = 2J(t) - M_2(t) = \int_{-1}^{1} dx x E(x, 0, t) . \tag{20}$$

In the isospin symmetric approximation the proton and neutron EMT FFs are similar. Therefore we introduce the nucleon transverse EMT densities instead of considering the proton and neutron EMT densities separately. In this approximation an unpolarized nucleon transverse EMT density takes the form

$$\rho_0^{(2)}(b) = \int_0^{\infty} \frac{dQ}{2\pi} j_0(bQ) A_{20}(Q^2) . \tag{21}$$

For a polarized nucleon one has the following transverse EMT density

$$\rho_T^{(2)}(\mathbf{b}) = \rho_0^{(2)}(b) - \sin(\phi_b - \phi_S) \times \int_0^{\infty} \frac{Q^2 dQ}{4\pi M_N} j_1(bQ) B_{20}(Q^2) . \tag{22}$$

3 Results

Now let us discuss the energy-momentum form factors of the nucleons. First of all, it is necessary to notice that in the case of exact isospin symmetry the energy-momentum form factors of the protons and neutrons cannot be distinguished in free space. The same result holds for the nucleons embedded in isospin symmetric nuclear matter. The situation changes if one introduces isospin breaking effects in the mesonic sector. In the case of in-medium nucleons the isospin asymmetric nuclear environment can generate differences in EMT form factors of the nucleons even if one has isospin symmetry in the mesonic sector in free space. For simplicity we concentrate in this work on the isopin symmetric case for both, free space as well as in medium nucleons, considering an isospin symmetric nuclear environment.

The energy-momentum form factors of the nucleons as functions of t are presented in Fig. 1 for free space nucleons and in-medium nucleons at normal nuclear matter density ρ_0.

Finally, in Fig. 2 we present the transverse energy-momentum densities inside an unpolarized and polarized nucleon for the fixed value of $b_x = 0$.

Our complete results will appear in some detail elsewhere [10].

Acknowledgments

This work is supported by the Basic Science Research Program through the National Research Foundation (NRF) of Korea funded by the Korean government (Ministry of Education, Science and Technology), Grant No. 2011-0023478 (J.H.Jung and U.Yakhshiev) and Grant No. 2012004024 (H.Ch.Kim). J.-H.Jung. acknowledges also partial support by the "Fonds zur Förderung der wissenschaftlichen Forschung in Österreich via FWF DK W1203-N16."

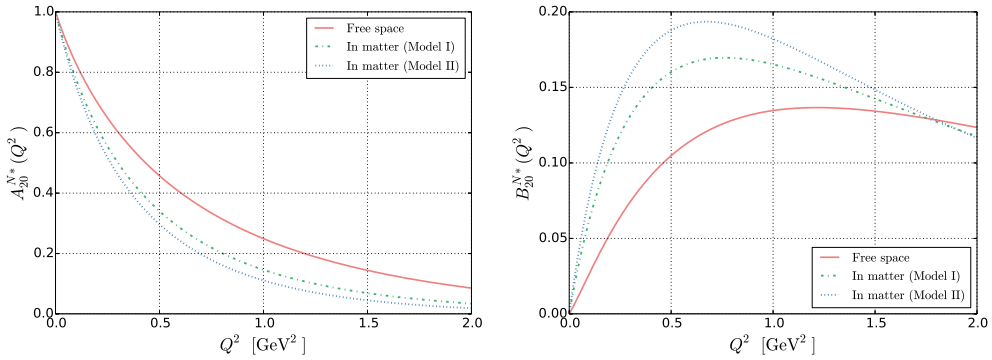

Fig. 1. The EMT form factors of the nucleon, A_{20} and B_{20}, as functions of t. The solid curve depicts the form factors in free space. The dotted and dotted-dashed ones represent, respectively, those from Model I and Model II in nuclear medium at the normal nuclear matter density ρ_0.

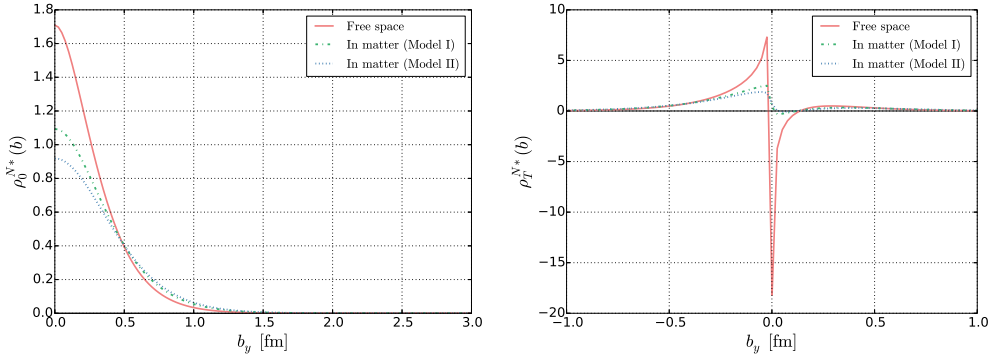

Fig. 2. Transverse energy-momentum densities inside an unpolarized and polarized nucleon with $b_x = 0$ fixed. The solid curve depicts the form factors in free space. The dotted and dotted-dashed ones represent, respectively, those from model I and model II in nuclear matter.

References

1. X. D. Ji, Phys. Rev. D **55**, 7114 (1997).
2. X. D. Ji, Phys. Rev. Lett. **78**, 610 (1997).
3. M. V. Polyakov, Phys. Lett. B **555**, 57 (2003).
4. U. Yakhshiev and H. -Ch. Kim, Phys. Lett. B **726**, 375 (2013).
5. K. Goeke, M. V. Polyakov and M. Vanderhaeghen, Prog. Part. Nucl. Phys. **47** 401 (2001).
6. J. -H. Jung, U. T. Yakhshiev and H. -Ch. Kim, Phys. Lett. B **723**, 442 (2013).
7. H. -Ch. Kim, P. Schweitzer and U. T. Yakhshiev, Phys. Lett. B **718**, 625 (2012).
8. J. -H. Jung, U. Yakhshiev and H. -Ch. Kim, J. Phys. G **41**, 055107 (2014).
9. J. -H. Jung, U. Yakhshiev, H. -Ch. Kim and P. Schweitzer Phys. Rev. D **89**, 114021 (2014).
10. J. -H. Jung, U. T. Yakhshiev and H. -Ch. Kim, in preparation.
11. T. Ericson and W. Weise, *Pions and Nuclei* (Clarendon, Oxford, 1988).

BLED WORKSHOPS
IN PHYSICS
VOL. 16, NO. 1
p. 9

Proceedings of the Mini-Workshop
Exploring Hadron Resonances
Bled, Slovenia, July 5 - 11, 2015

η MAID-2015: update with new data and new resonances*

V. L. Kashevarov, L. Tiator, M. Ostrick

Institut für Kernphysik, Johannes Gutenberg-Universität, D-55099 Mainz, Germany

Abstract. Recent data for η and η′ photoproduction on protons obtained by the A2 Collaboration at MAMI are presented. The total cross section for η photoproduction demonstrates a cusp at the energy corresponding to the η′ threshold. The new data and existing data from GRAAL, CBELSA/TAPS, and CLAS collaborations have been analyzed by an expansion in terms of associated Legendre polynomials. The isobar model ηMAID updated with η′ channel and new resonances have been used to fit the new data. The new solution ηMAID-2015 reasonably good describes the data in the photon beam energy region up to 3.7 GeV.

1 Introduction

The unitarity isobar model ηMAID [1] was developed in 2002 for η photo- and electroproduction on nucleons. The model includes a nonresonant background, which consists of nucleon Born terms in the s and u channels and the vector meson exchange in the t channel, and s-channel resonance excitations. The Born terms are evaluated with the pseudoscalar coupling. The vector meson contribution is obtained by the ρ and ω meson exchange in the t channel with pole-like Feynman propagators. For each partial wave the resonance contribution is parameterized by the Breit-Wigner function with energy dependent widths. The ηMAID-2003 version includes eight resonances, $N(1520)3/2^-$, $N(1535)1/2^-$, $N(1650)1/2^-$, $N(1675)5/2^-$, $N(1680)5/2^+$, $N(1700)3/2^-$, $N(1710)1/2^+$, $N(1720)3/2^+$, and was fitted to proton data for differential cross sections and beam asymmetry at photon beam energies up to 1400 MeV. The ηMAID-2003 version describes not only the experimental data available in 2002, but even a bump structure around W=1700 MeV in η photoproduction on the neutron, which was observed a few years later. However, this version fails to reproduce the new polarization data obtained in Mainz [2].

The aim of this work is to extend the ηMAID-2003 version to higher energies, to improve a description of the new polarization data, and to include the η′ photoproduction channel.

* Talk presented by V. L. Kashevarov

2 Truncated Legendre analysis

The full angular coverage of differential cross sections and polarization observables allow us to perform a fit with a Legendre series truncated to a maximum orbital angular momentum ℓ_{max}:

$$\frac{d\sigma}{d\Omega} = \sum_{n=0}^{2\ell_{max}} A_n^{\sigma} P_n^0(\cos\Theta_\eta), \tag{1}$$

$$T(F)\quad \frac{d\sigma}{d\Omega} = \sum_{n=1}^{2\ell_{max}} A_n^{T(F)} P_n^1(\cos\Theta_\eta), \tag{2}$$

$$\Sigma\quad \frac{d\sigma}{d\Omega} = \sum_{n=2}^{2\ell_{max}} A_n^{\Sigma} P_n^2(\cos\Theta_\eta), \tag{3}$$

where $P_n^m(\cos\Theta_\eta)$ are the associated Legendre polynomials. The spin-dependent cross sections, $Td\sigma/d\Omega$, $Fd\sigma/d\Omega$, and $\Sigma d\sigma/d\Omega$ were obtained by multiplying the corresponding asymmetries with the differential cross sections obtained in Mainz. As an example, the results for the Legendre coefficients for differential

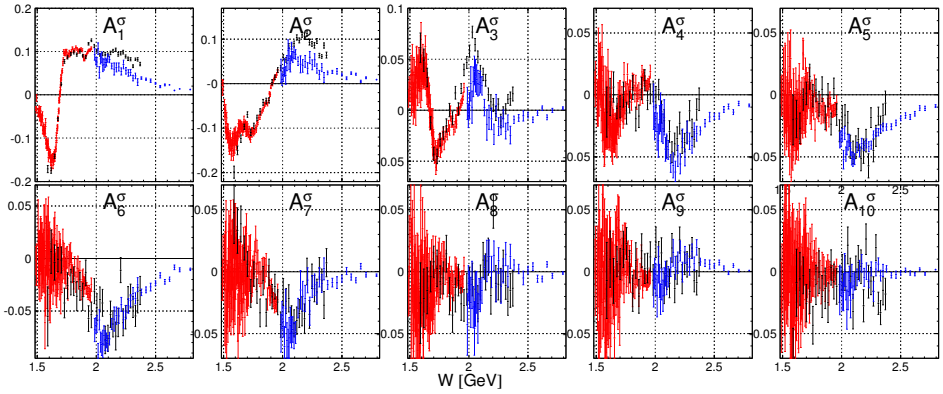

Fig. 1. Legendre coefficients in [μb/sr] up to $\ell_{max} = 5$ from our fits to the differential cross section of the $\gamma p \to \eta p$ reaction as function of the center-of-mass energy W. Red circles are fit results for preliminary A2/MAMI data [3], black and blue - for CBELSA/TAPS [4] and CLAS [5] data correspondingly.

cross sections are presented in Figs. 1 and 2. A non-zero A_{10} only posible with h-wave contribution, A_9 is dominated by the an interference between g and h waves, A_8 includes g, h waves and an interference between f and h waves, and so on. The first coefficient, A_0, was omitted in the figures because of it includes all possible partial-wave amplitudes and just only reflects the magnitude of the total cross section, see Fig. 3.

Non-zero values of the A_7 and A_8 coefficients point to a contribution of the g wave at energies above W=2 GeV for both η and η′ channels. The errors in

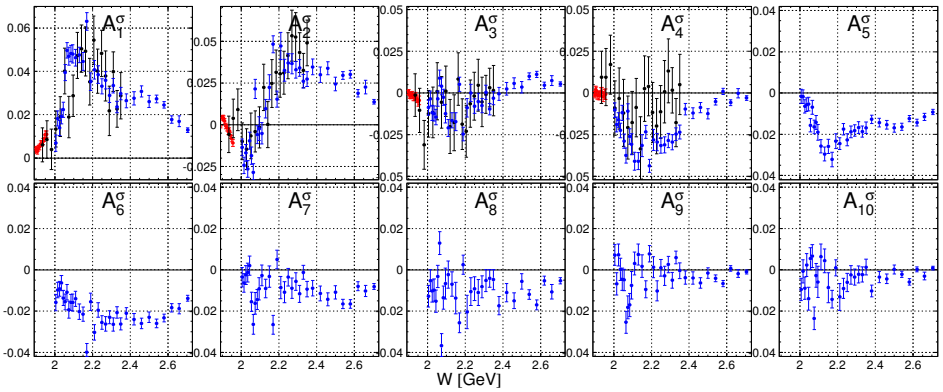

Fig. 2. The same as Fig. 1, but for the $\gamma p \to \eta' p$ reaction.

the determination of the coefficients A_9 and A_{10} do not allow any conclusions about the contribution of h wave in these reactions. Polarization observables for η photoprduction were measured below W=1.9 GeV. The Legendre fit for these data shows the sensitivity to small partial-wave contributions and indicates pd interferences below W=1.6 GeV and df interferences above W=1.6 GeV [2].

3 Updated ηMAID

New ηMAID-2015 model is based on the ηMAID-2003 version. The following main changes were made:

- 12 additional resonances were added: $N(1860)5/2^+$, $N(1875)3/2^-$, $N(1880)1/2^+$, $N(1895)1/2^-$, $N(1900)3/2^+$, $N(1990)7/2^+$, $N(2000)5/2^+$, $N(2060)5/2^-$, $N(2120)3/2^-$, $N(2190)7/2^-$, $N(2220)9/2^+$, and $N(2250)9/2^-$;
- electromagnetic couplings for the vector mesons were updated according to Ref. [6];
- hadronic vector and tensor couplings for the vector mesons were fixed from Ref. [7];
- data base for the fit was updated.

The new model was fitted to data of differential cross sections from the A2 Collaboration at MAMI [3] and CLAS Collaboration [5], polarisation observables T, F [2] and Σ [8], [9]. The main variable parameters for each resonance: Breit-Wigner mass, total width, branching ratio to ηp (or η′p) decay, photoexcitation helicity amplitudes $A_{1/2}$ and $A_{3/2}$, a relative sign between the $N^* \to \eta N$ and the $N^* \to \pi N$ couplings. Besides, the hadronic pseudoscalar coupling for the Born term contribution, cutoffs for dipole formfactors of the vector mesons, damping factors for the partial widths and the electromagnetic form factor of the resonances were also fitted. Branching ratios for hadronic decays of the resonances besides the investigated channel were fixed.

As an initial parameter set for the Breit-Wigner parameters the last BnGa solution [10] was used. As initial parameter limits uncertainties from Refs. [6]

and [10] were used. As the first step, for each resonance $A_{1/2}$ and $A_{3/2}$ are fixed because of a strong correlation with the branching ratio. On the second step the branching ratios obtained on the first step are fixed, but $A_{1/2}$ and $A_{3/2}$ are variable, and so on. After few iterations the initial limits are changed if necessary. The fits for the η and $\eta\prime$ channels were done independently.

The fit results for the total cross sections and the polarization observables are presented in Figs. 3-6 together with corresponding experimental data. We used the differential cross section from the CLAS Collabration [5] in this fit because of their much smaller statistical errors, larger energy covering, and better agreement with the high statistic data from A2/MAMI [3] in an overlapping energy region. Unfortunately, the total cross section was not determined in Ref. [5] and we calculated it using Legendre decomposition for the differential cross sections. Blue circles in Figs. 3 and 5 are results of this procedure.

In Fig. 3, there is a very interesting feature at energy ~1900 MeV, which could be explained by a cusp due to the opening of a new channel, $\eta\prime$ photoproduction. The main resonance, which is responsible for this effect is the $N(1895)1/2^-$. The Breit-Wigner parameters of this state were determined by the fit as following: $M = 1896 \pm 1$ MeV, $\Gamma_{tot} = 93 \pm 13$ MeV, $\Gamma_{\eta p} = (14 \pm 3)\%$, $\Gamma_{\eta\prime p} = (6.5 \pm 2)\%$, and $A_{1/2} = (-17.4 \pm 1.5) 10^{-3} GeV^{-1/2}$. Fig. 4 demonstrates a significant improvement of description for T and F asymmetries (red lines) in comparison with the ηMAID-2003 version (blue lines).

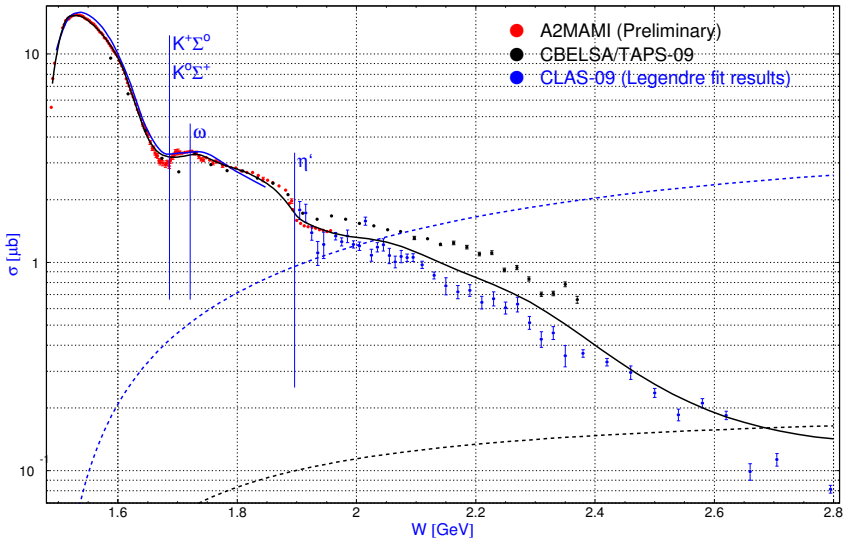

Fig. 3. Total cross section of the $\gamma p \to \eta p$ reaction. Solid blue curve is ηMAID-2003 isobar model [1], black solid curve: new ηMAID-2015 solution. Prediction of ηMAID-2003 for background contribution is shown by blue dashed line, background of ηMAID-2015 - black dashed line. Vertical lines correspond to thresholds of $K\Sigma$, ω, and $\eta\prime$ photoproductions.

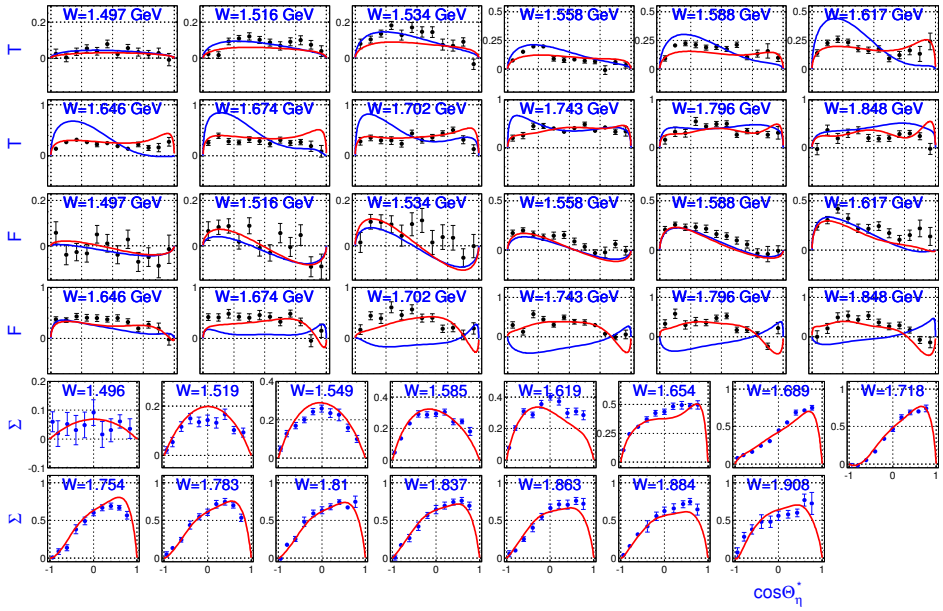

Fig. 4. ηMAID-2015 solution for the η channel (red lines). Black circles: A2/MAMI-15 data [2] for T and F asymmetries, blue circles: GRAAL-07 data [8] for Σ. Blue lines: ηMAID-2003 prediction [1].

A very good agreement with the experimental data was obtained for the cross section of the $\gamma p \to \eta' p$ reaction (see Fig. 5). The main contributions to this reaction come from $N(1895)1/2^-$, $N(1900)3/2^+$, $N(1880)1/2^+$, $N(2150)3/2^-$, and $N(2000)5/2^+$ resonances. Other resonance contributions are much smaller then the background. The new ηMAID-2015 solution describes shape of the GRAAL data for Σ near threshold, but not the magnitude (see Fig. 6). To explain, why the magnitude of the asymmetry is larger at lower energy, it is probably necessary to include below threshold resonances using the more realistic approach applied in Ref. [11] for the Roper resonance at η-meson photoproduction.

4 Summary and conclusions

In summary, we have presented new version ηMAID-2015. The model describes available data for the $\gamma p \to \eta p$ and $\gamma p \to \eta' p$ reactions reasonably well. The cusp at W~1900 MeV in $\gamma p \to \eta p$ reaction was explained as a threshold effect from the η' channel. Parameters of $N(1895)1/2^-$ resonance, responsible for this effect, were determined. A further improvement could be achieved by adding below threshold resonances and using Regge trajectories for the vector mesons in t channel. Furthermore, polarization observables which should come soon from A2/MAMI, CBELSA/TAPS, and CLAS Collaborations will help to improve the model.

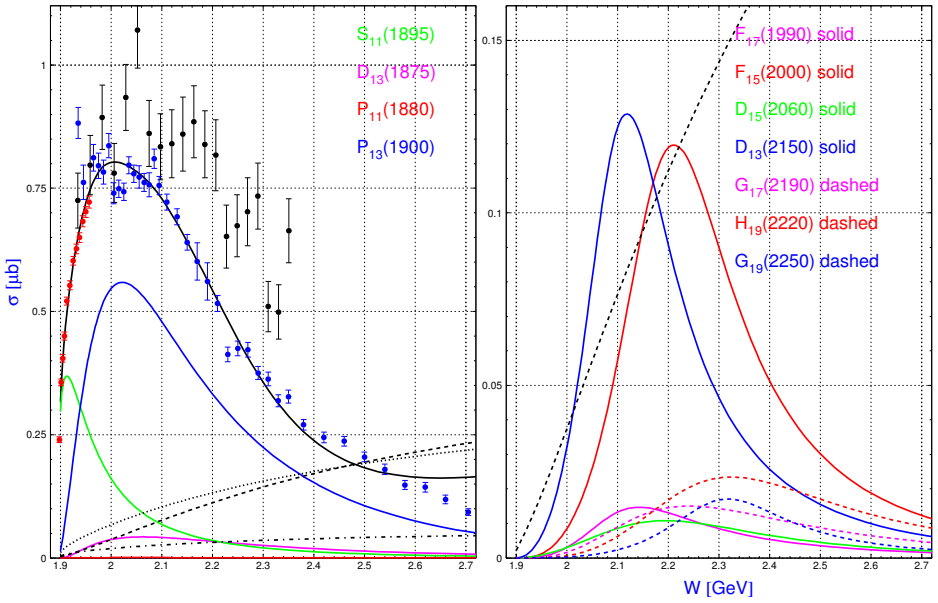

Fig. 5. Total cross section of the $\gamma p \rightarrow \eta' p$ reaction. Red circles: A2/MAMI-15 data [3], black circles: CBELSA/TAPS-09 [4], blue circles: data obtained from the Legendre fit to the differential cross sections of the CLAS Collaboration [5]. Solid black line: ηMAID-2015 solution. Background contribution is shown by dashed black line. Black dotted and dot-dashed lines are partial contributions of the Born terms and the vector mesons correspondingly. Other curves are partial contributions of resonances.

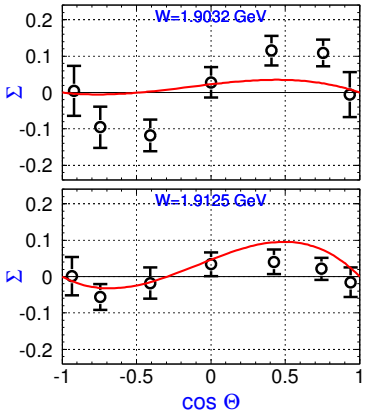

Fig. 6. Beam asymmetry Σ. Data from Ref. [9], red curves are ηMAID-2015 solution.

Acknowledgment

This work was supported by the Deutsche Forschungsgemeinschaft (SFB 1044).

References

1. W. -T. Chiang, S. N. Yang, L. Tiator, and D. Drechsel, Nucl. Phys. **A700**, 429 (2002).
2. J. Akondi *et al.* (A2 Collaboration at MAMI), Phys. Rev. Lett. **113**, 102001 (2014).
3. P. Adlarson *et al.* (A2 Collaboration at MAMI), Submitted to Phys. Rev. Lett.
4. V. Crede *et al.* (CBELSA/TAPS Collaboration), Phys. Rev. C **80**, 055202 (2009).
5. M. Williams *et al.* (CLAS Collaboration), Phys. Rev. C **80**, 045213 (2009).
6. K. A. Olive *et al.* (Particle Data Group), Chin. Phys. C **38**, 090001 (2014).
7. J. M. Laget *et al.*, Phys. Rev. C **72**, 022202(R) (2005).
8. O. Bartalini *et al.* (The GRAAL Collaboration), Eur. Phys. J. A **33**, 169 (2007).
9. G. Mandaglio *et al.*, EPJ Web of Conferences **72** 00016 (2014); P. Levi Sandri *et al.*, arXiv:1407.6991v2.
10. A. V. Anisovich, R. Beck, E. Klempt, V. A. Nikonov, A. V. Sarantsev, U. Thoma, Eur. Phys. J. A **48**, 15 (2012).
11. I. G. Aznauryan, Phys. Rev. C **68**, 065204 (2003).

BLED WORKSHOPS
IN PHYSICS
VOL. 16, NO. 1
p. 16

Proceedings of the Mini-Workshop
Exploring Hadron Resonances
Bled, Slovenia, July 5 - 11, 2015

Analytic structure of nonperturbative quark propagators and meson processes*

Dalibor Kekez[a] and Dubravko Klabučar[b]

[a] Rugjer Bošković Institute, Bijenička c. 54, 10000 Zagreb, Croatia
[b] Physics Department, Faculty of Science, Zagreb University, Bijenička c. 32, Zagreb 10000, Croatia

Abstract. The analytic structure of certain *Ansätze* for quark propagators in the nonperturbative regime of QCD is investigated. When choosing physically motivated parameterization of the momentum-dependent dressed quark mass function $M(p^2)$, with definite analytic structure, it is highly nontrivial to predict and control the analytic structure of the corresponding nonperturbative quark propagator. The issue of the Wick rotation relating the Minkowski-space and Euclidean-space formulations is also highly nontrivial in the nonperturbative case. A propagator form allowing the Wick rotation and enabling equivalent calculations in Minkowski and Euclidean spaces is achieved. In spite of its simplicity, this model yields good qualitative and semi-quantitative description of some pseudoscalar meson processes.

Lattice studies of QCD are complemented by the continuum QCD studies utilizing Dyson–Schwinger equations (DSE). Both *ab initio* DSE studies and DSE studies for models of QCD provide an important approach for the study of phenomena in hadronic physics both at zero and finite temperatures and densities – see, for example, Refs. [1, 2]. Just like lattice QCD studies, the large majority of DSE calculations (including those of our group, *e.g.*, [3]) are implemented in the Euclidean metric.

Nevertheless, solutions of the Bethe–Salpeter equation require analytic continuation of DSE solutions for dressed quark propagators $S_q(p)$, into the complex p^2–plane. Similar situation is with the processes that involve quark propagators (QP) and Bethe–Salpeter amplitudes: it is not enough to know propagators and the Bethe–Salpeter amplitude only in the spacelike region, for real and positive p^2. It is important to know the analytic properties in the whole p^2 complex plane.

Alkofer *et al.* [4] have explored the analytic structure of the Landau gauge gluon and quark propagators. They have proposed some simple analytic *Ansätze* for these propagators. Based on their *Ansätze*, Jiang *et al.* [5] provide an analytical approach to calculating the pion decay constant f_π and and the pion mass M_π at finite density.

We want to investigate and further improve the analytic structure of the quark propagator $S(p)$. It can be conventionally parameterized (in Minkowski

* Talk delivered by Dubravko Klabučar

space) as

$$S(p) = -\sigma_v(-p^2)\,\not{p} + \sigma_s(-p^2) = Z(-p^2)\frac{\not{p} + M(-p^2)}{p^2 - M^2(-p^2)} \ ,$$

and correspondingly in Euclidean space as

$$S(p) = i\not{p}\,\sigma_v(p^2) + \sigma_s(p^2) = \frac{Z(p^2)}{-i\not{p} + M(p^2)} = Z(p^2)\frac{i\not{p} + M(p^2)}{p^2 + M^2(p^2)} \ ,$$

where $M(x)$ is the dressed quark mass function and $Z(x)$ is the wave function renormalization. Alkofer et al. [4] have explored the analytic structure of the quark (and gluon) propagator in the Landau gauge, using numerical solutions of the pertinent Dyson-Schwinger equations and fits to lattice data as inputs. Their *Ansätze* for Z and M (or σ_v and σ_s) include meromorphic functions (poles on the real axes or/and pairs of the complex conjugate poles) and functions with branch cut structures. Positivity violation in the spectral representation of the propagator shows the presence of the negative–norm contributions to the spectral function, i.e., the absence of asymptotic states from the physical part of the state space, which is sufficient (but not necessary) criterion for the confinement. While in the gluon propagator a clear evidence for positivity violation is found, the similar analysis shows that there is probably no such violation in the quark propagator [4]. The propagator with pairs of complex conjugate poles violates causality. It has been argued [6,7] that the corresponding S-matrix remains both causal and unitary (see also Ref. [1]).

Furthermore, complex conjugate poles can pose a problem for the analytic continuation from Minkowski to Euclidean space (Wick rotation) used by lattice gauge theory and functional methods. It has been also shown that complex conjugate poles in $S(p)$ cause thermodynamical instabilities at nonvanishing temperature and density [8].

Of crucial importance is the following question: Is it possible to find an analytic *Ansatz* for the quark propagator solely with branching cut (or cuts) on the real timelike axes, with no additional structures (isolated singularities or cuts) in the complex plane? Such an *Ansatz* could be used for practical calculation of the processes involving quark loops.

Because of a complicated interplay between analytic structure of the functions Z and M on one side, and σ_s and σ_v on the other side, the approximation $A = 1$ has been applied. Then, the problem reduces to finding of appropriate functions $M(x)$ and $\sigma(x) = 1/(x + M^2(x))$. The most rigorous constraint is that the propagator $S(p) \to 0$ for all directions $|p^2| \to \infty$ in the complex p^2 plane [9]. Furthermore, for large and positive values of $x = p^2$ (spacelike momenta), function $M(x)$ must be positive and approach to zero from above [4]. In the Euclidean regime, for real and positive values of x, the mass function should be fitted to match the form known from lattice and Dyson-Schwinger calculations.

Number of *Ansätze* for the quark mass function has been investigated. When choosing certain parametrization of the function $M(x)$, with definite analytic structure, it is highly nontrivial to predict and control the analytic structure of the accompanying $\sigma(x)$ function. Relevant mathematical theory and possibly related theorems (like Rouches theorem) are hardly applicable for this concrete problem.

The best results were achieved with the *Ansatz* of the form $M(x) = \log(R(x))$, where R is a rational function with certain good properties. The function $M(x)$ has a few cuts on the real timelike axes, while the propagator dressing function $\sigma(x)$ has both branch cuts and poles on the real timelike axes. No additional structure are present in the complex momentum plane. The quark propagator based on this *Ansatz* should allow for the Wick rotation and equivalent calculation in Minkowski and Euclidean spacetime.

Future work will include an improved fitting of the mass function $M(x)$ and refinement of calculation with $Z(x) = 1$. Furthermore, we are planning to check whether our *Ansatz* satisfies the requirements of positivity violation.

The quark propagator obtained in this way, endowed with good analytic properties, should then be tried and adjusted so that it gives good results in various applications: the $\gamma\gamma$-transition and charge form factors of pions, σ and ρ form factors and decays, are just some of the interesting potential applications of the quark propagator *Ansatz* with good analytic structure. It is also necessary to investigate the related issue of the Bethe-Salpeter equation in Minkowski space. The quark loop contribution to various processes should also be studied using these improved quark propagators. Besides the processes like $\pi, \eta, \eta' \to \gamma\gamma$ that are described by an anomalous triangle diagram, there are interesting anomalous processes based on the pentagon diagram, like $\eta, \eta' \to 4\pi$. (We could expect new results from high-statistics η' experiments like BES-III, ELSA, CB-at-MAMIC, CLAS at Jefferson Lab.) The non–anomalous processes $\eta \to 3\pi$ is especially interesting because it is sensitive to the isospin violation. While the average u and d-quark mass, $(m_u + m_d)/2$, is well known, there exists significant uncertainty in their mass difference, $m_d - m_u$. The $\eta \to 3\pi$ decay is particularly suitable for $m_d - m_u$ difference determination because of the suppressed electromagnetic contributions [10,11].

Since the microscopic understanding of strongly interacting matter (both in hadronic phase and in quark-gluon phase) is of great importance also for the physics of heavy ion collisions and compact stars, extending the quark propagator *Ansatz* with good analytic structure to finite densities and temperatures should also be investigated. This is necessary, for example (to name one concrete task), for extending our analyses of the η-η' complex [12,13] to finite densities and temperatures. Of particular interest is extending to finite density our analysis of the possible $U_A(1)$ symmetry restoration [14] in the η-η' complex.

Acknowledgement

This work has been supported in part by the Croatian Science Foundation under the project number 8799. The authors acknowledge the partial support of the COST Action MP1304 Exploring fundamental physics with compact stars (NewCompStar).

References

1. C. D. Roberts and S. M. Schmidt, *Prog.Part.Nucl.Phys.* **45** (2000) S1–S103.

2. R. Alkofer and L. von Smekal, *Phys.Rept.* **353** (2001) 281.
3. D. Kekez and D. Klabučar, Phys. Rev. D **71** (2005) 014004 [hep-ph/0307110], and our references therein.
4. R. Alkofer, W. Detmold, C. Fischer, and P. Maris,*Phys.Rev.* **D70** (2004) 014014.
5. Y. Jiang *et al.*, *Phys.Rev.* **C78** (2008) 025214; Y. Jiang *et al.*, *Phys.Rev.* **D78** (2008) 116005.
6. U. Habel, R. Konning, H. Reusch, M. Stingl, and S. Wigard, *Z.Phys.* **A336** (1990) 435–447.
7. U. Habel, R. Konning, H. Reusch, M. Stingl, and S. Wigard, *Z.Phys.* **A336** (1990) 423–433.
8. S. Benić, D. Blaschke and M. Buballa, Phys. Rev. D **86** (2012) 074002.
9. R. Oehme and W. t. Xu, Phys. Lett. B **384** (1996) 269.
10. D. Sutherland, *Phys.Lett.* **23** (1966) 384.
11. J. Bell and D. Sutherland, *Nucl.Phys.* **B4** (1968) 315–325.
12. For analytic, closed form results for the masses and mixing in the η-η' complex, and for our earlier results on the η-η' complex, see [13].
13. S. Benić, D. Horvatić, D. Kekez and D. Klabučar, Phys. Lett. B **738** (2014) 113.
14. S. Benić, D. Horvatić, D. Kekez and D. Klabučar, Phys. Rev. D **84**, 016006 (2011) [arXiv:1105.0356 [hep-ph]], and our references therein.

BLED WORKSHOPS
IN PHYSICS
VOL. 16, NO. 1
p. 20

Proceedings of the Mini-Workshop
Exploring Hadron Resonances
Bled, Slovenia, July 5 - 11, 2015

Comparing mesons and $W_L W_L$ TeV-resonances*

Antonio Dobado[a], Rafael L. Delgado[a], Felipe J. Llanes-Estrada[a] and Domenec Espriu[b]

[a] Dept. Fisica Teorica I, Univ. Complutense, 28040 Madrid, Spain
[b] Institut de Ciencies del Cosmos (ICCUB), Marti Franques 1, 08028 Barcelona, Spain

Abstract. Tantalizing LHC hints suggest that resonances of the Electroweak Symmetry Breaking Sector might exist at the TeV scale. We recall a few key meson-meson resonances in the GeV region that could have high-energy analogues which we compare, as well as the corresponding unitarized effective theories describing them. While detailed dynamics may be different, the constraints of unitarity, causality and global-symmetry breaking, incorporated in the Inverse Amplitude Method, allow to carry some intuition over to the largely unmeasured higher energy domain. If the 2 TeV ATLAS excess advances one such new resonance, this could indicate an anomalous $q\bar{q}W$ coupling.

1 Non-linear EFT for $W_L W_L$ and hh

The Electroweak Symmetry Breaking Sector of the Standard Model (SM) has a low-energy spectrum composed of the longitudinal $W_L^\pm$, Z_L and the Higgs-like h bosons. Various dynamical relations suggest that the longitudinal gauge bosons are a triplet under the custodial $SU(2)_c$, and h is a singlet. This is analogous to hadron physics where pions fall in a triplet and the η meson is a singlet. The global symmetry breaking pattern, $SU(2) \times SU(2) \to SU(2)_c$ is shared between the two fields.

The resulting effective Lagrangian, employing Goldstone bosons $\omega^a \sim W_L$, Z_L as per the Equivalence Theorem (valid for energies sufficiently larger than M_W, M_Z), in the non-linear representation, is [1–3],

$$\begin{aligned}\mathcal{L} = \frac{1}{2}\left[1 + 2a\frac{h}{v} + b\left(\frac{h}{v}\right)^2\right]\partial_\mu\omega^i\partial^\mu\omega^j\left(\delta_{ij} + \frac{\omega^i\omega^j}{v^2}\right) + \frac{1}{2}\partial_\mu h\partial^\mu h \\ + \frac{4a_4}{v^4}\partial_\mu\omega^i\partial_\nu\omega^i\partial^\mu\omega^j\partial^\nu\omega^j + \frac{4a_5}{v^4}\partial_\mu\omega^i\partial^\mu\omega^i\partial_\nu\omega^j\partial^\nu\omega^j + \frac{g}{v^4}(\partial_\mu h\partial^\mu h)^2 \\ + \frac{2d}{v^4}\partial_\mu h\partial^\mu h\partial_\nu\omega^i\partial^\nu\omega^i + \frac{2e}{v^4}\partial_\mu h\partial^\nu h\partial^\mu\omega^i\partial_\nu\omega^i \qquad (1)\end{aligned}$$

This Lagrangian is adequate to explore the energy region 1-3 TeV $\gg$ 100 GeV, and contains seven parameters. Their status is given in [1] and basically amounts to

* Talk delivered by Felipe J. Llanes-Estrada

$a \in (0.88, 1.3)$ (1 in the SM), $b \in (-1, 3)$ (1 in the SM) and the other, NLO parameters (vanishing in the SM) largely unconstrained. This is a reasonably manageable Lagrangian for LHC exploration of electroweak symmetry breaking in the TeV region, before diving into the space of the fully fledged effective theory [3].

Partial wave scattering amplitudes in perturbation theory $A^I_I(s) = A^{(LO)}_{IJ}(s) + A^{(NLO)}_{IJ}(s) \dots$ for $\omega\omega$ and hh, have been reported to NLO in [4]. For example, the LO amplitudes of $I = 0$, 1 and 2, and the $\omega\omega \to hh$ channel-coupling one are

$$A^0_0(s) = \frac{1}{16\pi v^2}(1 - a^2)s \qquad A^1_1(s) = \frac{1}{96\pi v^2}(1 - a^2)s$$
$$A^0_2(s) = -\frac{1}{32\pi v^2}(1 - a^2)s \qquad M^0(s) = \frac{\sqrt{3}}{32\pi v^2}(a^2 - b)s$$

and we see how any small separation of the parameters from the SM value $a^2 = b = 1$ leads to energy growth, and eventually to strong interactions. To NLO, the amplitudes closely resemble those of chiral perturbation theory

$$A^{(LO+NLO)}_{IJ}(s) = Ks + \left(B(\mu) + D \log \frac{s}{\mu^2} + E \log \frac{-s}{\mu^2} \right) s^2 \tag{2}$$

with a left cut carried by the $Ds^2 \log s$ term, a right cut in the $Es^2 \log(-s)$ term, and the $Ks + Bs^2$ tree-level polynomial. B, D and E can be found in [4] and satisfy perturbative renormalizability (in the chiral sense).

2 Resonances

The perturbative amplitudes in Eq. (2) do not make sense for large s (TeV-region) where they violate unitarity $\mathrm{Im}A_{IJ} = |A_{IJ}|^2$, relation satisfied only order by order in perturbation theory, namely $\mathrm{Im}A^{(NLO)}_{IJ} = |A^{(LO)}_{IJ}|^2$.

In hadron physics, the solution is to construct new amplitudes that satisfy unitarity exactly and reproduce the effective theory at low energy (see the lectures [5]) via dispersive analysis. This combination of dispersion relations with effective theory exploits all model-independent information in the two-body experimental data, and is known in both the electroweak symmetry breaking sector and the QCD sector of the Standard Model [7]. A salient example is the NLO Inverse Amplitude Method,

$$A_{IJ} = \frac{\left(A^{(LO)}_{IJ}\right)^2}{A^{(LO)}_{IJ} - A^{(NLO)}_{IJ}} \tag{3}$$

a simple formula that can be rigorously generalized to two channels of massless particles by upgrading the various A to matrices. The denominator of Eq. (3) allows for scattering resonances (poles in the 2nd Riemann sheet).

In meson physics, the most salient elastic resonance of the $\pi\pi$ system is the isovector $\rho(770)$ meson, that dominates low-energy dipion production in most experiments; for example, its prominence in COMPASS data [6] is visible in the

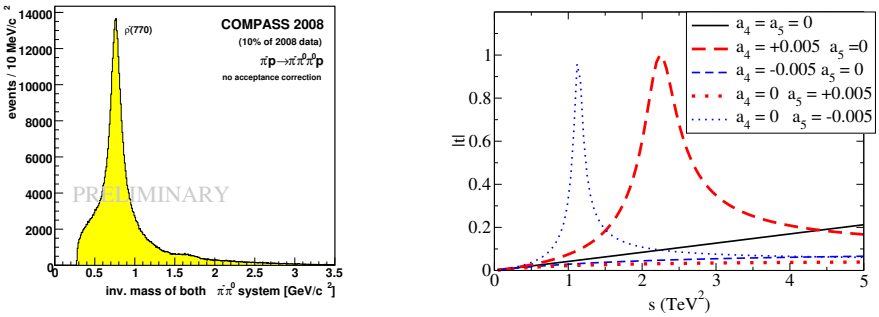

Fig. 1. Left: the physical ρ in the COMPASS ππ spectrum. (Reprinted from [6]. Copyright 2008, AIP Publishing LLC). Right: a possible equivalent *WW*, *WZ* state for various a_4, a_5.

left plot of figure 1. Independently of particular technicolor models, values of a_4 and a_5 at the 10^{-4}-10^{-3} level produce a ρ-like meson of the electroweak sector in the TeV region. The right panel of figure 1 demonstrates this.

The central attraction of the nuclear potential suggested the introduction of a scalar σ meson in the ππ spectrum whose existence was long disputed but that is now well established [8]. In addition to detailed dispersive analysis, it gives strength to the low-energy ππ spectrum if the ρ channel is filtered out by cautious quantum number choice, such as $J/\psi \to \omega\pi\pi$ that forces the pion subsystem to have positive charge conjugation because the other two mesons both have $C = (-1)$. An analysis of BES data by D. Bugg is shown in the left plot of fig. 2. The right plot shows the equivalent resonance in $\omega\omega \sim W_L W_L$, that appears for

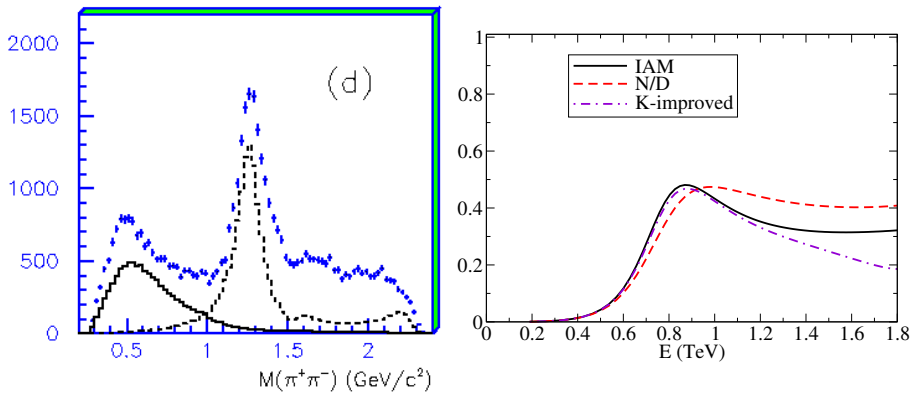

Fig. 2. Left: ππ spectrum with positive charge conjugation clearly showing an enhancement at low invariant mass, related to the $f_0(500)$ (or σ) meson; (Reprinted from [9] with permission. Copyright 2008, AIP Publishing LLC). Right: IJ = 00 ωω scattering in the IAM and other unitarization methods producing an equivalent electroweak resonance.

$a \neq 1$ and/or $b \neq a^2$ (if the resonance is induced by b alone it is a pure coupled channel one [4], that also has analogues in hadron physics, though less straightforward ones).

The same BES data also reveals another salient meson resonance, the $f_2(1270)$. Partial waves with $J = 2$ cannot be treated with the NLO IAM, as $A_0^{2\,LO} = 0$ but a similar structure has been obtained with the N/D or K-matrix unitarization methods, and we show it in figure 3.

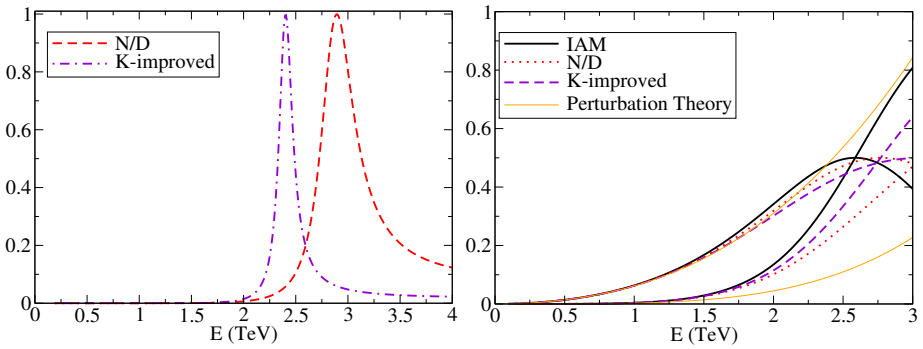

Fig. 3. Left: generating an $IJ = 02$ resonance in the electroweak sector is possible with adequate values of a_4, a_5. Right: positive values of $a^2 - 1$ also generate an isotensor $I = 2$ resonance, though this is more disputed [2]. In hadron physics the isotensor wave is repulsive, and thus, not resonant.

3 ATLAS excess in two-jet events

Renewed interest in TeV-scale resonances is due to a possible excess in ATLAS data [10] plotted in figure 4 together with comparable, older CMS data [11] that does not show such an enhancement. The excess is seen in two-jet events tagged as vector boson pairs by invariant mass reconstruction (82 and 91 GeV respectively). The experimental error makes the identification loose, so that the three-channels cross-feed and we should not take seriously the excess to be seen in all three yet. Because WZ is a charged channel, an $I = 0$ resonance cannot decay there. Likewise ZZ cannot come from an $I = 1$ resonance because the corresponding Clebsch-Gordan coefficient $\langle 1010|10\rangle$ vanishes. A combination of both $I = 0, 1$ could explain all three signals simultaneously (as would also an isotensor $I = 2$ resonance).

A relevant relation imported from hadron physics that the IAM naturally incorporates restricts the width of a vector boson. This one-channel KSFR relation [12] links the mass and width of the vector resonance with the low-energy constants v and a in a quite striking manner,

$$\Gamma^{IAM} = \frac{M^3_{IAM}}{96\pi v^2}(1 - a^2)\,. \tag{4}$$

For $M \sim 2$ TeV and $\Gamma \sim 0.2$ TeV (see fig. 4), we get $a \sim 0.73$ which is in tension with the ATLAS-deduced bound $a|_{2\sigma} > 0.88$ at 4-5σ level; Eq. (4) predicts that a 2 TeV $J = 1$ resonance, with current low-energy constants, needs to have $\Gamma < 50$ GeV, a fact confirmed by more detailed calculations [1,2]. However scalar resonances tend to be substantially broader.

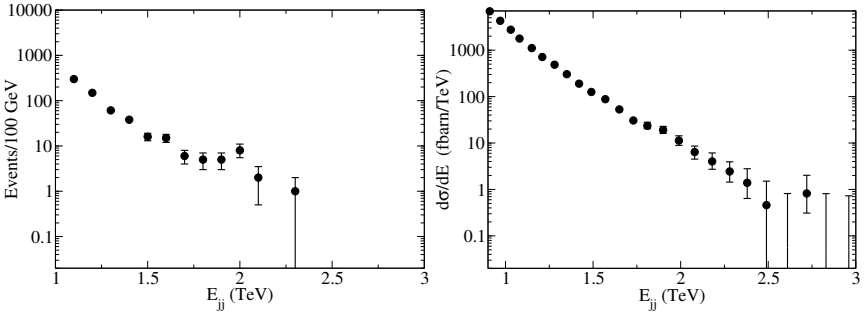

Fig. 4. Left: replot of the ATLAS data [10] for $WZ \to 2$ jet, with a slight excess at 2 TeV (also visible in the other isospin combinations WW and ZZ, not shown). The jet analysis is under intense scrutiny [15]. Right: equivalent CMS data [11] with vector-boson originating jets. No excess is visible at 2 TeV (though perhaps some near 1.8-1.9 TeV).

The cross section for the reaction $pp \to W^+Z+X$ for a given WZ Mandelstam s, and with the E^2 total energy in the proton-proton cm frame, can be written [13] in standard LO QCD factorization as

$$\frac{d\sigma}{ds} = \int_0^1 dx_u \int_0^1 dx_{\bar{d}} \delta(s - x_u x_{\bar{d}} E_{tot}^2 f(x_u) f(x_{\bar{d}}) \hat{\sigma}(u\bar{d} \to \omega^+ z) \,. \tag{5}$$

The parton-level cross section $\hat{\sigma}$ is calculated, with the help of the factorization theorem, from the effective Lagrangian in Eq. (1) above. Following [13], we would

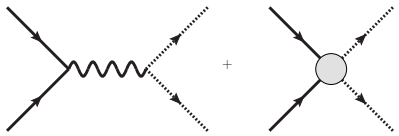

Fig. 5. Production of a pair of Goldstone bosons by $u\bar{d}$ annihilation through a W-meson and anomalous BSM vertex enhancing it.

expect an amplitude (from the left diagram of figure 5) given by $\mathcal{M} = \bar{u}\gamma^\mu_L v(-ig/\sqrt{8})^2(i/q^2)(k_1 - k_2)_\mu$ in perturbation theory. Further, dispersive analysis reveals the need of a vector form factor in the presence of strong final state rescattering, to guarantee Watson's final state theorem; the phase of the production amplitude must be equal to that of the elastic $\omega\omega$ scattering amplitude. If the later is represented by the Inverse Amplitude Method, the form factor in the $W\omega\omega$ vertex is $F_V(s) = \left[1 - \frac{A_{11}^{(1)}(s)}{A_{11}^{(0)}(s)}\right]^{-1}$. The resulting cross section [13] was found to be slightly below the CMS bound, and perhaps insufficient to explain

the possible ATLAS excess. With current precision this statement should not be taken to earnestly, but it is nonetheless not too soon to ask ourselves what would happen in the presence of additional non-SM fermion couplings.

Thus, an original contribution of this note is to add to Eq. (1) a term [1]

$$\mathcal{L}_{\text{fermion anomalous}} = \frac{\delta_1}{v^2}\bar{\psi}_L \omega \not{\partial}\omega\psi_L \tag{6}$$

(for a derivation see, e.g. [14]). The parton level cross-section is then

$$\left[\frac{d\hat{\sigma}}{d\Omega}\right]_{cm} = \frac{1}{64\pi^2 s}\frac{g^4}{32}\sin^2\theta\left(1+\frac{\delta_1 s}{v^2}\right)^2 |F_V(s)|^2\,, \tag{7}$$

and if $\delta_1 \neq 0$ additional production strength appears in the TeV region. The sign of this δ_1 might be determined from the line shape due to interference with the background [16].

4 Conclusion

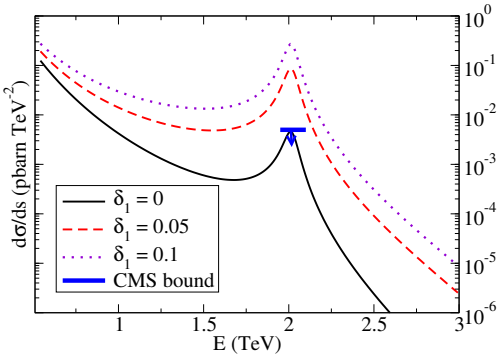

Fig. 6. Tree-level W production of $\omega\omega$ [13] with final-state resonance; non-zero parameters are a=0.9, b=a^2, $a_4 = 7\times10^{-4}$ (at $\mu = 3$ TeV). Also shown is a CMS cross-section upper bound (see fig. 4). This can be exceeded with the δ_1 coupling of Eq. (6).

The 13 TeV LHC run II entails larger cross sections and allows addressing the typical σ, ρ-like $\omega\omega$ resonances, at the edge of the run I sensitivity limit as shown in fig. 6. The large rate at which such a resonance would have to be produced to explain the ATLAS excess (at the 10fbarn level [17]) is a bit puzzling, though it can be incorporated theoretically with the δ_1 parameter. Hopefully this ATLAS excess will soon be refuted or confirmed. In any case, the combination of effective theory and unitarity that the IAM encodes is a powerful tool to describe data up to $E = 3$ TeV in the electroweak sector if new, strongly interacting phenomena

[1] This is only one of the possible additional operators. There is a second one with R fields, and several custodially breaking others. The gauge-invariant version of Eq. (6) actually modifies the fermion-gauge coupling by a factor $(1+\delta_1)$: this cannot be excluded because it would be the quantity that is actually well measured in β decay. The triple gauge boson vertex would then need not coincide with this coupling. However the latter is much less precisely known and there is room for deviations at the 5-10% level.

appear, with only few independent parameters. The content of new, Beyond the Standard Model theories, can then be matched onto those parameters for quick tests of their phenomenological viability.

Acknowledgements

FLE thanks the organizers of the Bled workshop "Exploring hadron resonances" for hospitality and encouragement. Work supported by Spanish Excellence Network on Hadronic Physics FIS2014-57026-REDT, and grants UCM:910309, MINECO:FPA2014-53375-C2-1-P, FPA2013-46570, 2014-SGR-104, MDM-2014-0369; its completion was possible at the Institute for Nuclear Theory of the Univ. of Washington, Seattle, with DOE support.

References

1. R.L.Delgado, A.Dobado and F.J.Llanes-Estrada, J. Phys. G **41**, 025002 (2014); *ibid*, JHEP **1402**, 121 (2014); R.L.Delgado, A.Dobado, M.J.Herrero and J.J.Sanz-Cillero, JHEP **1407**, 149 (2014).
2. P. Arnan, D. Espriu and F. Mescia, arXiv:1508.00174 [hep-ph]. D. Espriu and F. Mescia, Phys. Rev. D **90**, 015035 (2014). D. Espriu, F. Mescia and B. Yencho, Phys. Rev. D **88**, 055002 (2013). D. Espriu and B. Yencho, Phys. Rev. D **87**, no. 5, 055017 (2013).
3. R. Alonso *et al.*, JHEP **1412**, 034 (2014); G.Buchalla, O.Cata, A.Celis and C.Krause, arXiv:1504.01707 [hep-ph].
4. R. L. Delgado, A. Dobado and F. J. Llanes-Estrada, Phys. Rev. Lett. **114**, 221803 (2015).
5. T. N. Truong, EFI-90-26-CHICAGO, EP-CPT-A965-0490, UCSBTH-90-29, C90-01-25.
6. F. Nerling [COMPASS Collaboration], AIP Conf. Proc. **1257**, 286 (2010) [arXiv:1007.2951 [hep-ex]].
7. A. Dobado, M. J. Herrero and T. N. Truong, Phys. Lett. B **235**, 129 (1990); A. Dobado and J. R. Pelaez, Nucl. Phys. B **425**, 110 (1994) [Nucl. Phys. B **434**, 475 (1995)] [hep-ph/9401202].
8. J. R. Pelaez, Phys. Rept.(in press) arXiv:1510.00653 [hep-ph].
9. D. V. Bugg, AIP Conf.Proc.**1030**,3 (2008) [arXiv:0804.3450 hep-ph].
10. G. Aad *et al.* [ATLAS Collaboration], arXiv:1506.00962 [hep-ex].
11. V. Khachatryan *et al.* [CMS Collaboration], JHEP **1408**, 173 (2014).
12. R. L. Delgado, A. Dobado and F. J. Llanes-Estrada, Phys. Rev. D **91**, 075017 (2015).
13. A. Dobado, F. K. Guo and F. J. Llanes-Estrada, Commun. Theor. Phys. (in press), arXiv:1508.03544 [hep-ph].
14. E. Bagan, D. Espriu and J. Manzano, Phys. Rev. D **60**, 114035 (1999).
15. D. Goncalves, F. Krauss, M. Spannowsky, arXiv:1508.04162 [hep-ph].
16. C. H. Chen and T. Nomura, arXiv:1509.02039 [hep-ph].
17. ATLAS contribution to the 3rd Annual LHC Physics Conference, St. Petersburg, 31/8 to 5/9 2015, ATLAS-CONF-2015-045.

Bled Workshops
in Physics
Vol. 16, No. 1
p. 27

Proceedings of the Mini-Workshop
Exploring Hadron Resonances
Bled, Slovenia, July 5 - 11, 2015

Resonances in the Constituent-Quark Model*

R. Kleinhappel and W. Plessas

Theoretical Physics, Institute of Physics, University of Graz, A-8010 Graz, Austria

Abstract. We give a short account of the present description of baryon resonances within the relativistic constituent-quark model, where resonances are usually treated as excited bound states, and point to ways for a more realistic theory producing the resonances as complex poles in the momentum/energy planes, i.e. with real mass values and finite widths.

Nowadays the relativistic constituent-quark model, especially the one relying on a dynamics of linear confinement and a hyperfine interaction of Goldstone-boson exchange [1, 2], can provide a reasonable description of the baryon spectra (see, e.g., the recent review in ref. [3]. It is even possible to reproduce - with only a few exceptions - the real mass values of all known baryon ground and resonant states with flavors u, d, s, c, and b in a universal framework in close agreement with phenomenology or data from lattice chromodynamics (QCD) [4–7]. Herein baryons are considered as relativistic bound states of three confined constituent quarks Q interacting mutually. The Q's are supposed to be quasi-particles with dynamical masses generated by the spontaneous breaking of chiral symmetry (SBχS) of low-energy QCD [8, 9]. The most important ingredients in the three-Q invariant mass operator turn out to be SBχS and relativistic invariance [10].

Solving the three-Q mass-operator eigenvalue problem provides also access to the baryon eigenfunctions (see, e.g., their rest-frame spatial representations in ref. [12]). They can be subject to tests in various baryon reactions. While their structures appear to be quite reasonable for the baryon ground states, the resonance wave functions are obviously affected by shortcomings.

In particular, the electromagnetic form factors of the nucleons as well as their electric radii and magnetic moments are reproduced in good agreement with phenomenology [13], even with regard to their flavor contents [14]. Similarly, the electromagnetic form factors, electric radii, and magnetic moments of the Δ and hyperon ground states are found well compatible with available data from experiment and lattice QCD [15, 16]. The same is true with regard to the axial form factors and axial charges [16–18]. Likewise, the gravitational form factor $A(Q^2)$ of the nucleons is reasonably reproduced [3]. In addition, for the strong form factors of the πNN and πNΔ a microscopic explanation is provided that conforms with the ones usually adopted in πN and $\pi\Delta$ dynamical models [19].

* Talk delivered by by W. Plessas

Disturbing shortcomings of the three-Q constituent-quark model appear with regard to direct predictions for hadronic decays of the π, η, and K meson modes. First fully relativistic results in general show an undershooting of the experimental decay widths [12, 20–22]. This hints to missing ingredients in the adopted approach. The problems may either be connected with an improper treatment of the meson-decay vertex or missing degrees of freedom from the decay channels.

In order to remedy the situation we have recently adhered to a coupled-channels formalism, taking into account mesonic decays channels explicitly. First attempts along a toy model for mesons yielded promising results [23]. At least it could be shown, how finite resonance widths well develop in such an approach.

Further studies concerned explicit pionic effects both on the ground state and resonance masses (including the resonance widths), exemplified for the nucleon and the Δ. Details of the formalism and first results were presented at previous Bled Workshops [24–26]. While the pionic effects on the nucleon mass appear reasonable, the analogous treatment of the Δ does not yet enhance especially its π-decay width enough in order to make it compatible with the relatively large phenomenological value [26]. Further ingredients appear to be necessary. We are presently in the course of extending the coupled-channels theory accordingly.

Acknowledgment

The authors are grateful to Bojan Golli, Mitja Rosina, and Simon Sirca for their continuous efforts of organizing every year the Bled Mini-Workshops. These meetings serve as a valuable institution of exchanging ideas and of mutual learning among an ever growing community of participating colleagues engaged in hadronic physics.

This work was supported by the Austrian Science Fund, FWF, through the Doctoral Program on *Hadrons in Vacuum, Nuclei, and Stars* (FWF DK W1203-N16).

References

1. L. Y. Glozman, W. Plessas, K. Varga and R. F. Wagenbrunn, Phys. Rev. D **58**, 094030 (1998)
2. L. Y. Glozman, Z. Papp, W. Plessas, K. Varga and R. F. Wagenbrunn, Phys. Rev. C **57**, 3406 (1998)
3. W. Plessas, Int. J. Mod. Phys. A **30**, no. 02, 1530013 (2015)
4. J. P. Day, W. Plessas, and K. S. Choi, arXiv:1205.6918 [hep-ph]
5. J. P. Day, K. S. Choi, and W. Plessas, Few-Body Syst. **54**, 329 (2013)
6. J. P. Day, W. Plessas, and K. S. Choi, in: *Looking into Hadrons* (Proceedings of the Mini-Workshop, Bled, Slovenia, 2013), ed. by B. Golli, M. Rosina, and S. Sirca. DMFA, Ljubljana (2013); p. 6
7. J. P. Day, PhD Thesis, University of Graz (2013)
8. W. Plessas, in: *Quark Masses and Hadron Spectra* (Proceedings of the Mini-Workshop, Bled, Slovenia, 2014), ed. by B. Golli, M. Rosina, and S. Sirca. DMFA, Ljubljana (2014); p. 34

9. M. Rosina, in: *Quark Masses and Hadron Spectra* (Proceedings of the Mini-Workshop, Bled, Slovenia, 2014), ed. by B. Golli, M. Rosina, and S. Sirca. DMFA, Ljubljana (2014); p. 50
10. W. Plessas, Mod. Phys. Lett. A **28**, no. 26, 1360022 (2013)
11. W. Plessas, PoS LC **2010**, 017 (2010); arXiv:1011.0156 [hep-ph]
12. T. Melde, W. Plessas and B. Sengl, Phys. Rev. D **77**, 114002 (2008)
13. R. F. Wagenbrunn, S. Boffi, W. Klink, W. Plessas, and M. Radici, Phys. Lett. B **511**, 33 (2001)
14. M. Rohrmoser, K. S. Choi, and W. Plessas, Acta Phys. Polon. Supp. **6**, 371 (2013)
15. K. Berger, R. F. Wagenbrunn, and W. Plessas, Phys. Rev. D **70**, 094027 (2004)
16. K. S. Choi and W. Plessas, Few-Body Syst. **54**, 1055 (2013)
17. L. Y. Glozman, M. Radici, R. F. Wagenbrunn, S. Boffi, W. Klink, and W. Plessas, Phys. Lett. B **516**, 183 (2001)
18. S. Boffi, L. Y. Glozman, W. Klink, W. Plessas, M. Radici, and R. F. Wagenbrunn, Eur. Phys. J. A **14**, 17 (2002)
19. T. Melde, L. Canton, and W. Plessas, Phys. Rev. Lett. **102**, 132002 (2009)
20. T. Melde, W. Plessas, and R. F. Wagenbrunn, Phys. Rev. C **72**, 015207 (2005); ibid. C **74**, 069901 (2006)
21. B. Sengl, T. Melde, and W. Plessas, Phys. Rev. D **76**, 054008 (2007)
22. T. Melde, W. Plessas, and B. Sengl, Phys. Rev. C **76**, 025204 (2007)
23. R. Kleinhappel, W. Plessas, and W. Schweiger, Few-Body Syst. **54**, 339 (2013)
24. R. Kleinhappel, W. Plessas, and W. Schweiger, in: *Understanding Hadron Spectra* (Proceedings of the Mini-Workshop, Bled, Slovenia, 2011), ed. by B. Golli, M. Rosina, and S. Sirca. DMFA, Ljubljana (2011); p. 36
25. R. Kleinhappel, W. Plessas, and W. Schweiger, in: *Hadronic Resonances* (Proceedings of the Mini-Workshop, Bled, Slovenia, 2012), ed. by B. Golli, M. Rosina, and S. Sirca. DMFA, Ljubljana (2012); p. 20
26. R. Kleinhappel, L. Canton, W. Plessas, and W. Schweiger, in: *Quark Masses and Hadron Spectra* (Proceedings of the Mini-Workshop, Bled, Slovenia, 2014), ed. by B. Golli, M. Rosina, and S. Sirca. DMFA, Ljubljana (2014); p. 22

BLED WORKSHOPS
IN PHYSICS
VOL. 16, NO. 1
p. 30

Proceedings of the Mini-Workshop
Exploring Hadron Resonances
Bled, Slovenia, July 5 - 11, 2015

Unquenched quark-model calculation of excited ρ resonances and P-wave ππ phase shifts*

Susana Coito[a], George Rupp[b], Eef van Beveren[c]

[a]Institute of Modern Physics, CAS, Lanzhou 730000, China
[b]CeFEMA, Instituto Superior Técnico, Universidade de Lisboa, 1049-001 Lisboa, Portugal
[c]Centro de Física Computacional, Departamento de Física, Universidade de Coimbra, 3004-516 Coimbra, Portugal

Abstract. The ρ(770) vector resonance, its radial recurrences, and the corresponding P-wave ππ phase shifts are investigated in an unquenched quark model with all classes of relevant decay channels included, viz. pseudoscalar-pseudoscalar, vector-pseudoscalar, vector-vector, vector-scalar, axialvector-pseudoscalar, and axialvector-vector, totalling 26 channels. Two of the few model parameters are fixed at previously used values, whereas the other three are adjusted to the ρ(770) resonance and the lower P-wave ππ phases. Preliminary results indicate the model's capacity to reproduce these phases as well as the ρ mass and width. However, at higher energies the phase shifts tend to rise too sharply. A possible remedy is an extension of the model so as to handle resonances in the final states for most of the included decay channels. Work in progress.

1 Introduction

The radial recurrences of the ρ(770) vector resonance play a crucial role in light-meson spectroscopy, owing to the several observed states in the PDG tables [1], up to 1.9 GeV, and the corresponding P-wave pion-pion phase shifts and inelasticities measured in several experiments [1]. These resonances may shed a lot of light on the underlying quark-confinement force as well as the strong-decay mecanism, both assumed to result from low-energy QCD. However, there are two serious problems, one experimental and the other theoretical. First of all, excited ρ states listed in the PDG tables are far from well established, even the generally undisputed ρ(1450) [1] resonance. For example, under the entry of the latter state in the PDG meson listings, experimental observations have been collected with masses in the range 1250–1582 MeV. The state of lowest mass here corresponds to the $\omega\pi^0$ resonance at 1.25 GeV first observed by Aston *et al.* in 1980 [2]. Several other experiments have confirmed such a vector ρ′ resonance in the mass interval 1.25–1.3 GeV, both in the $\omega\pi^0$ [3] and ππ [4] channels. More recently, a combined $\mathcal{S}$-matrix and Breit-Wigner (BW) analysis [5], using P-wave ππ data from the early 1970s, not only confirmed a ρ(1250), but even found it to be much

* Talk delivered by George Rupp

more important for a good fit to the data than the $\rho(1450)$. In view of these findings, it is simply inconceivable that no separate $\rho(1250)$ entry has been created in the PDG tables, and to make things worse, the latter analysis [5] is not even included in the PDG references. The reason for these omissions seems to be based on theory bias, which is the second problem. Indeed, the renowned relativised quark model for mesons by Godfrey & Isgur [6] predicted the first radial ρ excitation at 1.45 GeV. As a matter of fact, practically all quark models employing the usual Coulomb-plus-linear confining potential find a ρ' at about the same mass and cannot accommodate a $\rho(1250)$ (see, however, Ref. [7]).

Unfortunately, no fully unquenched lattice calculations including both $q\bar{q}$ and two-meson interpolating fields have been carried out so far beyond the ground-state $\rho(770)$ [8]. Nevertheless, in the strange-meson sector such a calculation was done recently [9], reproducing the $K^\star(892)$ resonance in P-wave elastic $K\pi$ scattering, with mass and width close to the experimental values. Moreover, the first radial excitation was identified as well, tentatively at 1.33 GeV, which should correspond to the $K^\star(1410)$ [1] resonance. The latter is thus determined on the lattice to be a normal quark-antiquark resonance. From simple quark-mass considerations, one is led to conclude the same for the ρ' originally found by Aston *et al.* [2] at 1.25 GeV, which contradicts the speculation in Ref. [10] that it *"has necessarily to be an exotic"*. Note that including meson-meson interpolators is absolutely crucial to reliably predict the mass of an excited resonance like the $K^{\star\prime}$, since an also unquenched lattice calculation without considering decay, by partly the same authors [11], predicted a $K^{\star\prime}$ mass a full 300 MeV heavier than in Ref. [9].

In the present work, we analyse the issue of radial ρ recurrences by attempting to describe the elastic and inelastic P-wave $\pi\pi$ phase shifts in the context of an unquenched quark model that has been successfully applied to several problematic mesons (see e.g. Ref. [12] for a very brief recent review). In this so-called Resonance-Spectrum-Expansion (RSE) model, the manifest non-perturbative inclusion of all relevant two-meson channels alongside a confined $q\bar{q}$ sector allows for a phenomenlogical decription of excited meson resonances in the same spirit as the referred lattice calculation [9]. An additional advantage is that the RSE model yields an exactly unitary and analytic $\mathcal{S}$-matrix for any number of included quark-antiquark and two-meson channels, whereas the lattice still faces serious problems in the case of inelastic resonances and highly excited states.

2 RSE modelling of P-wave $\pi\pi$ scattering

The general expressions for the RSE off-energy-shell $\mathcal{T}$-matrix and corresponding on-shell $\mathcal{S}$-matrix have been given in several papers (see e.g. Ref. [13]). In the present case of P-wave $\pi\pi$ scattering, the quantum numbers of the system are $I^G J^{PC} = 1^+ 1^{--}$, which couples to the $I=1$ quark-antiquark state $(u\bar{u}-d\bar{d})/\sqrt{2}$ in the spectroscopic channels $^3S_1$ and $^3D_1$. In the meson-meson sector, we only consider channels allowed by total angular momentum J, isospin I, parity P, and G-parity G. The included combinations are pseudoscalar–pseudoscalar (PP), vector-pseudoscalar (VP), vector-vector (VV), vector-scalar (VS), axialvector-pseudoscalar (AP), and axialvector-vector (AV), with mesons from the lowest-lying pseudoscalar,

vector, scalar, and axialvector nonets listed in the PDG [1] tables. Here, "axialvector" may refer to $J^{PC} = 1^{++}$, $J^{PC} = 1^{+-}$, or $J^{P} = 1^{+}$ for mesons with no definite C-parity. This choice of meson-meson channels is motivated by the observed two- and multi-particle decays of the ρ recurrences up to the $\rho(1900)$ [1], which include several intermediate states containing resonances from the referred nonets. For instance, the PDG lists [1] under the 4π decays of the $\rho(1450)$ the modes $\omega\pi$, $a_1(1260)\pi$, $h_1(1170)\pi$, $\pi(1300)\pi$, $\rho\rho$, and $\rho(\pi\pi)_{\text{S-wave}}$, where $(\pi\pi)_{\text{S-wave}}$ is probably dominated by the $f_0(500)$ [1] scalar resonance. By the same token, the 6π decays of the $\rho(1900)$ will most likely include important contributions from modes as $b_1(1235)\rho$, $a_1(1260)\omega$, ... For consistency of our calculation, we generally include complete nonets in the allowed decays, and not just individual modes observed in experiment. The only exception is the important $\pi(1300)\pi$ P′P mode, because no complete nonet of radially excited pseudoscalar mesons has been observed so far [1]. The included 26 meson-meson channels are given in Table 1.

Nonets	Two-Meson Channels	L
PP	$\pi\pi$, KK	1
VP	$\omega\pi$, $\rho\eta$, $\rho\eta'$, K^*K	1
VV	$\rho\rho$, K^*K^*	1
VS	$\rho f_0(500)$, $\omega a_0(980)$, $K^*K_0^*(800)$	0, 2
AP	$a_1(1260)\pi$, $b_1(1235)\eta$, $b_1(1235)\eta'$, $h_1(1170)\pi$, $K_1(1270)K$, $K_1(1400)K$	0
AV	$a_1(1260)\omega$, $b_1(1235)\rho$, $f_1(1285)\rho$, $K_1(1270)K^*$, $K_1(1400)K^*$	0
P′P	$\pi(1300)\pi$	1

Table 1. Included classes of decay channels containing mesons listed [1] in the PDG tables, with the respective orbital angular momenta. Note that the included P′P decay mode is incomplete (see text above).

Notice that the VS channels count twice, because they can have L=0 or L=2. However, the S-wave only couples to the $^3S_1$ $q\bar{q}$ channel and the D-wave only to the $^3D_1$. The relative couplings between the $q\bar{q}$ and meson-meson channels are determined using the scheme of Ref. [14], based on overlaps of harmonic-oscillator (HO) wave functions. Special care is due in the cases of flavour mixing (η, η'), and mixing of the C-parity eigenstates $^3P_1$ and $^1P_1$ [13], as the strange axialvector mesons $K_1(1270)$ and $K_1(1400)$ have no definite C-parity.

Coming now to describing the data, we have to adjust the model parameters. Two of these, namely the non-strange constituent quark mass and the HO oscillator frequency, are as always fixed [13] at the values $m_n = m_u = m_d = 406\,\text{MeV}$ and $\omega = 190$ MeV. This yields a largely degenerate bare ρ spectrum with energy levels 1097 MeV ($1\,^3S_1$), 1477 MeV ($2\,^3S_1/1\,^3D_1$), 1857 MeV ($3\,^3S_1/2\,^3D_1$), 2237 MeV ($4\,^3S_1/3\,^3D_1$), ... This bare spectrum is then deformed upon unquenching, that is, by allowing $q\bar{q}$ pair creation. This results in real or complex mass shifts due to meson-loop contributions, depending on decay channels being closed or open, respectively. Note that these shifts are non-perturbative and can

only be determined, for realistic coupling strengths, by numerically finding the poles of the $\mathcal{S}$-matrix. The adjustable parameters are the overall dimensionless coupling constant λ, the "string-breaking" radius r_0 for transitions between the $q\bar{q}$ and two-meson channels, and a range parameter α for weakening subthreshold contributions via a form factor. The coupling λ is usually in the range 3–5, r_0 should be of the order of 1 fm for systems made of light quarks (with mass m_n), and the α value used in several previous papers is 4 GeV^{-2} (see e.g. Ref. [15]).

In view of these strong limitations, it is quite remarkable that we can obtain a good fit to the P-wave $\pi\pi$ phase shifts up to 1.2 GeV with the choice $\lambda = 5.3$, $r_0 = 0.9$ fm, and $\alpha = 4$ GeV^{-2}. Moreover, the corresponding $\rho(770)$ pole comes out at the very reasonable energy $E = (754 - i67)$ MeV. At higher energies, though, the $\pi\pi$ phases tend to rise too fast and no good description has been obtained so far, also due to the very little fitting freedom. As for the poles of the higher ρ recurrences, we find at least four in the energy range 1.2–2.0 GeV, in agreement with the PDG [1] and also Ref. [5], albeit at yet quite different energies. In particular, there are two poles between 1.2 and 1.5 GeV, in qualitative agreement with Ref. [5]. However, these pole positions are extremely sensitive to the precise values of the parameteres λ, r_0, and α, so that they should not be taken at face value as long as no good fit is achieved of the observables above 1.2 GeV.

A possibility to improve the fit is by allowing different decay radii for the several classes of decay channels (PP, VP, VV, VS, AP, AV, P′P), which would be logical in view of the detailed, channel-dependent transition potentials derived in Ref. [14]. Such an additional flexibility will neither affect the exact solvability of the RSE $\mathcal{T}$-matrix, nor its analyticity.

An addditional possible model extension we shall discuss in the next section.

3 Resonances in asymptotic states

The decay channels listed in Table 1 contain several resonances, some of which are even extremely broad, with widths exceeding 300 MeV. So treating the corresponding thresholds as being sharp, at well-defined real energies, is certainly an approximation, which may produce too sudden effects at threshold openings. Ideally, one would like to describe a resonance in the final state via a smooth function of real energy, corresponding to an experimental cross section in which the resonance is observed. By discretising such a function, one could in principle describe each final-state resonance through a large number of effective thresholds. However, this would lead to a proliferation of channels and to a true explosion of Riemann sheets, making the tracing of complex poles impracticable.

An alternative way to handle a resonance in asymptotic states is to replace its real mass by a complex one, on the basis of the PDG [1] resonance mass and total width. However, this inevitably destroys unitarity of the $\mathcal{S}$-matrix. Nevertheless, its symmetry will be unaffected, which can be used to define a new matrix that is unitary again, and so take over the role of $\mathcal{S}$. Here, we closely follow the derivation given in Ref. [16].

An arbitrary symmetric matrix $\mathcal{S}$ can be decomposed, via Takagi [17] factorisation, as

$$\mathcal{S} \;=\; V D V^{\mathsf{T}} \,, \tag{1}$$

where V is unitary and D is a real non-negative diagonal matrix. Then we get

$$\mathcal{S}^\dagger \mathcal{S} = (V^{\mathsf{T}})^\dagger D V^\dagger V D V^{\mathsf{T}} = (V^{\mathsf{T}})^\dagger D^2 V^{\mathsf{T}} = U^\dagger D^2 U, \tag{2}$$

where we have defined $U \equiv V^{\mathsf{T}}$, which is obviously unitary, too. So the diagonal elements of $D = \sqrt{U \mathcal{S}^\dagger \mathcal{S} U^\dagger}$ are the square roots of the eigenvalues of the positive Hermitian matrix $\mathcal{S}^\dagger \mathcal{S}$, which are all real and non-negative. Moreover, since $\mathcal{S} = \mathbf{1} + 2i\mathcal{T}$ is manifestly non-singular, the eigenvalues of $\mathcal{S}^\dagger \mathcal{S}$ are even all non-zero and U is unique. Thus, we may define

$$\mathcal{S}' \;\equiv\; \mathcal{S} U^\dagger D^{-1} U \,. \tag{3}$$

Then, using Eq. (1) and $V = U^{\mathsf{T}}$, we have

$$\mathcal{S}' \;=\; U^{\mathsf{T}} D U U^\dagger D^{-1} U \;=\; U^{\mathsf{T}} U \,, \tag{4}$$

which is obviously symmetric. But it is also unitary, as

$$(U^{\mathsf{T}} U)^\dagger = U^\dagger (U^\dagger)^{\mathsf{T}} = U^{-1} (U^{-1})^{\mathsf{T}} = (U^{\mathsf{T}} U)^{-1} \,. \tag{5}$$

So $\mathcal{S}'$ has the required properties to be defined as the scattering matrix for a process with complex masses in the asymptotic states. Note that this empirical method has been applied very successfully to the enigmatic $X(3872)$ charmonium state in Ref. [16].

4 Conclusions

We have presented preliminary results of an unquenched quark-model study aimed at determining the complex pole positions of vector ρ recurrences up to 2 GeV, motivated by the poor status of these resonances in the PDG tables [1] and their importance for light-meson spectroscopy. The employed RSE model was applied in the past to a variety of problematic mesons, with very good results [12]. The here included classes of meson-meson channels cover most of the observed strong decays. The three adjustable model parameters were fitted to the P-wave $\pi\pi$ phase shifts up to about 1.2 GeV, allowing a good reproduction of these data and a very reasonable $\rho(770)$ resonance pole position.

However, at energies above 1.2 GeV the thus calculated phases rise too fast, and a globally good fit including the higher $\pi\pi$ phases is not feasible with only three parameters. A possible model extension amounts to allowing different decay radii for the different classes of meson-meson channels, which will not spoil the nice model features. Another extension to be considered is the use of complex physical masses for the final-state resonances in nearly all channels of Table 1. This will require a redefinition of the $\mathcal{S}$-matrix so as to restore manifest unitarity, which can be done with an empirical algebraic procedure, exploiting the symmetry of $\mathcal{S}$.

All this work is in progress.

References

1. K. A. Olive *et al.* [Particle Data Group Collaboration], Chin. Phys. C **38** (2014) 090001.
2. D. Aston *et al.* [Bonn-CERN-Ecole Poly-Glasgow-Lancaster-Manchester-Orsay-Paris-Rutherford-Sheffield Collaboration], Phys. Lett. B **92** (1980) 211 [Erratum ibid. **95** (1980) 461].
3. D. P. Barber *et al.* [LAMP2 Group Collaboration], Z. Phys. C **4** (1980) 169.
4. L. M. Kurdadze *et al.*, JETP Lett. **37** (1983) 733 [Pisma Zh. Eksp. Teor. Fiz. **37** (1983) 613]; S. Dubnicka and L. Martinovic, J. Phys. G **15** (1989) 1349; D. Aston *et al.*, Nucl. Phys. Proc. Suppl. **21** (1991) 105; A. Bertin *et al.* [OBELIX Collaboration], Phys. Lett. B **414** (1997) 220.
5. Y. S. Surovtsev and P. Bydzovsky, Nucl. Phys. A **807** (2008) 145.
6. S. Godfrey and N. Isgur, Phys. Rev. D **32** (1985) 189.
7. E. van Beveren, G. Rupp, T. A. Rijken, and C. Dullemond, Phys. Rev. D **27** (1983) 1527.
8. C. B. Lang, D. Mohler, S. Prelovsek, and M. Vidmar, Phys. Rev. D **84** (2011) 054503 [Erratum ibid. **89** (2014) 059903] [arXiv:1105.5636 [hep-lat]].
9. S. Prelovsek, L. Leskovec, C. B. Lang, and D. Mohler, Phys. Rev. D **88** (2013) 5, 054508 [arXiv:1307.0736 [hep-lat]].
10. A. Donnachie, Y. S. Kalashnikova, and A. B. Clegg, Z. Phys. C **60** (1993) 187.
11. G. P. Engel, C. B. Lang, D. Mohler, and A. Schäfer, PoS Hadron **2013** (2013) 118 [arXiv:1311.6579 [hep-ph]].
12. G. Rupp, E. van Beveren, and S. Coito, Acta Phys. Polon. Supp. **8** (2015) 139 [arXiv:1502.05250 [hep-ph]].
13. S. Coito, G. Rupp, and E. van Beveren, Phys. Rev. D **84** (2011) 094020 [arXiv:1106.2760 [hep-ph]].
14. E. van Beveren, Z. Phys. C **21** (1984) 291 [hep-ph/0602246].
15. S. Coito, G. Rupp, and E. van Beveren, Phys. Rev. D **80** (2009) 094011 [arXiv:0909.0051 [hep-ph]].
16. S. Coito, G. Rupp, and E. van Beveren, Eur. Phys. J. C **71** (2011) 1762 [arXiv:1008.5100 [hep-ph]].
17. T. Takagi, Japan J. Math. **1** (1924) 82.

BLED WORKSHOPS
IN PHYSICS
VOL. 16, NO. 1
p. 36

Proceedings of the Mini-Workshop
Exploring Hadron Resonances
Bled, Slovenia, July 5 - 11, 2015

The pion-cloud contribution to the electromagnetic nucleon structure*

D. Kupelwieser and W. Schweiger

Institute of Physics, University of Graz, A-8010 Graz, Austria

Abstract. The present contribution continues and extends foregoing work on the calculation of electroweak form factors of hadrons using the point-form of relativistic quantum mechanics. Here we are particularly interested in studying pionic effects on the electromagnetic structure of the nucleon. To this aim we employ a hybrid constituent-quark model that comprises, in addition to the 3q valence component, also a 3q+π non-valence component. With a simple wave function for the 3q component we get reasonable results for the nucleon form factors. In accordance with other authors we find that the pionic effect is significant only below $Q^2 \lesssim 0.5$ GeV^2.

In a series of papers [1–4] we have developed and advocated a method for the calculation of the electroweak structure of few-body bound states that is based on the point form of relativistic quantum mechanics. All types of interactions are introduced in a Poincaré-invariant way via the Bakamjian-Thomas construction [5]. Our strategy is then to determine the invariant 1-γ-exchange (1-W-exchange) amplitude, extract the electroweak current of the bound state, analyze its covariant structure and determine the form factors. The dynamics of the exchanged gauge boson is thereby fully taken into account by means of a coupled-channel formulation.

Here we are interested in the electromagnetic structure of the nucleon as resulting from a hybrid constituent-quark model in which the nucleon is not just a 3q bound state, but contains, in addition, a 3q+π non-valence component. Transitions between these two components can happen via emission and absorption of the pions by the quarks. In addition, quarks are subject to an *instantanous* confining force. Typical for the point-form, all four components of the momentum operator are interaction dependent, whereas the generators of Lorentz transformations stay free of interactions. This entails simple rotation and boost properties and angular-momentum addition works like in non-relativistic quantum mechanics. The point-form version of the Bakamjian-Thomas construction allows to separate the overall motion of the system from the internal motion in a neat way:

$$\hat{P}^\mu = \hat{\mathcal{M}}\,\hat{V}^\mu_{\text{free}} = \left(\hat{\mathcal{M}}_{\text{free}} + \hat{\mathcal{M}}_{\text{int}}\right)\hat{V}^\mu_{\text{free}}\,, \tag{1}$$

i.e. the 4-momentum operator factorizes into an interaction-dependent mass operator $\hat{\mathcal{M}}$ and a free 4-velocity operator $\hat{V}^\mu_{\text{free}}$. Bakamjian-Thomas-type mass

* Talk delivered by W. Schweiger

operators are most conveniently represented in terms of velocity states $|V;\mathbf{k}_1,\mu_1;\mathbf{k}_2,\mu_2;\ldots;\mathbf{k}_n,\mu_n\rangle$, which specify the system by its overall velocity V ($V_\mu V^\mu = 1$), the CM momenta $\mathbf{k}_i$ of the individual particles and their (canonical) spin projections μ_i [2].

We now want to calculate the 1γ-exchange amplitude for elastic electron scattering off a nucleon that consists of a 3q and a 3q+π component. A multichannel formulation that takes not only the dynamics of electron and quarks, but also the dynamics of the photon and the pion fully into account has to comprise all states which can occur during the scattering process (i.e. $|3q,e\rangle$, $|3q,\pi,e\rangle$, $|3q,e,\gamma\rangle$, $|3q,\pi,e,\gamma\rangle$). What one then needs, in principle, are scattering solutions of the mass-eigenvalue equation

$$\begin{pmatrix} \hat{M}^{\text{conf}}_{3qe} & \hat{K}_\pi & \hat{K}_\gamma & 0 \\ \hat{K}^\dagger_\pi & \hat{M}^{\text{conf}}_{3q\pi e} & 0 & \hat{K}_\gamma \\ \hat{K}^\dagger_\gamma & 0 & \hat{M}^{\text{conf}}_{3qe\gamma} & \hat{K}_\pi \\ 0 & \hat{K}^\dagger_\gamma & \hat{K}^\dagger_\pi & \hat{M}^{\text{conf}}_{3q\pi e\gamma} \end{pmatrix} \begin{pmatrix} |\psi_{3qe}\rangle \\ |\psi_{3q\pi e}\rangle \\ |\psi_{3qe\gamma}\rangle \\ |\psi_{3q\pi e\gamma}\rangle \end{pmatrix} = \sqrt{s} \begin{pmatrix} |\psi_{3qe}\rangle \\ |\psi_{3q\pi e}\rangle \\ |\psi_{3qe\gamma}\rangle \\ |\psi_{3q\pi e\gamma}\rangle \end{pmatrix}, \quad (2)$$

which evolve from an asymptotic electron-nucleon in-state $|eN\rangle$ with invariant mass $\sqrt{s}$. The diagonal entries of this matrix mass operator contain, in addition to the relativistic kinetic energies of the particles in the particular channel, an instantaneous confinement potential between the quarks. The off-diagonal entries are vertex operators which describe the transition between the channels. In the velocity-state representation these vertex operators are directly related to usual quantum-field theoretical interaction-Lagrangean densities [2]. Since we only deal with pseudoscalar pion-quark coupling in the following, we have neglected the $\pi\gamma qq$-vertex (that would show up for pseudovector pion-quark coupling).

To proceed, we reduce Eq. (2) to an eigenvalue problem for $|\psi_{3qe}\rangle$ by means of a Feshbach reduction,

$$\left[\hat{M}^{\text{conf}}_{3qe} + \hat{K}_\pi(\sqrt{s} - \hat{M}^{\text{conf}}_{3q\pi e})^{-1}\hat{K}^\dagger_\pi + \hat{V}^{\text{opt}}_{1\gamma}(\sqrt{s})\right]|\psi_{3qe}\rangle = \sqrt{s}\,|\psi_{3q\pi e}\rangle\,, \quad (3)$$

where $\hat{V}^{\text{opt}}_{1\gamma}(\sqrt{s})$ is the 1γ-exchange optical potential. The invariant 1γ-exchange electron-nucleon scattering amplitude is now obtained by sandwiching $\hat{V}^{\text{opt}}_{1\gamma}(\sqrt{s})$ between (the appropriately normalized valence component of the) physical electron-nucleon states $|eN\rangle$, i.e. eigenstates of $[\hat{M}^{\text{conf}}_{3qe} + \hat{K}(\sqrt{s} - \hat{M}^{\text{conf}}_{3q\pi e})^{-1}\hat{K}^\dagger]$. The crucial point is now to observe that, due to instantaneous confinement, propagating intermediate states do not contain free quarks, they rather contain either physical nucleons N or bare baryons $\tilde{B}$, the latter being eigenstates of the pure confinement problem. As a consequence one can reformulate the scattering amplitude in terms of pure hadronic degrees of freedom with the quark substructure being hidden in vertex form factors. This is graphically represented in Fig. 1. The analytical expressions for the bare nucleon form factors follow from this reformulation.[1]

[1] For details of their extraction and a discussion of the problems connected with wrong cluster properties associated with the Bakamjian-Thomas construction we refer to Refs. [1,2,4].

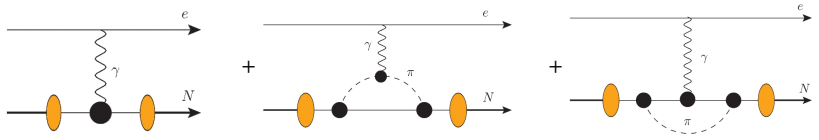

Fig. 1. Diagrams representing the 1γ-exchange amplitude for electron scattering off a "physical" nucleon N, i.e. a bare nucleon dressed by a pion cloud. The time orderings of the γ-exchange are subsumed under a covariant photon propagator. Black blobs represent vertex form factors for the coupling of a photon or pion to the bare nucleon $\tilde{N}$. A vertex form factor is also assumed at the photon-pion vertex. The ovals represent the wave function (i.e. essentially the square root of the probability $P_{\tilde{N}/N}$) for finding the bare nucleon in the physical nucleon.

If nucleonic excitations are neglected in the pion loop, we just need the electromagnetic $\gamma\tilde{N}\tilde{N}$ and strong $\pi\tilde{N}\tilde{N}$ vertex form factors (for the bare nucleon $\tilde{N}$) as well as the electromagnetic pion form factor. The electromagnetic pion form factor can be taken from Ref. [1], where it has been calculated within the same approach as here using a harmonic-oscillator model for the $u\bar{d}$ bound-state wave function of the π^+. What enters the analytical expressions for the form factors of the bare nucleon is its 3q bound-state wave function. Instead of solving the bound-state problem for a particular confinement potential, we rather use a simple model for this wave function, i.e. $\Phi_{\tilde{N}}\left(\tilde{\mathbf{k}}_i\right) = \mathcal{N}\left[(\sum \tilde{\omega}_i)^2 + \beta^2\right]^{-\gamma}$, with $\tilde{\mathbf{k}}_i$ and $\tilde{\omega}_i$ denoting the quark momenta and energies in the rest frame of the nucleon. The same wave function has been used in a corresponding front-form calculation [6], from which we also take the values of the parameters β, γ for later comparison. The normalization $\mathcal{N}$ has to be fixed such that the whole nucleon wave function, including the 3q+π component, is normalized to one. Unlike the authors of Ref. [6], who took a phenomenological $\pi\tilde{N}\tilde{N}$ vertex form factor, we have calculated both, the electromagnetic form factors of the bare nucleon as well as the strong $\pi\tilde{N}\tilde{N}$ vertex form factor with the same microscopic input, namely the 3q bound-state wave function $\Phi_{\tilde{N}}$.

With the model sketched above we achieve good agreement with the experimental data for proton electric and magnetic form factors (see Fig. 2). Our neutron magnetic form factor is also in reasonable agreement with the corresponding experimental data, the reproduction of the neutron electric form factor seems to be less satisfactory. But here one has to notice that it is a rather small quantity and the error bars on the experimental data points are, in general, large. The size of the pionic contribution to all the nucleon form factors is comparable with the one found in Ref. [6]. A significant effect of the 3q+π component on the form factors is only observed for momentum transfers $Q^2 \lesssim 0.5$ GeV^2, where it leads to a welcome modification of the Q^2-dependence.

Improvements of the model can be made in several directions:

i) Take a more sophisticated 3q wave function of the (bare) nucleon, containing, e.g., a mixed $SU(6)$ spin-flavor-symmetry component like in Ref. [6].
ii) Replace the pseudoscalar by the pseudovector $\pi\tilde{N}\tilde{N}$ coupling, which guarantees correct properties in the chiral limit.

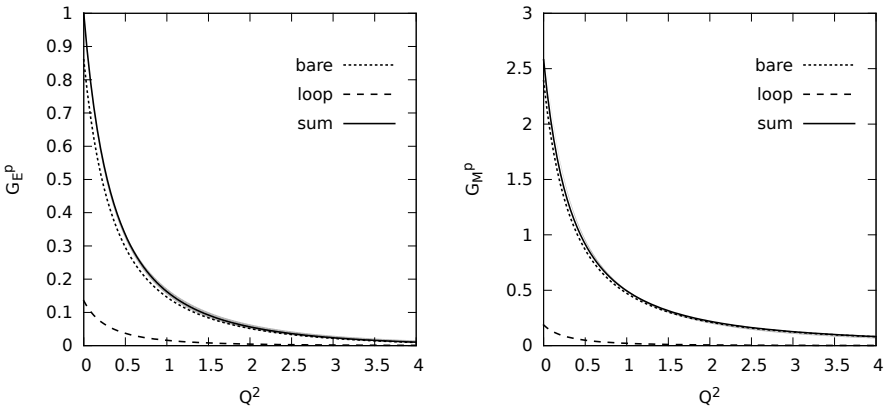

Fig. 2. The proton electric (left) and magnetic (right) form factors as predicted by our model (solid line). The 3q valence contribution is indicated by the dotted line, the contribution due to the 3q+π non-valence component by the dashed line. The shaded area (which is hardly visible) is a parameterization of the experimental data (including uncertainties) [7].

iii) Account for other baryons, different from the nucleon, within the loop, the lightest and most important of them being the Δ.

The ultimate goal should, of course, be a consistent description of the baryon spectrum and the structure of the baryons. This means that one should not start with a model for the nucleon wave function, but rather with a 3q+3qπ hybrid model and fit the parameters of the confinement potential and the πqq coupling strength to the baryon mass spectrum. This would give us the masses and wave functions of the (bare) baryons which are required as an input for the calculation of the strong and electromagnetic form factors of the baryons.

Acknowledgment: D. Kupelwieser acknowledges the support of the "Fonds zur Förderung der wissenschaftlichen Forschung in Österreich" (FWF DK W1203-N16).

References

1. E. P. Biernat, W. Schweiger, K. Fuchsberger and W. H. Klink, Phys. Rev. C **79**, 055203 (2009).
2. E. P. Biernat, W. H. Klink and W. Schweiger, Few Body Syst. **49**, 149 (2011).
3. M. Gomez-Rocha and W. Schweiger, Phys. Rev. D **86**, 053010 (2012).
4. E. P. Biernat and W. Schweiger, Phys. Rev. C **89**, 055205 (2014).
5. B. Bakamjian and L. H. Thomas, Phys. Rev. **92** (1953) 1300.
6. B. Pasquini and S. Boffi, Phys. Rev. D **76**, 074011 (2007).
7. A. J. R. Puckett [GEp-III Collaboration], in *Exclusive Reactions at High Momentum Transfer IV* ed. by A. Radyushkin, World Scientific, 222 (2011); arXiv:1008.0855 [nucl-ex].

BLED WORKSHOPS
IN PHYSICS
VOL. 16, NO. 1
p. 40

Proceedings of the Mini-Workshop
Exploring Hadron Resonances
Bled, Slovenia, July 5 - 11, 2015

Partial wave analysis of η photoproduction data with analyticity constraints*

M. Hadzimehmedovic[a], V. Kashevarov[c], K. Nikonov[c], R. Omerovic[a], H. Osmanovic[a], M. Ostrick[c], J. Stahov[a], A. Svarc[b], L. Tiator[c]

[a] University of Tuzla, Faculty of Science, Bosnia and Herzegovina
[b] Rudjer Boskovic Institute, Zagreb, Croatia
[c] Institut für Kernphysik, Johannes Gutenberg Universtät Mainz, Germany

Abstract. We perform partial wave analysis of the η photoproduction on data. The obtained multipoles are consistent with the fixed-t analyticity and fixed-s analyticity. A fixed-t analyticity is imposed using Pietarinen expansion method. The invariant amplitudes obey the required crossing symmetry.

1 Introduction

A big problem in partial wave analyses are ambiguities of partial wave solutions. More than one set of partial waves describe equally well the experimental data. A first attempt to solve this problem was to require smoothness of partial waves as a function of energy. It was shown that this criteria was not enough to achieve a unique partial wave solution [1]. Furthermore, it was shown that more stringent constraints, based on the analytic properties of invariant amplitudes from Mandelstam hypothesis, should be taken into consideration. An efficient method for imposing the fixed-t analyticity on invariant amplitudes was proposed by E. Pietarinen [2–5] and was used in Karlsruhe-Helsinki partial wave analysis of πN scattering data KH80 [6–8]. In our partial wave analysis of η-photoproduction data we follow main ideas from Karlsruhe-Helsinki analysis. The method consists of two separate analyses: Fixed-t amplitude analysis (FT AA) and a single energy partial wave analysis (SE PWA). The two analyses are coupled in such a way that results from one are used as a constraint in another in an iterative procedure. The resulting partial waves (multipoles) describe experimental data adequately and are consistent with fixed-t and fixed-s analyticity as well.

2 Preparing experimental data for partial wave analysis

Our data base consists of the following experimental data:
— Differential cross sections at 120 energies in the range 710 MeV $\leq E_{lab} \leq$ 1395 MeV [9];

* Talk presented by J. Stahov

— Beam asymmetry Σ at 15 energies in the range 724 MeV − 1472 MeV [10];
— Target asymmetry T at 12 energies in the range 725 MeV − 1350 MeV [11];
— Double asymmetry F at 12 energies in the range 725 MeV − 1350 MeV [11].
In SE PWA experimental data are required at a predetermined set of energies. Experimental values of beam asymmetry, target asymmetry and double polarization asymmetry are interpolated to 113 energies, where data on differential cross sections are available. A spline fit method with $\chi^2/dp = 0.7$ (DP-number of data points) was used. FT AA requires experimental data at predetermined set of t values. Using the same method, data previously prepared for SE PWA were shifted to 40 t values in the range $t \in [-1.00\,\mathrm{GeV}^2, -0.05\,\mathrm{GeV}^2]$.

3 Fixed-t amplitude analysis

Following definition in Ref. [12], in description of η-meson photoproduction, we use crossing symmetric invariant amplitudes B_1, B_2, B_6, and B_8/ν. For a given value of variable t amplitudes are represented by two Pietarinen expansions in the form

$$F_k(\nu^2, t) = F_{kN}(\nu^2, t) + (1 + z_1) \sum_{i=1}^{N_1} b_{1i}^{(k)} z_1^i + (1 + z_2) \sum_{i=1}^{N_2} b_{2i}^{(k)} z_2^i, \qquad (1)$$

where F_k stands for invariant amplitudes B_k. F_{kN} are explicitly known nucleon pole contributions and s, u and $\nu = (s - u)/4m$ with the proton mass m are Mandelstam variables. The conformal variables z_1 and z_2 are defined as

$$z_1 = \frac{\alpha_1 - \sqrt{\nu_{th1}^2 - \nu^2}}{\alpha_1 + \sqrt{\nu_{th1}^2 - \nu^2}}, \qquad z_2 = \frac{\alpha_2 - \sqrt{\nu_{th2}^2 - \nu^2}}{\alpha_2 + \sqrt{\nu_{th2}^2 - \nu^2}}. \qquad (2)$$

ν_{th1} and ν_{th2} correspond to the π and η photoproduction thresholds ($\gamma p \to \pi^0 p$ and $\gamma p \to \eta p$). N_1 and N_2 are number of parameters in expansion (1) (in our applications N_1, $N_2 \approx 15$). α_1 and α_2 are parameters which determine distribution of points on a unit circle ($|z_1| = |z_2| = 1$). Coefficients $b_1^{(k)}$ and $b_2^{(k)}$ in expansion (1) are determined by minimizing a quadratic form

$$\chi^2 = \chi^2_{data} + \chi^2_{PW} + \Phi. \qquad (3)$$

The term χ^2_{data} is the standard exspression containing all the data at a fixed-t value

$$\chi^2_{data} = \sum_D \sum_{n=1}^{N_D} \frac{(D_n^{exp}(\nu^2, t) - D_n^{fit}(\nu^2, t))^2}{\Delta^2_{D_n}}, \qquad (4)$$

where D stands for measurable quantities ($\sigma_0 = d\sigma/d\Omega$, $\sigma_0 \cdot T$, $\sigma_0 \cdot F$, $\sigma_0 \cdot \Sigma$). The sum goes over all N_D available experimental values of measured quantities D for a given t value. D_n^{fit} are predicted values in terms of coefficients in expansion (1).

A second term χ^2_{PW} is also a usual χ^2 expression containing as "data" the helicity amplitudes calculated from the partial wave solution

$$\chi^2_{PW} = q \sum_{k=1}^{4} \sum_{i=1}^{N_D} \left\{ \frac{\left[\mathrm{Re}\, H_k^{fit}\left(t, \nu_i^2\right) - \mathrm{Re}\, H_k^{PW}\left(t, \nu_i^2\right) \right]^2}{(\varepsilon_R)^2_{ki}} + \frac{\left[\mathrm{Im}\, H_k^{fit}\left(t, \nu_i^2\right) - \mathrm{Im}\, H_k^{PW}\left(t, \nu_i^2\right) \right]^2}{(\varepsilon_I)^2_{ki}} \right\}. \tag{5}$$

In the first iteration H_k^{PW} are calculated from an initial, already existing solution. In the subsequent iterations H_k^{PW} are calculated from partial waves obtained in the single energy partial wave analysis (SE PWA) of the same set of experimental data. The weight factor q and errors ε_{ki} are unknown. They are adjusted in such a way that $\chi^2_{data} \approx \chi^2_{PW}$. Φ is Pietarinen's penalty function in the form

$$\Phi = \Phi_1 + \Phi_2 + \Phi_3 + \Phi_4, \tag{6}$$

where Φ_k is defined as

$$\Phi_k = \lambda_{1k} \sum_{i=1}^{N_1} \left(b_{1i}^{(k)} \right)^2 (i+1)^3 + \lambda_{2k} \sum_{i=1}^{N_2} \left(b_{2i}^{(k)} \right)^2 (i+1)^3 .$$

$\lambda_{11}, \lambda_{21}, \ldots, \lambda_{14}, \lambda_{24}$ are weight factors determined according to the convergence test function method [5]. The final result of the fixed-t amplitude analysis consists of 40 sets of coefficients $b_1^{(k)}$ and $b_2^{(k)}$. The invariant amplitudes may be calculated at any c.m. energy W and scattering angle θ in the physical region. Helicity amplitudes are used as a constraint in a SE PWA. Helicity amplitudes in terms of invariant amplitudes are given in the Appendix.

3.1 Single energy partial wave analysis

In the single energy partial wave analysis we minimize a quadratic form:

$$\chi^2 = \chi^2_{data} + \chi^2_{FT}. \tag{7}$$

χ^2_{data} is again a standard expression containing all the data at a given energy. For a given observable D, measured at N_D angles θ_i, contribution to the χ^2_{data} reads:

$$\left(\chi^2_{data}\right)_D = \sum_{i=1}^{N} \left[\frac{D_{exp}(\theta_i) - D_{fit}(\theta_i)}{\Delta_{Di}} \right]^2,$$

$$\chi^2_{data} = \sum_{D} \left(\chi^2_{data}\right)_D .$$

$D_{exp}(\theta_i)$ are experimental values of observable D with corresponding experimental errors Δ_{Di}. $D_{fit}(\theta_i)$ are values of observable D calculated from partial waves which are parameters in the fit. The second term χ^2_{FT} is also a usual χ^2

expression containing as "data" the helicity amplitudes H_k from the fixed-t amplitude analysis. It has the form

$$\chi^2_{FT} = \sum_{k=1}^{4} \sum_{i=1}^{Nc} \left\{ \left[\frac{\mathrm{Re}\, H_k(\theta_i) - \mathrm{Re}\, H_k^{fit}(\theta_i)}{(\varepsilon_R)_{ki}} \right]^2 + \left[\frac{\mathrm{Im}\, H_k(\theta_i) - \mathrm{Im}\, H_k^{fit}(\theta_i)}{(\varepsilon_I)_{ki}} \right]^2 \right\}.$$

The angles θ_i are calculated using the formula

$$\cos\theta_i = \frac{t_i - m_\eta^2 + 2k\omega}{2kq}, \quad \cos\theta_i \in [-1.00, +1.00], \tag{8}$$

where m_η, q, and ω are mass, c.m. momentum and c.m. energy of the η meson, and k is the c.m. momentum of the photon. N_c is the number of angles at which constraining amplitudes are given. Errors of real and imaginary parts (ε_R), (ε_I) are not determined. They are adjusted in such a way that $\chi^2_{data} \approx \chi^2_{FT}$. After performing SE PWA at predetermined N_D energies, the obtained partial wave values are used as a constraint in the fixed-t amplitude analysis. The "data" in the term χ^2_{PW} of (3) are to be calculated using these partial waves.

Our iterative procedure is shown in Fig 1.

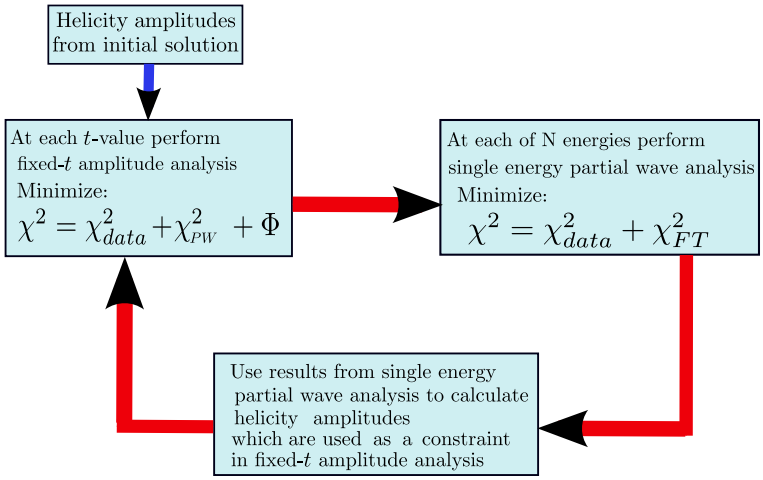

Fig. 1. (Color online) Iterative procedure in a combined single energy partial wave analysis and fixed-t amplitude analysis.

To make our analysis easier to follow, we give more details about important steps after preparing input data as described in section 2.

1. Take an initial solution (MAID [13] or Bonn-Gatchina [14, 15]) and calculate all four invariant amplitudes $B_i(W, t)$ at all t values and energies where input data are available.
2. Perform the Pietarinen expansion for all invariant amplitudes using equation (1) with conformal variables defined in formula (2).

3. Calculate helicity amplitudes from invariant amplitudes (see Appendix).
4. For all t values perform a non-linear fit of observables minimizing the quadratic form (3). As starting values of parameters $b_1^{(k)}$ and $b_2^{(k)}$ take coefficients obtained in step 2. Calculate term χ^2_{PW} using initial solution to calculate H_k^{PW}. This step completes the FT AA.
5. At a given energy W calculate helicity amplitudes $H_k(W, \cos\theta_i)$, where $\cos\theta_i$ are given by formula (8). Use coefficients $b_1^{(k)}$ and $b_2^{(k)}$ from FT AA for corresponding t-values.
6. Perform a non-linear SE PWA using helicity amplitudes obtained in step 5 as a constraint. As starting values for partial waves (multipoles) use the same initial solution as in step 1.
7. Use results from step 6 in step 1 and perform next iteration. Our preliminary results show that, depending on the strength of constraints, it is enough to perform 2-3 iterations to get a stable final solution.

In Fig. 2 fits of invariant amplitudes are shown at $t = -0.15$ GeV^2. Multipoles with $L \leq 3$, obtained after two iterations, are shown in Figs. 3 and 4. The Eta-Maid2015b solution was chosen as a starting solution in both analyses, FT AA and SE PWA.

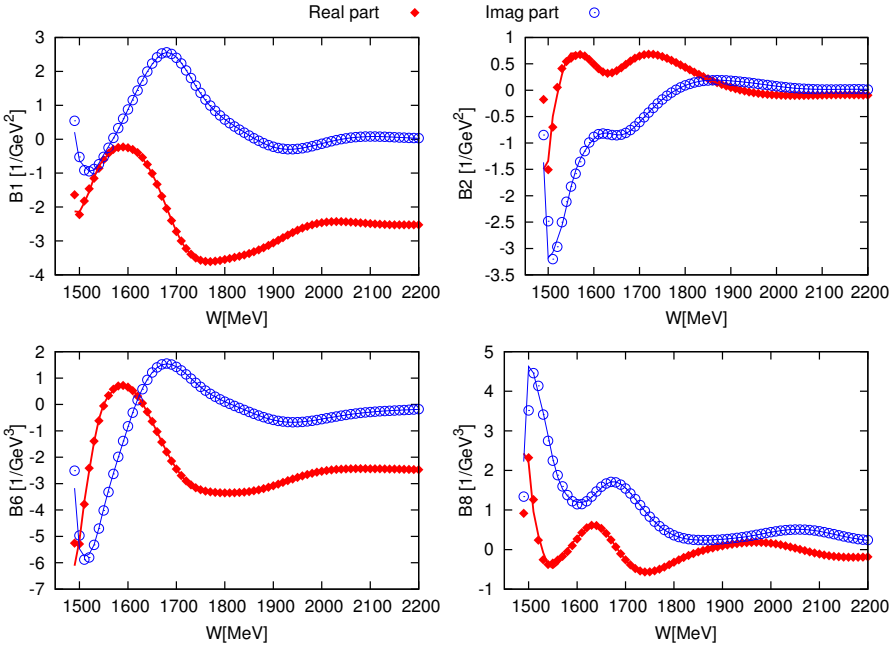

Fig. 2. (Color online) Red diamonds and blue circles show initial real and imaginary values of invariant amplitudes. As initial solution invariant amplitudes for $t = -0.15$ GeV^2 from etaMAID2015b [13] are used. The red and blue lines show the Pietarinen fits to real and imaginary parts of invariant amplitudes, respectively

.

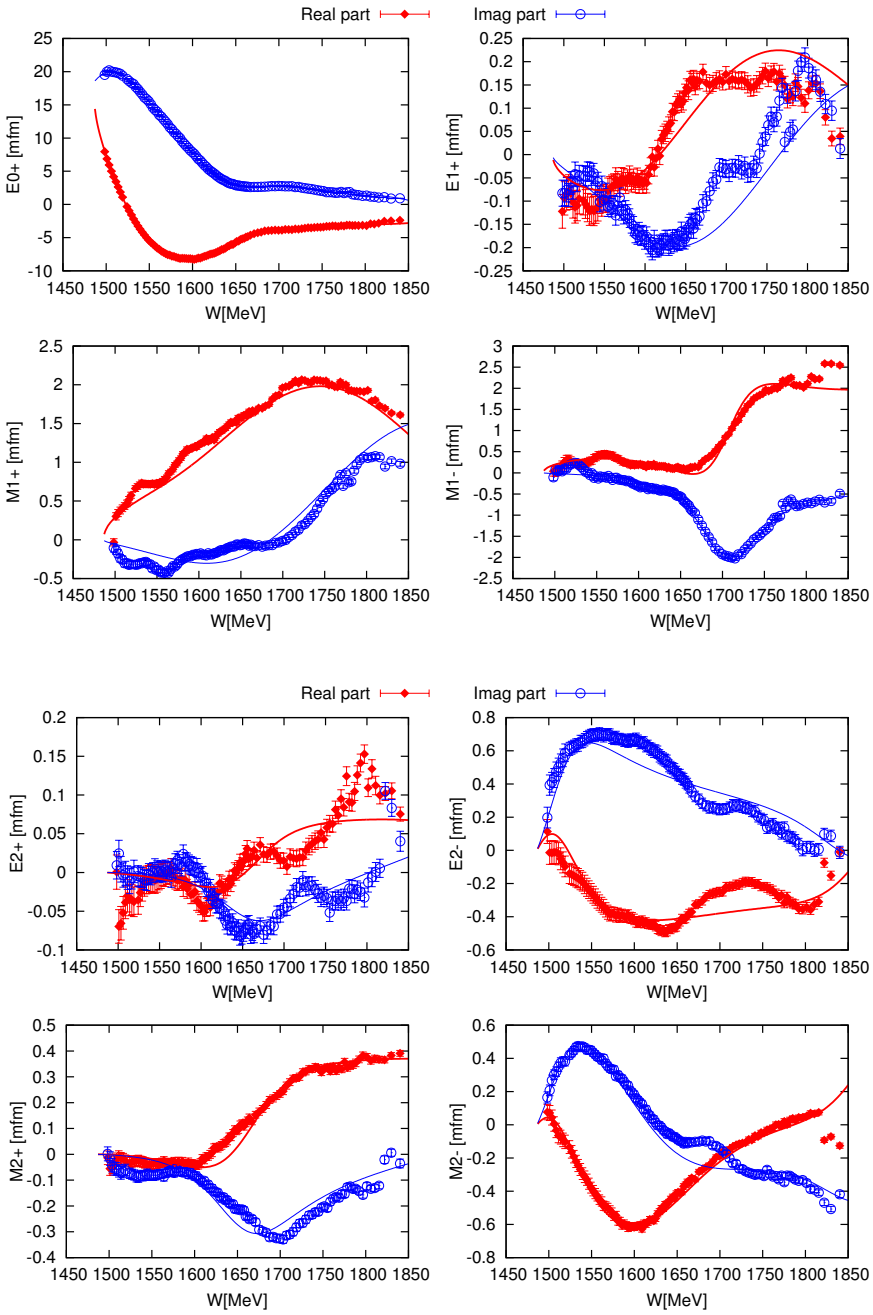

Fig. 3. (Color online) Real and imaginary parts of multipoles obtained from SE PWA in 2nd iteration are shown as red diamonds and blue circles. The initial solution etaMAID2015b is given as red and blue solid lines.

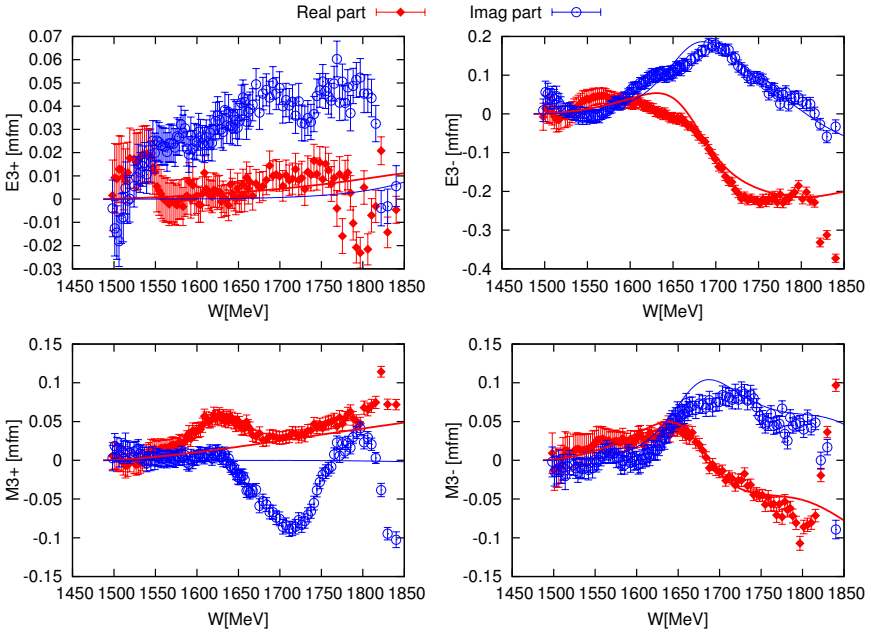

Fig. 4. [Continued from previous page.] Caption as in Fig. 3.

4 Conclusions

A SE PWA with fixed-t constraints has been performed and multipoles, consistent with crossing symmetry and fixed-t analyticity, have been obtained. The helicity amplitudes from fixed-t show good consistency with fixed-s analyticity. It implies that our amplitudes are consistent with both, fixed-t and fixed-s analyticity.

Acknowledgment

This work was supported in part by the Federal Ministry of Education and Science, Bosnia and Herzegovina, Grant No. 05-39-3545-1/14 and by the Deutsche Forschungsgemeinschaft, Collaborative Research Center 1044.

Appendix

A Multipole expansion of invariant amplitudes

In partial wave analysis of pseudoscalar meson photoproduction it is convenient to work with CGLN amplitudes [16] giving simple representations in terms of

electric and magnetic multipoles and derivatives of Legendre polynomials

$$\begin{aligned}
F_1 &= \sum_{l=0}^{\infty}[(lM_{l+} + E_{l+})P'_{l+1}(x) + ((l+1)M_{l+} + E_{l-})P'_{l-1}(x)],\\
F_2 &= \sum_{l=1}^{\infty}[(l+1)M_{l+} + lM_{l-}]P'_l(x),\\
F_3 &= \sum_{l=1}^{\infty}[(E_{l+} - M_{l+})P''_{l+1} + (E_{l-} + M_{l-})P''_{l-1}(x)],\\
F_4 &= \sum_{l=2}^{\infty}[M_{l+} - E_{l+} - M_{l-} - E_{l-}]P''_l(x).
\end{aligned} \tag{A.1}$$

Another common set of amplitudes are helicity amplitudes, which are linearly related to the CGLN amplitudes

$$\begin{aligned}
H_1 &= -\frac{1}{\sqrt{2}}\sin\theta\cos\frac{\theta}{2}(F_3 + F_4),\\
H_2 &= \sqrt{2}\cos\frac{\theta}{2}[(F_2 - F_1) + \frac{1-\cos\theta}{2}(F_3 - F_4)],\\
H_3 &= \frac{1}{\sqrt{2}}\sin\theta\sin\frac{\theta}{2}(F_3 - F_4),\\
H_4 &= \sqrt{2}\sin\frac{\theta}{2}[(F_1 + F_2) + \frac{1+\cos\theta}{2}(F_3 + F_4)].
\end{aligned} \tag{A.2}$$

The relations between CGLN and invariant amplitudes are given by

$$\begin{pmatrix} F_1\\ F_2\\ F_3\\ F_4 \end{pmatrix} = M \cdot \begin{pmatrix} B_1\\ B_2\\ B_6\\ B_8 \end{pmatrix}, \tag{A.3}$$

with the matrix M:

$$M = \frac{1}{2W(s-m^2)} \begin{pmatrix} \frac{(s-m^2)}{a_1} & -\frac{(s-m^2)}{a_2} & 0 & 0\\ 0 & 0 & -\frac{(t-m_\eta^2)(m-W)}{2a_3} & -\frac{(t-m_\eta^2)(m+W)}{2a_4}\\ -\frac{2(m+W)}{a_1} & \frac{2(m-W)}{a_2} & -\frac{(t-m_\eta^2)}{a_3} & -\frac{(t-m_\eta^2)}{a_4}\\ -\frac{(m+W)}{a_1} & \frac{(m-W)}{a_2} & -\frac{(s-u)}{2a_3} & -\frac{(s-u)}{2a_4} \end{pmatrix}. \tag{A.4}$$

and

$$\begin{aligned}
a_1 &= \frac{\sqrt{(E_1+m)(E_2+m)}}{8\pi W},\\
a_2 &= \frac{\sqrt{(E_1-m)(E_2-m)}}{8\pi W},\\
a_3 &= \frac{\sqrt{(E_1-m)(E_2-m)}(E_2+m)}{8\pi W} = a_2\cdot(E_2+m),
\end{aligned}$$

$$a_4 = \frac{\sqrt{(E_1+m)(E_2+m)}(E_2-m)}{8\pi W} = a_1 \cdot (E_2 - m)\,,$$

$$s + t + u = \sum = 2m^2 + m_\eta^2, \qquad \nu = \frac{s-u}{4m}\,,$$

where E_1 and E_2 are c.m. energies of the incoming and outgoing nucleons and W is the total c.m. energy.

References

1. J. E. Bowcock and H. Burkhardt, Rep. Prog. Phys. **38** 1099 (1975).
2. E. Pietarinen, Nucl. Phys. B **49** 315 (1972).
3. E. Pietarinen, Nucl. Phys. B **55**, 541 (1973).
4. E. Pietarinen, Nucl. Phys. B **107**, 21 (1976).
5. E. Pietarinen, Nuovo Cim. **12A** 522 (1972).
6. G. Höhler, *Pion Nucleon Scattering*, Part 2, Landolt-Börnstein: Elastic and Charge Exchange Scattering of Elementary Particles, Vol. **9b** (Springer-Verlag, Berlin, 1983).
7. G. Höhler, F. Kaiser, R. Koch, E. Pietarinen, Physik Daten 12N1 1 (1979).
8. R. Koch, E. Pietarinen, Nucl. Phys. A **336**, 331 (1980).
9. E. F. McNicoll et al. (Crystal Ball Collaboration at MAMI), Phys. Rev. C **82**, 035208 (2010).
10. O. Bartalini at al., Eur. Phys. J. A **33** 169 (2007).
11. C.S. Akondi et al. (A2 Collaboration at MAMI) Phys. Rev. Lett. **113**, 102001 (2014).
12. I. G. Aznauryan, Phys. Rev. C **67**, 015209 (2003).
13. V. Kashevarov, Proceedings from Mini-Workshop Bled 2015.
14. A.V. Anisovich, R. Beck, E. Klempt, V.A. Nikonov, A.V. Sarantsev, and U. Thoma, Eur. Phys. J. A **48** 15 (2012).
15. A.V. Anisovich, E. Klempt, V.A. Nikonov, A.V. Sarantsev, U. Thoma, Eur. Phys. J. A **47** 153 (2011).
16. G. F. Chew, M. L. Goldberger, F. E. Low, Y. Nambu, Phys. Rev. **106** 1345 (1957).

BLED WORKSHOPS
IN PHYSICS
VOL. 16, NO. 1
p. 49

Proceedings of the Mini-Workshop
Exploring Hadron Resonances
Bled, Slovenia, July 5 - 11, 2015

Progress in Neutron Couplings*

W. J. Briscoe and I. Strakovsky

The George Washington University, Washington, DC 20052, USA

Abstract. An overview of the GW SAID group effort to analyze pion photoproduction on the neutron-target will be given. The disentanglement the isoscalar and isovector EM couplings of N^* and Δ^* resonances does require compatible data on both proton and neutron targets. The final-state interaction plays a critical role in the state-of-the-art analysis in extraction of the $\gamma n \to \pi N$ data from the deuteron target experiments. It is important component of the current JLab, MAMI-C, SPring-8, CBELSA, and ELPH programs.

1 Introduction

The N^* family of nucleon resonances has many well established members [1], several of which exhibit overlapping resonances with very similar masses and widths but with different J^P spin-parity values. Apart from the $N(1535)1/2^-$ state, the known proton and neutron photo-decay amplitudes have been determined from analyses of single-pion photoproduction. The present work reviews the region from the threshold to the upper limit of the SAID analyses, which is CM energy W = 2.5 GeV. There are two closely spaced states above $\Delta(1232)3/2^+$: $N(1520)3/2^-$ and $N(1535)1/2^-$. Up to W $\sim$ 1800 MeV, this region also encompasses a sequence of six overlapping states: $N(1650)1/2^-$, $N(1675)5/2^-$, $N(1680)5/2^+$, $N(1700)3/2^-$, $N(1710)1/2^+$, and $N(1720)3/2^+$.

One critical issue in the study of meson photoproduction on the nucleon comes from isospin. While isospin can change at the photon vertex, it must be conserved at the final hadronic vertex. Only with good data on both proton and neutron targets can one hope to disentangle the isoscalar and isovector electromagnetic (EM) couplings of the various N^* and Δ^* resonances (see Refs. [2]), as well as the isospin properties of the non-resonant background amplitudes. The lack of $\gamma n \to \pi^- p$ and $\gamma n \to \pi^0 n$ data does not allow us to be as confident about the determination of neutron EM couplings relative to those of the proton. For instance, the uncertainties of neutral EM couplings of 4^* low-lying N^* resonances, $\Delta(nA_{1/2})$ vary between 25 and 140% while charged EM couplings, $\Delta(pA_{1/2})$, vary between 7 and 42%. Some of the N^* baryons [$N(1675)5/2^-$, for instance] have stronger EM couplings to the neutron relative to the proton, but the parameters are very uncertain [1]. One more unresolved issue relates to the second P_{11}, $N(1710)1/2^+$. That is not seen in the recent πN partial-wave analysis

* Talk presented by I. Strakovsky

(PWA) [3], contrary to other PWAs used by the PDG14 [1]. A recent brief review of its status is given in Ref. [4].

Additionally, incoherent pion photoproduction on the deuteron is interesting in various aspects of nuclear physics, and particularly, provides information on the elementary reaction on the neutron, i.e., $\gamma n \to \pi N$. Final-state interaction (FSI) plays a critical role in the state-of-the-art analysis of the $\gamma n \to \pi N$ interaction as extracted from $\gamma d \to \pi NN$ measurements. The FSI was first considered in Refs. [5] as responsible for the near-threshold enhancement (Migdal-Watson effect) in the NN mass spectrum of the meson production reaction $NN \to NNx$. In Ref. [6], the FSI amplitude was studied in detail.

2 Complete Experiment in Pion Photoproduction

Originally, PWA arose as the technology to determine amplitude of the reaction via fitting scattering data. That is a non-trivial mathematical problem – loking for a solution of ill-posed problem following to Hadamard, Tikhonov *et al.* Resonances appeared as a by-product (bound states objects with definite quantum numbers, mass, lifetime and so on).

There are 4 independent invariant amplitudes for a single pion photoproduction. In order to determine the pion photoproduction amplitude, one has to carry out 8 independent measurements at fixed (s, t) (the extra observable is necessary to eliminate a sign ambiguity).

There are 16 non-redundant observables and they are not completely independent from each other, namely 1 unpolarized, $d\sigma/d\Omega$; 3 single polarized, Σ, T, and P; 12 double polarized, E, F, G, H, C_x, C_z, O_x, O_z, L_x, L_z, T_x, and T_z measurements. Additionally, there are 18 triple-polarization asymmetries [9 (9) for linear (circular) polarized beam and 13 of them are non-vanishing] [7]. Obviously, the triple-polarization experiments are not really necessary from the theoretical point of view while such measurements will play a critical role to keep systematics under control.

3 Neutron Database

Experimental data for neutron-target photoreactions are much less abundant than those utilizing a proton target, constituting only about 15% of the present worldwide known GW SAID database [8]. The existing $\gamma n \to \pi^- p$ database contains mainly differential cross sections and 15% of which are from polarized measurements. At low to intermediate energies, this lack of neutron-target data is partially compensated by experiments using pion beams, e.g., $\pi^- p \to \gamma n$, as has been measured, for example, by the Crystal Ball Collaboration at BNL [9] for the inverse photon energy E = 285 – 689 MeV and $\theta = 41^\circ - 148^\circ$, where θ is the inverse production angle of π^- in the CM frame. This process is free from complications associated with the deuteron target. However, the disadvantage of using the reaction $\pi^- p \to \gamma n$ is the 5 to 500 times larger cross sections for $\pi^- p \to \gamma n \to \gamma nn$,

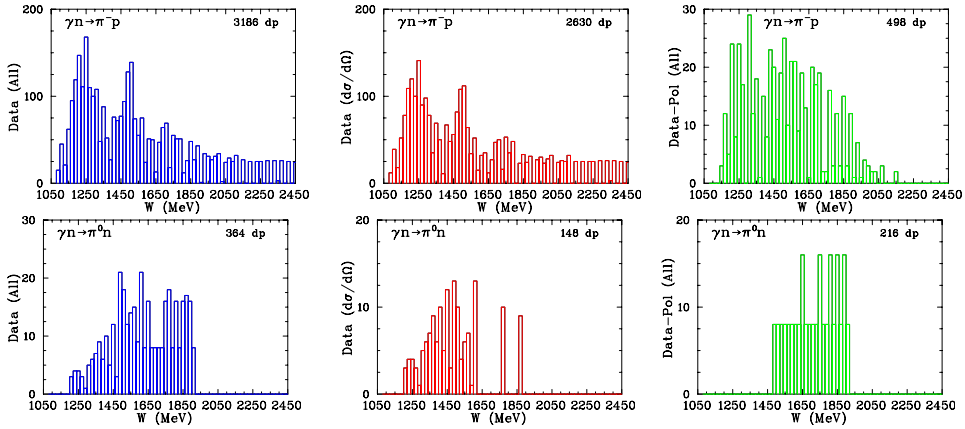

Fig. 1. Data available for single pion photoproduction of the neutron as a function of CM energy W [8]. The number of data points, dp, is given in the upper right hand side of each subplot. **Top panel**: The first subplot (blue) shows the total amount of $\gamma n \to \pi^- p$ data available for all observables, the second subplot (red) shows the amount of $d\sigma/d\Omega$, data available, the third subplot (green) shows the amount of P observables data available. **Bottom panel**: The first subplot (blue) shows the total amount of $\gamma n \to \pi^0 n$ data available for all observables, the second subplot (red) shows the amount of $d\sigma/d\Omega$ data available, the third subplot (green) shows the amount of P observables data available.

depending on E and θ, which causes a large background, and there were no tagging high flux pion beams.

Figure 1 summarizes the available data for single pion photoproduction on the neutron below W = 2.5 GeV. Some high-precision data for the $\gamma n \to \pi^- p$ and $\gamma n \to \pi^0 n$ reactions have been measured recently. We applied our GW-ITEP FSI corrections, covering a broad energy range up to E = 2.7 GeV [6], to the CLAS and A2 Collaboration $\gamma d \to \pi^- pp$ measurements to get elementary cross sections for $\gamma n \to \pi^- p$ [10, 11]. In particular, the new CLAS cross sections have quadrupled the world database for $\gamma n \to \pi^- p$ above E = 1 GeV. The FSI correction factor for the CLAS (E = 1050 – 2700 MeV and $\theta = 32^\circ - 157^\circ$) and MAMI (E = 301 – 455 MeV and $\theta = 45^\circ - 125^\circ$) kinematics was found to be small, $\Delta\sigma/\sigma < 10\%$.

Obviously, that is not enough to have compatible proton and neutron databases, specifically the energy binning of the CLAS measurements is 50 MeV or, in the worst case, 100 MeV while A2 Collaboration measurements are able to have 2 to 4 MeV binning. The forward direction, which is doable for A2 vs. CLAS, is critical for evaluation of our FSI treatment.

4 Neutron Data from Deuteron Measurements

The determination of the $\gamma d \to \pi^- pp$ differential cross sections with the FSI, taken into account (including all key diagrams in Fig. 2), were done, as we did recently [6, 10, 11], for the CLAS [10] and MAMI data [11]. The SAID of GW Data Analysis Center (DAC) phenomenological amplitudes for $\gamma N \to \pi N$ [12], $NN \to NN$ [13], and $\pi N \to \pi N$ [3] were used as inputs to calculate the diagrams

in Fig. 2. The Bonn potential (full model) [14] was used for the deuteron description. In Refs. [10, 11], we calculated the FSI correction factor R(E,θ) dependent on photon energy, E, and pion production angle in CM frame θ and fitted recent CLAS and MAMI $d\sigma/d\Omega$ versus the world $\gamma N \to \pi N$ database [8] to get new neutron multipoles and determine neutron resonance EM couplings [10].

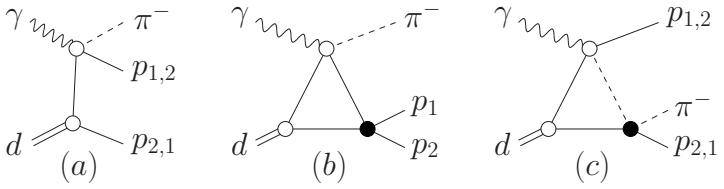

Fig. 2. Feynman diagrams for the leading components of the $\gamma d \to \pi^- pp$ amplitude. (a) Impulse approximation (IA), (b) pp-FSI, and (c) πN-FSI. Filled black circles show FSI vertices. Wavy, dashed, solid, and double lines correspond to the photons, pions, nucleons, and deuterons, respectively.

Results of calculations and comparison with the experimental data on the differential cross sections, $d\sigma_{\gamma d}/d\Omega$, where Ω and θ are solid and polar angles of outgoing π^- in the laboratory frame, respectively, with z-axis along the photon beam for the reaction $\gamma d \to \pi^- pp$ are given in Fig. 3 for a number of the photon energies, E.

The FSI corrections for the CLAS and MAMI quasi-free kinematics were found to be small, as mentioned above. As an illustration, Fig. 4 shows the FSI correction factor $R(E,\theta) = (d\sigma/d\Omega_{\pi p})/(d\sigma^{IA}/d\Omega_{\pi p})$ for the $\gamma n \to \pi^- p$ differential cross sections as a function of the pion production angle in the CM $(\pi - p)$ frame, θ, for different energies over the range of the CLAS and MAMI experiments. Overall, the FSI correction factor $R(E,\theta) < 1$, while the effect, i.e., the (1 - R) value, vary from 10% to 30%, depending on the kinematics, and the behavior is very smooth versus pion production angle. We found a sizeable FSI-effect from S-wave part of pp-FSI at small angles. A small but systematic effect $|R - 1| << 1$ is found in the large angular region, where it can be estimated in the Glauber approach, except for narrow regions close to $\theta \sim 0^\circ$ or $\theta \sim 180^\circ$. The $\gamma n \to \pi^0 n$ case is much more complicate vs. $\gamma n \to \pi^- p$ because $\pi^0 n$ final state can come from both γn and γp initial interactions [16]. The leading diagrams for $\gamma d \to \pi^0 pn$ are similar as given on Fig. 2.

5 New Neutron Amplitudes and neutron EM Couplings

The solution, SAID GB12 [10], uses the same fitting form as SAID recent SN11 solution [17], which incorporated the neutron-target CLAS $d\sigma/d\Omega$ for $\gamma n \to \pi^- p$ [10] and GRAAL Σs for both $\gamma n \to \pi^- p$ and $\gamma n \to \pi^0 n$ [18, 19] (Fig. 5). This fit form was motivated by a multichannel K-matrix approach, with an added phenomenological term proportional to the πN reaction cross section. However, these new CLAS cross sections departed significantly from our predictions at the

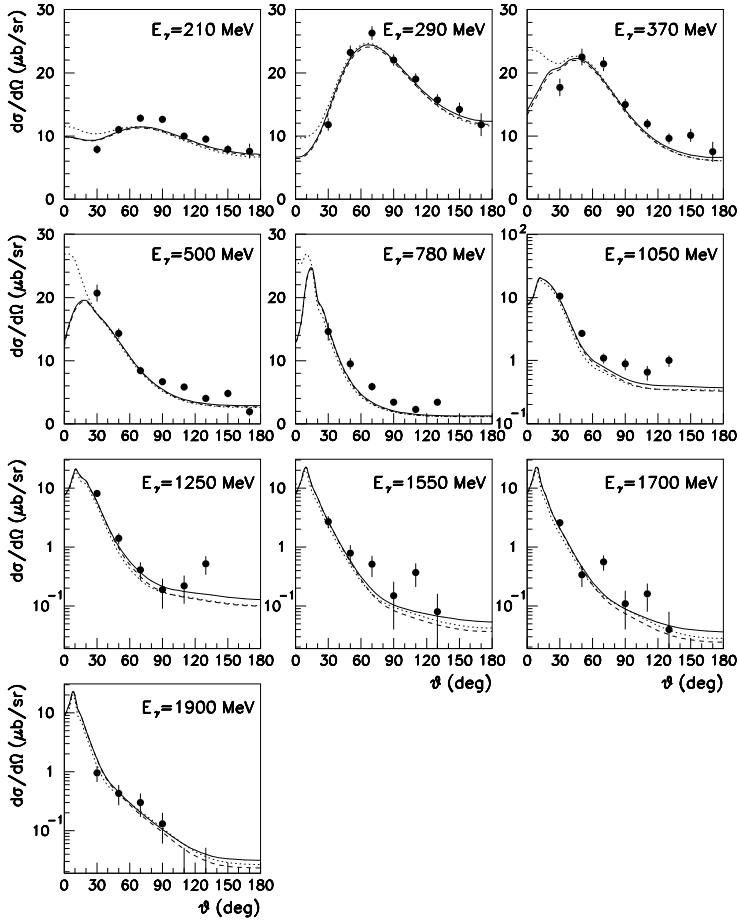

Fig. 3. The differential cross section, $d\sigma_{\gamma d}/d\Omega$, of the reaction $\gamma d \to \pi^- pp$ in the laboratory frame at different values of the photon laboratory energy E < 1900 MeV; θ is the polar angle of the outgoing π^-. Dotted curves show the contributions from the IA amplitude [Fig. 2(a)]. Successive addition of the NN-FSI [Fig. 2(b)] and πN-FSI [Fig. 2(c)] amplitudes leads to dashed and solid curves, respectively. The filled circles are the data from DESY bubble chamber [15].

higher energies, and greatly modified PWA result [10] (Fig. 5). Recently, the BnGa group reported a neutron EM coupling determination [21] using the CLAS Collaboration $\gamma n \to \pi^- p$ because $\pi^0 n$ final state can come from both γn and γp initial interact $d\sigma/d\Omega$ with our FSI [10] (Table 1). BnGa13 and SAID GB12 used the same (almost) data [10] to fit them while BnGa13 has several new Ad-hoc resonances.

Overall: the difference between MAID07 with BnGa13 and SAID GB12 is rather small but resonances may be essentially different (Table 1). The new BnGa13 [21] has some difference vs. GB12 [10], PDG14 [1], for instance, for N(1535)$1/2^-$, N(1650)$1/2^-$, and N(1680)$5/2^+$.

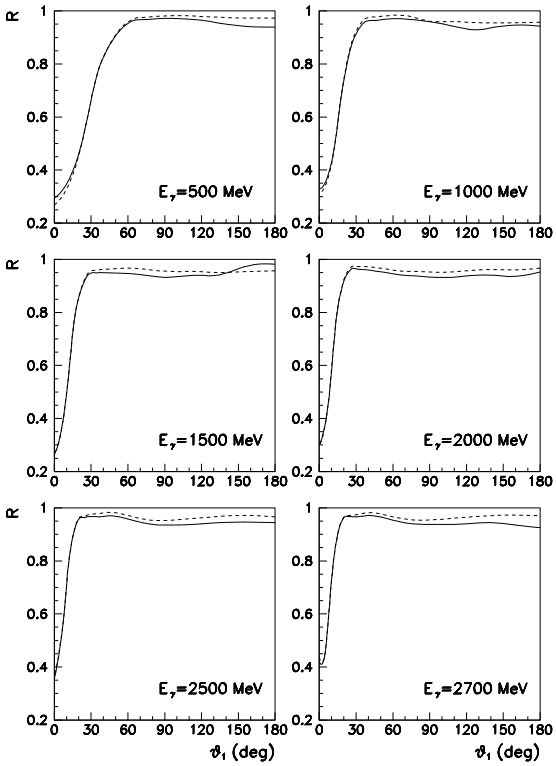

Fig. 4. The correction factor R(E,θ), where θ is the polar angle of the outgoing π^- in the rest frame of the pair π^-+ fast proton. The kinematic cut, $P_p > 200$ MeV/c, is applied. The solid (dashed) curves are obtained with both πN- and NN-FSI (only NN-FSI) taken into account.

6 Work in Progress

At MAMI in March of 2013, we collected deuteron data below E = 800 MeV with 4 MeV energy binning [23] and will have a new experiment below E = 1600 MeV [24] in the fall of 2016.

The experimental setup provides close to 4π sr coverage for outgoing particles. The photons from π^0 decays and charged particles are detected by the CB and TAPS detection system. The energy deposited by charged particles in CB and TAPS is, for the most part, proportional to their kinetic energy, unless they punch through crystals of the spectrometers. Clusters from the final-state neutrons provide information only on their angles. Separation of clusters from neutral particles and charged ones is based on the information from MWPC, PID, and TAPS veto. Separation of positive and negative pions can be based on the identification of the final-state nucleon as either a neutron or a proton. Since cluster energies from charged pions are proportional to their kinetic energy (unless their punch through the crystals), the energy of those clusters can be very low close to reaction threshold.

Table 1. Neutron helicity amplitudes A1/2 and A3/2 (in [(GeV)-1/2 × 10-3] units) from the SAID GB12 [10] (first row), previous SAID SN11 [17] (second row), recent BnGa13 by the Bonn-Gatchina group [21] (third row), recent Kent12 by the Kent State Univ. group [22] (forth row), and average values from the PDG14 [1] (fifth row).

Resonance	$nA_{1/2}$	Resonance	$nA_{1/2}$	$nA_{3/2}$	Ref.
$N(1535)1/2^-$	−58± 6	$N(1520)3/2^-$	−46± 6	−115± 5	SAID GB12
	−60± 3		−47± 2	−125± 2	SAID SN11
	−93±11		−49± 8	−113±12	BnGa13
	−49± 3		−38± 3	−101± 4	Kent12
	−46±27		−59± 9	−139±11	PDG14
$N(1650)1/2^-$	−40±10	$N(1675)5/2^-$	−58± 2	−80± 5	SAID GB12
	−26± 8		−42± 2	−60± 2	SAID SN11
	25±20		−60± 7	−88±10	BnGa13
	11± 2		−40± 4	−68± 4	Kent12
	−15±21		−43±12	−58±13	PDG14
$N(1440)1/2^+$	48± 4	$N(1680)5/2^+$	26± 4	−29± 2	SAID GB12
	45±15		50± 4	−47± 2	SAID SN11
	43±12		34± 6	−44± 9	BnGa13
	40± 5		29± 2	−59± 2	Kent12
	40±10		29±10	−33± 9	PDG14

Monte Carlo simulations, which tracks reaction products through a realistic model of the detector system together with the reconstruction program, is used to calculate acceptance to various channels. So to detect the reactions under study with our setup, we have to take data with almost open trigger. Acceptance for reaction $\gamma n \rightarrow \pi^0 n$ varies from 70% at 0.8 GeV to 30% at 1.5 GeV of the incident-photon energy. Acceptance of reaction $\gamma p \rightarrow \pi^+ n$ drops at higher beam energies as charged pions punch through the crystals, and the energy of the neutron cluster does not reflect its kinetic energy. Reaction $\gamma n \rightarrow \pi^- p$ above 0.8 GeV has an acceptance that is better than that for $\gamma p \rightarrow \pi^+ n$ as the energy and angles of the cluster from the outgoing proton can be used to reconstruct the reaction kinematics.

We are going to use our FSI technology to apply for the upcoming JLab CLAS (g13 run period) $d\sigma/d\Omega$ for $\gamma n \rightarrow \pi^- p$ covering E = 400 - 2500 MeV and $\theta = 18^\circ - 152^\circ$ [25]. This data set will bring about 11k new measurements which quadruple the world $\gamma n \rightarrow \pi^- p$ database. The ELPH facility at Tohoku Univ. will bring new $d\sigma/d\Omega$ for $\gamma n \rightarrow \pi^0 n$ below E = 1200 MeV [26].

7 Summary for Neutron Study

- The differential cross section for the processes $\gamma n \rightarrow \pi^- p$ was extracted from new CLAS and MAMI-B measurements accounting for Fermi motion effects in the IA as well as NN- and πN-FSI effects beyond the IA.
- Consequential calculations of the FSI corrections, as developed by the GW-ITEP Collaboration, was applied.
- New cross sections departed significantly from our predictions, at the higher energies, and greatly modified the fit result.

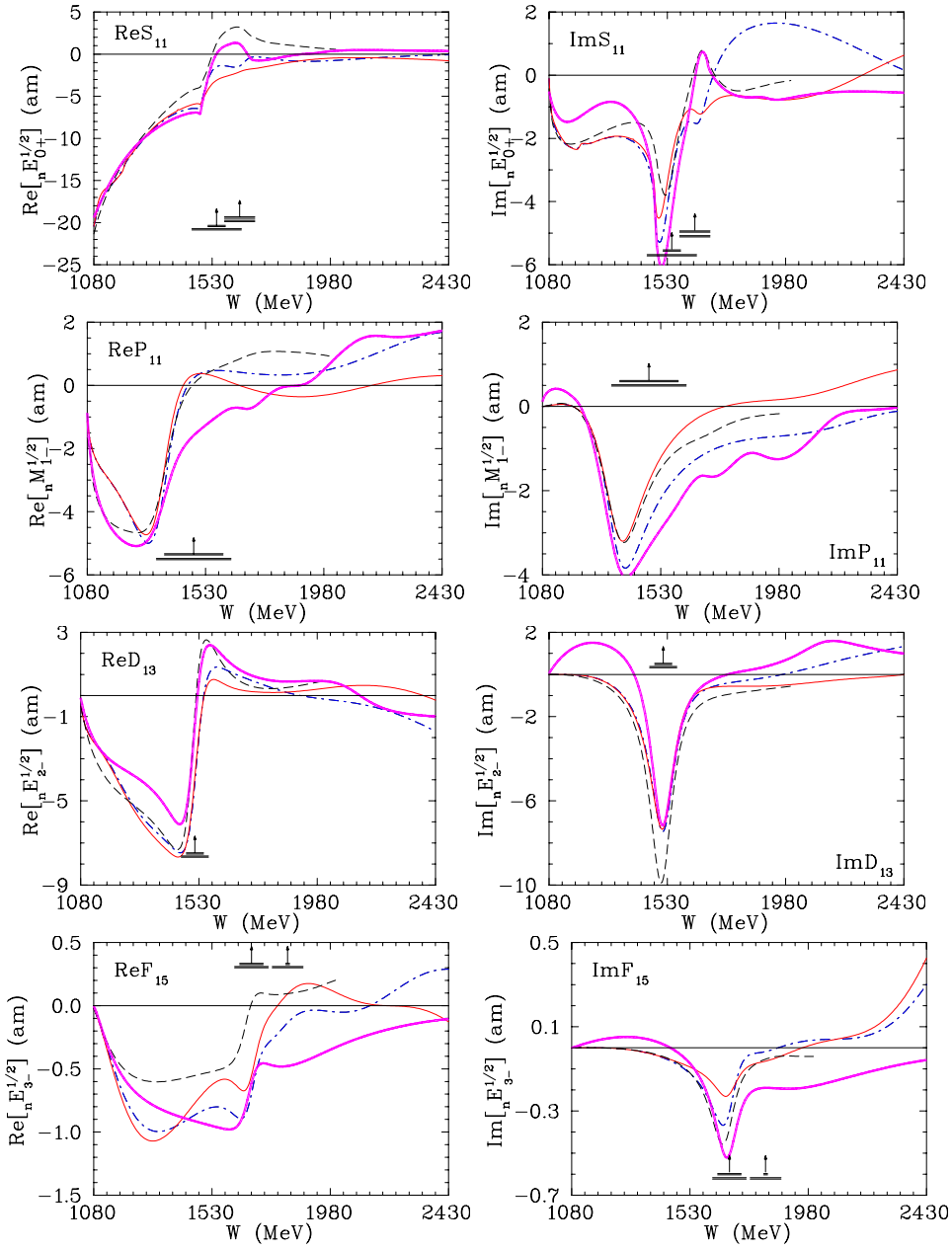

Fig. 5. Samples of neutron multipoles I = 1/2 and 3/2. Solid (dash-dotted) lines correspond to the SAID GB12 [10] (SN11 [17]) solution. Thick solid (dashed) lines give SAID GZ12 [10] solution (MAID07 [20]). Vertical arrows indicate mass (WR), and horizontal bars show full, Γ, and partial, $\Gamma_{\pi N}$, widths of resonances extracted by the Breit-Wigner fit of the πN data associated with the SAID solution WI08 [3].

- New $\gamma n \to \pi^- p$ and $\gamma n \to \pi^0 n$ data will provide a critical constraint on the determination of the multipoles and EM couplings of low-lying baryon resonances using the PWA and coupled channel techniques.

- Polarized measurements at JLab/JLab12, MAMI, SPring-8, CBELSA, and ELPH will help to bring more physics in.
- FSI corrections need to apply.

Acknowledgements

The authors are grateful to A. E. Kudryavtsev, V. V. Kulikov, M. Maremianov, V. E. Tarasov, and R. L. Workman for many useful communications and discussions. This material is based upon work supported by the U.S. Department of Energy, Office of Science, Office of Nuclear Physics, under Award Number DE-FG02-99-ER41110.

References

1. K. A. Olive *et al.* (Particle Data Group), Chin. Phys. C **38**, 090001 (2014).
2. K.M. Watson, Phys. Rev. **95**, 228 (1954); R.L. Walker, Phys. Rev. **182**, 1729 (1969).
3. R.A. Arndt, W.J. Briscoe, I.I. Strakovsky, and R.L. Workman, Phys. Rev. C **74**, 045205 (2006).
4. Ya.I. Azimov and I.I. Strakovsky, Proceedings of the *XVth International Conference on Hadron Spectroscopy* (Hadron 2013), Nara, Japan, Nov. 2013, PoS (Hadron 2014) 034.
5. A.B. Migdal, JETP **1**, 2 (1955); K.M. Watson, Phys. Rev. **88**, 1163 (1952).
6. V.E. Tarasov, W.J. Briscoe, H. Gao, A.E. Kudryavtsev, and I.I. Strakovsky, Phys. Rev. C **84**, 035203 (2011).
7. A.M. Sandorfi, B. Dey, A. Sarantsev, L. Tiator, and R. Workman, AIP Conf. Proc. **1432**, 219 (2012); K. Nakayama, private communication, 2014.
8. W.J. Briscoe, I.I. Strakovsky, and R.L. Workman, Institute of Nuclear Studies of The George Washington University Database; http://gwdac.phys.gwu.edu/analysis/pr_analysis.html .
9. A. Shafi *et al.*, Phys. Rev. C **70**, 035204 (2004).
10. W. Chen, H. Gao, W.J. Briscoe, D. Dutta, A.E. Kudryavtsev, M. Mirazita, M.W. Paris, P. Rossi, S. Stepanyan, I.I. Strakovsky, V.E. Tarasov, and R.L. Workman, Phys. Rev. C **86**, 015206 (2012).
11. W.J. Briscoe, A.E. Kudryavtsev, P. Pedroni, I.I. Strakovsky, V.E. Tarasov, and R.L. Workman, Phys. Rev. C **86**, 065207 (2012).
12. M. Dugger, J.P. Ball, P. Collins, E. Pasyuk, B.G. Ritchie, R.A. Arndt, W.J. Briscoe, I.I. Strakovsky, R.L. Workman *et al.* (CLAS Collaboration), Phys. Rev. C **76**, 025211 (2007).
13. R.A. Arndt, W.J. Briscoe, I.I. Strakovsky, and R.L. Workman, Phys. Rev. C **76**, 025209 (2007).
14. R. Machleidt, K. Holinde, and C. Elster, Phys. Rep. **149**, 1 (1987).
15. P. Benz *et al.* (Aachen-Bonn-Hamburg-Heidelberg-Muenchen Collaboration), Nucl. Phys. B **65**, 158 (1973).
16. V. Tarasov, A. Kudryavtsev, W. Briscoe, M. Dieterle, B. Krusche, I. Strakovsky, and M. Ostrick, to be published in Yad. Fiz. **79** (2016) [Phys. At. Nucl. **79** (2016)] ; arXiv:1503.06671 [hep.ph].
17. R.L. Workman, W.J. Briscoe, M.W. Paris, and I.I. Strakovsky, Phys. Rev. C **85**, 025201 (2012).
18. G. Mandaglio *et al.* (GRAAL Collaboration), Phys. Rev. C **82**, 045209 (2010).

19. R. Di Salvo *et al.* (GRAAL Collaboration), Eur. Phys. J. A **42**, 151 (2009).
20. D. Drechsel, S.S. Kamalov, and L. Tiator, Eur. Phys. J. A **34**, 69 (2007); http://www.kph.uni-mainz.de/MAID/ .
21. A. Anisovich, V. Burkert, E. Klempt, V.A. Nikonov, A.V. Sarantsev, and U. Thoma, Eur. Phys. J. A **49**, 67 (2013).
22. M. Shrestha and D.M. Manley, Phys. Rev. C **86**, 055203 (2012).
23. *Meson production off the deuteron. I*, Spokespersons: W.J. Briscoe and I.I. Strakovsky (A2 Collaboration), MAMI Proposal MAMI-A2-02/12, Mainz, Germany, 2012.
24. *Meson production off the deuteron. II*, Spokespersons: W.J. Briscoe, V.V. Kulikov, K. Livingston, and I.I. Strakovsky (A2 Collaboration), MAMI Proposal MAMI-A2-02/13, Mainz, Germany, 2013.
25. P. Mattione, Proceedings of the *XVth International Conference on Hadron Spectroscopy* (Hadron 2013), Nara, Japan, Nov. 2013, PoS (Hadron 2014) 096.
26. T. Ishikawa *et al.*, Proceedings of the *XVth International Conference on Hadron Spectroscopy* (Hadron 2013), Nara, Japan, Nov. 2013, PoS (Hadron 2014) 095.

BLED WORKSHOPS
IN PHYSICS
VOL. 16, NO. 1
p. 59

Proceedings of the Mini-Workshop
Exploring Hadron Resonances
Bled, Slovenia, July 5 - 11, 2015

Exciting Baryon Resonances with Meson Photoproduction*

L. Tiator[a], A. Svarc[b]

[a] Institut für Kernphysik, Johannes Gutenberg Universtät Mainz, Germany
[b] Rudjer Boskovic Institute, Zagreb, Croatia

Abstract. Light hadron spectroscopy is still an exciting field in nuclear and particle physics. Even 50 years after the discovery of the Roper resonance and more than 30 years after the pioneering work of Hoehler and Cutkosky many questions remain for baryon resonances. Nowadays the main excitation mechanism is photo- and electroproduction of mesons, studied at electron accelerator labs as MAMI, ELSA and JLab. In a combined effort, pole positions and residues are searched from partial waves, which are obtained in a partial wave analysis from recently measured polarization observables using analytical constraints from fixed-t dispersion relations. Special emphasis is placed on the pole structure of baryon resonances on different Riemann sheets.

1 Introduction

Fifty years ago the Roper resonance was found in partial wave analysis (PWA) of pion nucleon scattering [1]. In the following decades more than 30 N and Δ resonances were also found in PWA. For many of these resonances the properties are still uncertain and need to be improved in more precise experiments, which is nowadays only possible with photon and electron beams. Due to the helicity nature of the photon in the initial state, the number of invariant amplitudes is twice as large and the number of observables is a factor of four larger than in pion nucleon scattering. Therefore, a model independent determination of the partial waves and the underlying nucleon resonances is far more involved and improved analysis tools are required.

2 Resonances as poles on different Riemann sheets

Thresholds and resonance positions are commonly used as the most important and physical properties of partial waves in scattering and production reactions. However, at a closer look, resonance positions described in a Breit-Wigner ansatz appear different in different analyses, especially when also different reaction channels are analyzed. Also production thresholds, as $\pi\pi$N or $\pi\pi\pi$N are not the most relevant positions, where new dynamics is observed. E.g. at the $\pi\pi$N threshold,

* Talk presented by L. Tiator

$W = m_p + 2m_\pi = 1208$ MeV, no single partial wave shows a signature of inelasticity, even as this process is kinematically allowed.

The relevant properties of partial waves are the pole positions and well selected real or complex branch points (b.p.). Pole positions have long been realized as the fundamental resonance parameters that are not influenced by background contributions, which will be different for different reaction channels. In photoproduction, background is very small for η or η' production, but large or even very large for π and K production. In the latter case, the background is not very well known, even the coupling constants of the Born terms for (γ, K) are quite uncertain.

Real branch points coincide with thresholds, like $\pi N, \eta N, \eta' N$, complex branch points appear as effective branch points for 3- and more-body final states. A very important complex branch point is the $\pi\Delta$ b.p. with $W_{bp} = 135 + 1210 - 50i = (1345 - 50i)$ MeV and also the ρN b.p. with $W_{bp} = 763 - 72i + 938 = (1701 - 72i)$ MeV. These branch points play an important role in the P_{11} partial wave, other partial waves are also influenced by less amount. Their role is especially pronounced, if a pole position gets close to such a complex b.p., which is the case for $P_{11}(1440)$ with $W_p = (1365 - 95i)$ MeV and $P_{11}(1710)$ with $W_p = (1720 - 115i)$ MeV.

This knowledge is used in the Laurent-plus-Pietarinen expansion (L+P) of partial waves, recently developed by the Zagreb/Tuzla group and applied so far to πN scattering, pion photoproduction and coupled π, η channels [2, 3]. Photoproduction of η and η' and pion electroproduction analyses are in progress.

For a given partial wave, e.g. for $\pi N \to \pi N$ or $\gamma N \to \pi N$, $\alpha = \{L, J, T\}$ with angular momentum L, spin J and isospin T, the partial wave amplitude can in general be split in a resonance and a background part, where the background part is simply everything, that is missing in the resonance ansatz,

$$t_\alpha(W) = \frac{\beta\,\Gamma/2}{M - W - i\,\Gamma/2}\, e^{i\phi} \;+\; \text{b.g.}(W)\,.$$

In general, Γ, β, ϕ can be functions of W, in particular for a very simple case

$$\Gamma(W) = \frac{q_{\pi N}(W)}{q_{\pi N}(M)}\,\frac{M}{W}\,\beta_{\pi N}\,\Gamma_{total} \;+\; \{\pi\pi N,\, \pi\Delta,\, \eta N \;+\; \cdots\}$$

with the pion c.m. momentum

$$\begin{aligned} &q_{\pi N}(W) \\ &= \frac{\sqrt{(W^2 - (m_p + m_\pi)^2)(W^2 - (m_p - m_\pi)^2)}}{2W} \\ &= \frac{\sqrt{W - (m_p + m_\pi)}\,\sqrt{W + (m_p + m_\pi)}\,\sqrt{W - (m_p - m_\pi)}\,\sqrt{W + (m_p - m_\pi)}}{2W}\,. \end{aligned}$$

In the latter expression four square-root branch points show up, where only the first one is in the physical region and is the most important branch point for all partial waves.

The square-root function $\sqrt{x}$ has a branch point at $x = 0$ and is defined on two Riemann sheets (R.S.). Usually the branch cut (b.c.) is chosen to the left as in FORTRAN, C++ or Mathematica. However, any other direction can be freely chosen, according to the convenience of a particular application. In hadronic scattering processes it is often used to the right and an especially convenient way is a branch cut downwards along the negative imaginary axis. For all those definitions the formulas remain the same, except for the square-root function which has to be replaced accordingly by

$$\begin{aligned} \sqrt{z} &\to \sqrt{z} && \text{b.c. to the left,} \\ &\to i\sqrt{-(z+i\varepsilon)} && \text{b.c. to the right,} \\ &\to \sqrt{i}\sqrt{-iz} && \text{b.c. downwards.} \end{aligned}$$

It is important to note, that the $i\varepsilon$ term in Eq. (6) is needed to assure that the real axis (physical axis) belongs to the first Riemann sheet.

In principle it makes no difference, which angle for the branch cut is chosen. Traditionally most often it is the b.c. on the positive real axis to the right side. However, this convention often leads to confusions about the different Riemann sheets, as all sheets starting from real b.p. will overlap. Even b.c. turning into different directions at each different branch point are allowed. In the following we have chosen all branch cuts downwards, as this was once suggested by Dick Arndt [4]. In this convention, all resonances appear as poles on the lower half-plane in the **first** Riemann sheet. In his 'bible' [5], Hoehler defines the resonances as poles in the lower half-plane of the second Riemann sheet, and this convention, where all cuts are drawn to the right, is mostly used in the literature. However, one has to be very careful in numbering the R.S. when more than one threshold is open. Then the second R.S. is always the sheet, which is entered by a direct path from the physical axis down into the next R.S. by crossing one or more cuts. In our notation we give in addition to the somewhat arbitrary numbering also the $\pm$ signs for each branch cut, which makes the definition unique.

Generally with each new branch point the number of Riemann sheets gets doubled and of course all R.S. exist in the whole complex energy plane, also below the branch points. For a partial wave with 3 decay channels one must consider in principle 8 Riemann sheets. But less important decay channels are usually ignored in order to get the number of R.S. smaller. For the $\Delta(1232)$ in the P_{33} partial wave, it can be simplified by only two R.S., where the 2 poles in the first and second R.S. are symmetric above and below the real axis.

In Fig. 1 we show as the first non-trivial case the Roper resonance on four Riemann sheets. The Roper decays to almost 100% in πN and $\pi\Delta$, as the effective $\pi\pi N$ channel. Introducing a complex $\pi\Delta$ branch point leads to the very interesting situation, that the Roper pole appears very near to the b.p. in the first Riemann sheet. Another 2 poles show up in the upper half-plane of the second and third R.S. and are uninteresting. A lot of interest, however, caused the fourth pole, which is in the lower half-plane of the 4. R.S. and often this has been especially reported in mostly dynamical approaches. But certainly it is a shadow pole and

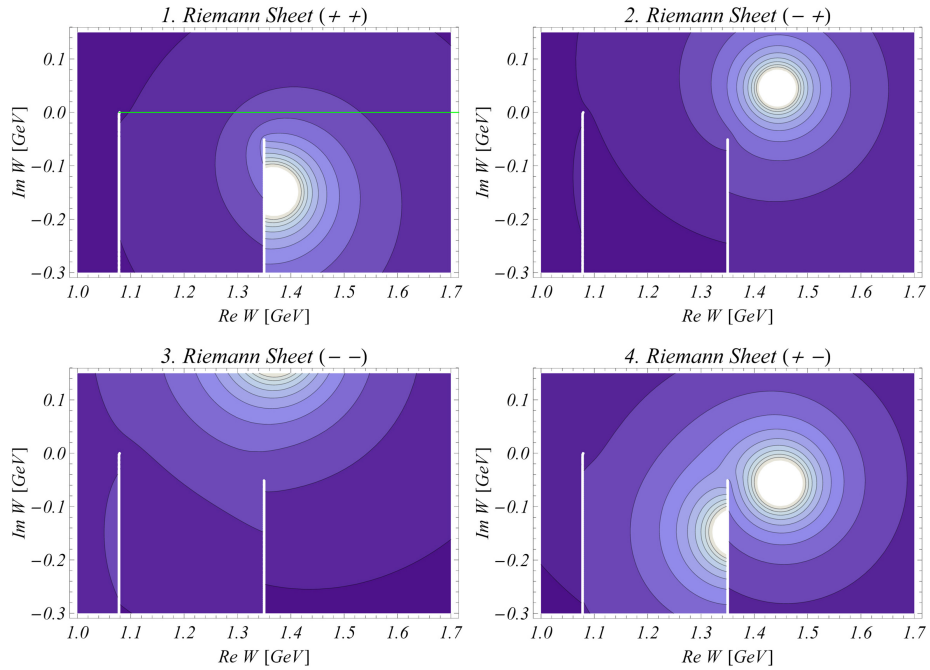

Fig. 1. Contour plots of the absolute magnitude of the P_{11} partial wave in the complex energy plane W with poles of the N(1440) P_{11} resonance on 4 different Riemann sheets. The white vertical lines show the branch cuts originating at the real b.p. πN and the complex b.p. $\pi\Delta$ and the green horizontal line shows the physical axis on the first Riemann sheet.

from Fig. 1(d) it can be judged how big the influence of this pole could be on the physical axis in Fig. 1(a). In fact it is practically negligible.

Another interesting case is the $N(1535)1/2^-$ resonance in the S_{11} partial wave. In Fig. 2 it appears in a normal scenario together with its partner $N(1650)1/2^-$ in the lower half-plane of the first Riemann sheet, if we again draw all branch cuts downwards. As it is long known and already stressed by Hoehler, the $N(1535)1/2^-$ pole sits very close near the ηN threshold and one can clearly see its influence also in the fourth R.S. Now, by a small change of parameters, this pole can move below the ηN cut and appears as a shadow pole in the fourth R.S., see Fig. 3. This scenario is realized in the Argonne-Osaka model [6], where the pole was found at $W_p = (1482 - 98i)$ MeV, only 4 MeV below ηN threshold. A shadow pole in the 4. R.S., so close to the branch point, without another counter part, certainly shows up with structure in the first R.S. and mocks a regular pole of the first R.S. However, all parameters of this shadow pole are a little bit surprising with different values compared to other PWA.

3 Complete experiments

A complete experiment is a set of measurements which is sufficient to predict all other possible experiments, provided that the measurements are free of uncer-

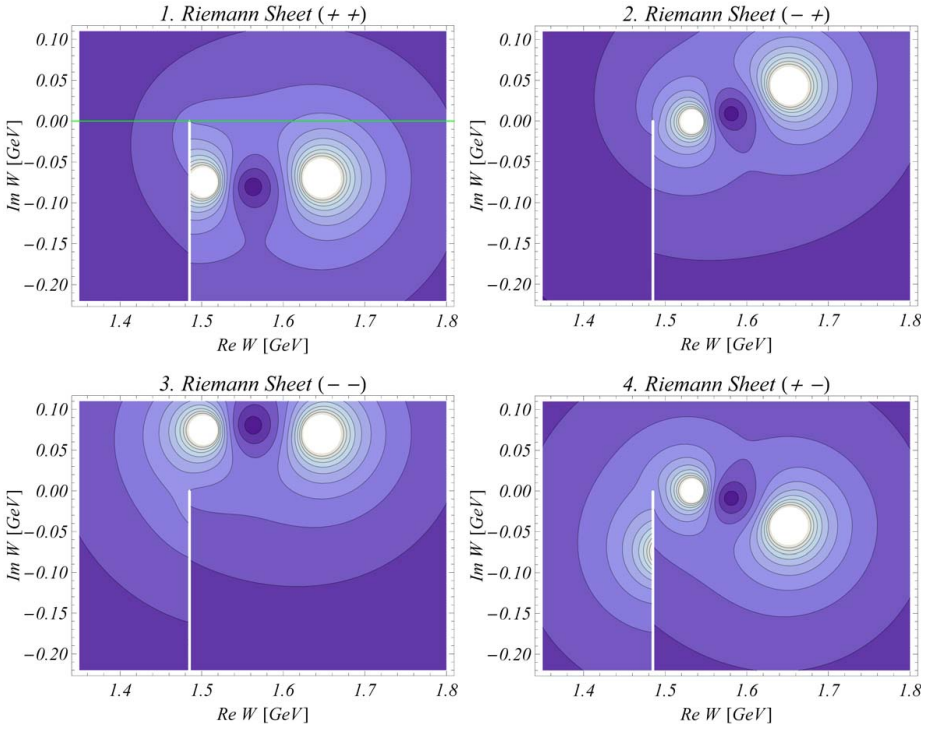

Fig. 2. Poles of N(1535) and N(1650) S_{11} resonances on 4 different Riemann sheets. The white vertical line shows the branch cut originating at the real b.p. ηN. The real b.p. πN is outside the plotted range. The green horizontal line shows the physical axis on the first Riemann sheet.

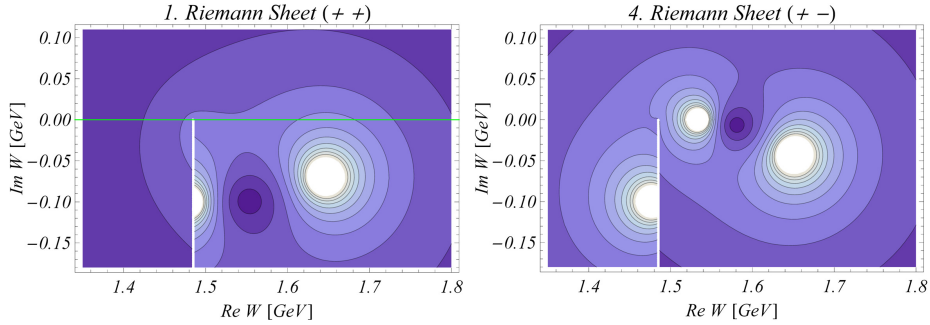

Fig. 3. Poles of N(1535) and N(1650) S_{11} resonances on the first and fourth Riemann sheets in an alternative scenario compared to Fig. 2. The N(1535) disappears form the first R.S. and appears as a shadow pole on the fourth R.S. Notation as in Fig. 2.

tainties. Using this maximal experimental information, the four complex CGLN, helicity or transversity amplitudes can be uniquely determined up to one overall energy- and angle-dependent phase, due to bilinear products of amplitudes for all observables. Starting in the 1970s many people studied the complete experi-

ment for pseudoscalar meson photoproduction and as a benchmark publication the work of Chiang and Tabakin [7] is considered who give tables where all possible combinations for such an experiment are given with the minimal number of 8 observables. In short, these 8 observables have to be chosen with beam, target and recoil polarization, which makes it in practise very difficult. Only in the last few years this goal has been achieved at JLab with $K\Lambda$ photoproduction, where the recoil polarization of the outgoing hyperon is given for free, due to its weak self-analyzing decay. For pion and eta photoproduction meanwhile at Mainz, Bonn and JLab all 8 observables with beam and target polarization are measured over a wide energy region and with almost full angular coverage. Most of them are currently analyzed and some are already published. The 2 missing observables with beam-recoil double polarization have only been measured in a pilot experiment at MAMI using secondary rescattering of the outgoing proton. Only a few data points with rather limited statistics were obtained [8].

However, as it was shown by Omelaenko [9] in 1981 and recently revisited by Wunderlich et al. [10, 11], a complete truncated partial wave analysis can be obtained with only 5 observables, where recoil observables can be completely avoided. Under these assumptions all partial wave amplitudes up to a finite angular momentum L_{max} can be uniquely determined up to an overall energy-dependent phase. At first this looks as a paradox situation, however, in this latter case of a truncated partial wave analysis, the summation over all partial waves is never the same as it is in the first case with the full angle dependent amplitudes. And in a realistic case, even $L_{max} = 5$ is hard to realize. Therefore, the difference should be understood in such a way, that with the complete experiment of 8 observables one gets the additional information with all partial waves beyond L_{max}. Wunderlich et al. further showed that the complexity of the ambiguity structure drastically increases, when partial waves are considered beyond S and P waves, the case that Omelaenko initially studied. In such a more realistic case with D and F waves an unrealistically high precision of the observables were needed in order to find a unique solution. This can only be obtained in simulations with numerical observables obtained from a model with 10 or more significant digits. In a truncated PWA the contributions from higher partial waves can either be ignored or added from a model, e.g. from Born terms and/or Regge trajectories.

Therefore, if a truncated partial wave analysis is performed from a complete experiment with realistic pseudo data or with experimental data, multiple solutions will appear, which can not be distinguished. The envelope of such a large range of equally good solutions will then produce partial wave amplitudes with very large error bands [12]. From this observation a somewhat pessimistic view can easily arise that a model-independent PWA is simply impossible.

4 Partial wave analysis with analytical constraints

The most common way to get a stable solution for single-energy (SE) PWA is a fit constrained by an energy-dependent solution in a model-dependent approach. This has been done mostly for pion photoproduction by SAID, MAID, BnGa groups, the latter also tried this for eta photoproduction. For low and dominant

partial waves this leads to similar solutions, but for smaller and higher partial waves all solutions will be different. Furthermore, the errors given in such SE analyses are just reflecting the statistical errors of the fitted experimental observables.

In a collaboration with groups from Mainz, Tuzla and Zagreb (MTZ) we are now analyzing data sets with analytical constraints from fixed-t dispersion relations. The method is similar to the pion nucleon PWA obtained in the 80s by Hoehler and Pietarinen and is described in detail in the contribution of Stahov to this workshop [13]. It enforces analyticity both in s and in t and in particular continuity in energy. Such constraints are based on fundamental symmetries and do not follow any model assumption. Finally, our goal of getting baryon resonance parameters in a model-independent way will be reached by analyzing the model-independent SE partial wave solutions obtained in the step before.

5 Baryon resonance analysis with the L+P method

Over the last few years Svarc et al. [2,3] have developed a very efficient resonance analysis method in order to find pole positions and residues from partial wave amplitudes over a large energy range. In this approach the most important properties of partial waves, poles and branch points are used as physical parameters and an expansion in terms of Pietarinen functions is used to describe the partial wave amplitudes over the whole energy range, giving more confidence on the obtained pole parameters of baryon resonances as with local methods like the speed-plot technique, first proposed by Hoehler.

The method is well described in articles with applications on pion nucleon scattering and pion photoproduction [2,3]. In summary, the set of equations which define the Laurent expansion + Pietarinen series method (L+P method) is given by

$$T(W) = \sum_{i=1}^{k} \frac{a_{-1}^{(i)}}{W - W_i} + B^L(W)$$

$$B^L(W) = \sum_{n=0}^{N_1} c_n X(W)^n + \sum_{n=0}^{N_2} d_n Y(W)^n + \sum_{n=0}^{N_3} e_n Z(W)^n + \cdots$$

$$X(W) = \frac{\alpha - \sqrt{x_P - W}}{\alpha + \sqrt{x_P - W}};\ Y(W) = \frac{\beta - \sqrt{x_Q - W}}{\beta + \sqrt{x_Q - W}};\ Z(W) = \frac{\gamma - \sqrt{x_R - W}}{\gamma + \sqrt{x_R - W}} + \cdots,$$

where $W_i, a_{-1}^{(i)}$ are the complex pole positions and corresponding residues and x_P, x_Q, x_R are real or complex branch points. Usually, the first b.p. x_P is used as an effective b.p. for the left-hand cuts, x_Q is the πN threshold and x_R is an effective multi-pion branch point, which can correspond to $\pi\Delta$, ηN, or any other channel. If necessary, a fourth Pietarinen etc. can be added. $c_n, d_n, e_n, \alpha, \beta, \gamma$ are real parameters and the number of terms N_1, N_2, N_3 of the Pietarinen series is typically between 10-20. In Fig. 4 we show four examples of pion photoproduction partial waves (multipoles) from MAID2007 SE solutions [14], where the L+P

method yields pole parameters consistent with PDG. Further details can be found in Ref. [3].

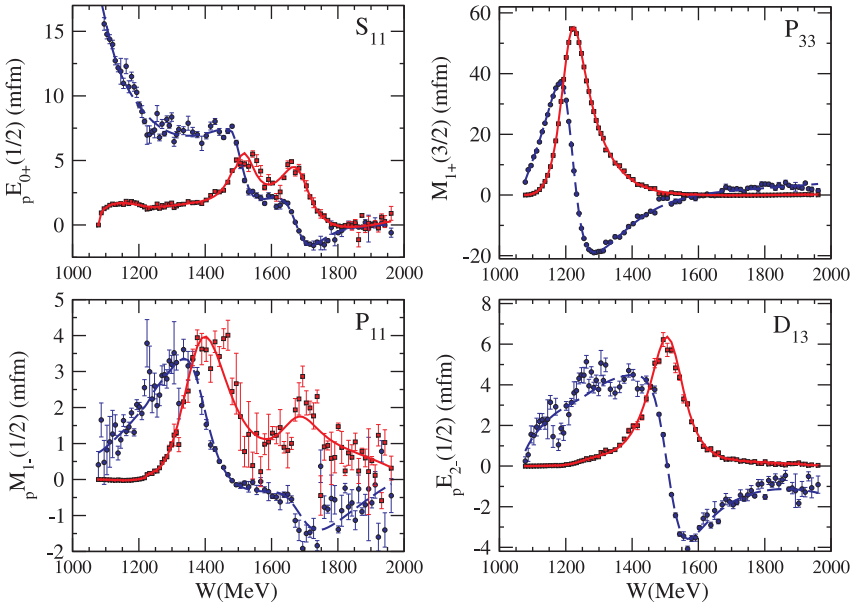

Fig. 4. L+P fit to MAID2007 SE solutions. Dashed blue, and full red lines denote real and imaginary parts of multipoles respectively.

6 Summary and conclusions

The study of baryon resonances is still an exciting field in hadron physics. While a large series of resonances are already known for a long time, in most cases only the dominant branching channels are well investigated. From still ongoing experiments at Mainz, Bonn and JLab, meson photo- and electroproduction data will be available partly with unprecedented precision and with different kind of beam, target and recoil polarization. With this large new database partial wave analyses can be obtained for various channels and more accurate and also new baryon resonance properties can be analyzed. In reactions different from πN also new resonances can be found, especially in the region $W > 1.8$ GeV, as it was already reported in a PWA mainly from new KΛ photoproduction data [15].

We would like to thank the Deutsche Forschungsgemeinschaft DFG for the support by the Collaborative Research Center 1044.

References

1. L. D. Roper, Phys. Rev. Lett. **12**, 340 (1964).

2. A. Svarc, M. Hadzimehmedovic, H. Osmanovic, J. Stahov, L. Tiator and R. L. Workman, Phys. Rev. C **88**, 035206 (2013).
3. A. Svarc, M. Hadzimehmedovic, H. Osmanovic, J. Stahov, L. Tiator and R. L. Workman, Phys. Rev. C **89**, 065208 (2014).
4. R. A. Arndt, R. L. Workman, Z. Li *et al.*, Phys. Rev. C **42**, 1853 (1990).
5. G. Höhler and H. Schopper, Berlin, Germany: Springer (1982) 407 P. (Landolt-Börnstein: Numerical Data and Functional Relationships In Science and Technology. New Ser., I/9B1)
6. H. Kamano, S. X. Nakamura, T.-S. H. Lee and T. Sato, Phys. Rev. C **88**, 035209 (2013).
7. W. T. Chiang and F. Tabakin, Phys. Rev. C **55**, 2054 (1997).
8. M. H. Sikora *et al.*, Phys. Rev. Lett. **112**, 022501 (2014).
9. A. S. Omelaenko, Sov. J. Nucl. Phys. **34**, 406 (1981).
10. Y. Wunderlich, R. Beck and L. Tiator, Phys. Rev. C **89**, 055203 (2014).
11. Y. Wunderlich, Proc. of the Mini-Workshop on Exploring Hadron Resonances, Bled (Slovenia), July 5-11, 2015, in this volume.
12. A.M. Sandorfi, S. Hoblit, H. Kamano, T.-S.H. Lee, J. Phys. G **38**, 053001 (2011).
13. J. Stahov et al., Proc. of the Mini-Workshop on Exploring Hadron Resonances, Bled (Slovenia), July 5-11, 2015, in this volume.
14. D. Drechsel, S. S. Kamalov, L. Tiator, Eur. Phys. J. A **34**, 69 (2007).
15. A. V. Anisovich, R. Beck, E. Klempt, V. A. Nikonov, A. V. Sarantsev and U. Thoma, Eur. Phys. J. A **48**, 15 (2012).

BLED WORKSHOPS
IN PHYSICS
VOL. 16, NO. 1
p. 68

Proceedings of the Mini-Workshop
Exploring Hadron Resonances
Bled, Slovenia, July 5 - 11, 2015

Complete experiments in pseudoscalar meson photoproduction

Yannick Wunderlich

Helmholtz-Institut f"ur Strahlen- und Kernphysik, Universit"at Bonn, Nussallee 14-16, 53115 Bonn, Germany

Abstract. The problem of extracting photoproduction amplitudes uniquely from so called complete experiments is discussed. This problem can be considered either for the extraction of full production amplitudes, or for the determination of multipoles. Both cases are treated briefly. Preliminary results for the fitting of multipoles, as well as the determination of their error, from recent polarization measurements in the Δ-region are described in more detail.

1 Introduction to the formalism

For the photoproduction of a single pseudoscalar mesons, i.e. $\gamma N \longrightarrow \mathcal{P}B$, it can be shown that the most general expression for the reaction amplitude, with spin and momentum variables specified in the center of mass frame (CMS), reads (cf. the work by CGLN [1])

$$F_{CGLN} = i\boldsymbol{\sigma}\cdot\hat{e}\,F_1 + \boldsymbol{\sigma}\cdot\hat{q}\;\boldsymbol{\sigma}\cdot\hat{k}\times\hat{e}\,F_2 + i\boldsymbol{\sigma}\cdot\hat{k}\;\hat{q}\cdot\hat{e}\,F_3 + i\boldsymbol{\sigma}\cdot\hat{q}\;\hat{q}\cdot\hat{e}\,F_4\,. \qquad (1)$$

Each spin-momentum structure in this expansion is multiplied by a complex function depending on the total energy W and meson scattering angle θ in the CMS. The 4 functions $\{F_i(W,\theta); i = 1,\ldots,4\}$ are called CGLN-amplitudes and contain all information on the dynamics of the reaction.

Since all particles in the reaction except for the meson $\mathcal{P}$ have spin, the preparation of the spin degrees of freedom in the initial state as well as the (generally more difficult) measurement of the polarization of the recoil baryon B facilitate the experimental determination of 16 polarization observables, summarized in Table 1. All observables are definable as asymmetries among different polarization states (see [2]). They contain the unpolarized differential cross section σ_0, the three single spin observables $\{\Sigma, T, P\}$ (corresponding to beam, traget and recoil polarization), as well as twelve double polarization observables which are divisible into the distinct classes of beam-target (BT), beam-recoil (BR) and target-recoil (TR) observables.

Once the equations connecting the measurable observables to the model independent production amplitudes are worked out (reference [2] contains instructions on how to do this), it becomes apparent that all of these relations can be

Table 1. The 16 polarization observables accessible in pseudoscalar meson photoproduction (for a more elaborate version of this Table, cf. [2]).

Beam		Target	Recoil	Target + Recoil
	-	- - -	x' y' z'	x' x' z' z'
	-	x y z	- - -	x z x z
unpolarized	σ_0	T	P	$T_{x'}$ $L_{x'}$ $T_{z'}$ $L_{z'}$
linearly pol.	Σ	H P G	$O_{x'}$ T $O_{z'}$	
circularly pol.		F E	$C_{x'}$ $C_{z'}$	

summarized by the relation

$$\check{\Omega}^{\alpha} = \frac{q}{k}\frac{1}{2}\sum_{i,j=1}^{4} F_i^* \hat{A}_{ij}^{\alpha} F_j = \frac{q}{k}\frac{1}{2}\langle F|\,\hat{A}^{\alpha}\,|F\rangle\,, \quad \alpha = 1,\ldots,16. \tag{2}$$

The 16 real profile functions $\check{\Omega}^{\alpha}$, connected to the polarization observables via $\check{\Omega}^{\alpha} = \sigma_0\Omega^{\alpha}$, are bilinear hermitean forms in the CGLN amplitudes and can be represented by the generally complex hermitean matrices $\hat{A}^{\alpha}$ (cf. [5] for a listing of those).

A change of the basis of spin quantization for the photoproduction reaction allows for the definition of different systems of spin amplitudes. Helicity amplitudes $H_i\,(W,\theta)$ or transversity amplitudes $b_i\,(W,\theta)$ are possible choices (cf. [4]). The different kinds of amplitdues are all related among each other in a linear and invertible way. Therefore, they can be seen as fully equivalent regarding their information content. The expressions for the polarization observables in the afore mentioned different systems of spin amplitudes retain the mathematical structure of equation (2), while the observables are now represented by different matrices

$$\check{\Omega}^{\alpha} = \frac{q}{k}\frac{1}{2}\langle H|\,\Gamma^{\alpha}\,|H\rangle = \frac{q}{k}\frac{1}{2}\langle b|\,\tilde{\Gamma}^{\alpha}\,|b\rangle\,. \tag{3}$$

The Γ^{α} (or $\tilde{\Gamma}^{\alpha}$ in case of transversity amplitudes) are a set of 16 hermitean unitary Dirac Γ-matrices (cf. [4,5]). They have useful properties, the exploitation of which facilitates the identification of complete experiments.

2 Complete experiments for spin amplitudes

Since photoproduction allows access to 16 polarization observables but needs 4 complex amplitudes for a model independent description (constituting just 8 real numbers), the fact can be anticipated that measuring all observables would mean an overdetermination for the problem of extracting amplitudes.

This issue has triggered investigations on so called complete experiments (cf. [3,4]), which are subsets of a minimum number of observables that allow for

a unique extraction of the amplitudes. Here one generally means unique only only up to an overall phase, since equations (2, 3) are invariant by a simultaneous rotation of all amplitudes by the same phase. Also, the complete experiment problem is first of all a precise mathematical problem disgregarding measurement uncertainties.

Chiang and Tabakin have published a solution to this problem (cf. [4]) that shall be depicted here. First of all it was noted that, using the fact that the $\tilde{\Gamma}$-matrices are an orthonormal basis of the complex 4×4-matrices, equation (3) can be inverted in order to yield expressions for the bilinear products

$$b_i^* b_j = \frac{1}{2} \sum_\alpha \left(\tilde{\Gamma}_{ij}^\alpha\right)^* \check{\Omega}^\alpha. \tag{4}$$

This relation allows for the determination of the moduli $|b_i|$ and relative phases ϕ_{ij}^b of the b_i and therefore fully constrains them up to an overall phase. Generalizations of equation (4) for helicity and CGLN amplitudes are possible (see [5]) but shall not be quoted here.

Another important property of the $\tilde{\Gamma}$ is that they imply quadratic relations among the observables known as the Fierz identities (see [4])

$$\check{\Omega}^\alpha \check{\Omega}^\beta = \sum_{\delta,\eta} C_{\delta\eta}^{\alpha\beta} \check{\Omega}^\delta \check{\Omega}^\eta, \tag{5}$$

where $C_{\delta\eta}^{\alpha\beta} = (1/16)\,\mathrm{Tr}\left[\tilde{\Gamma}^\delta \tilde{\Gamma}^\alpha \tilde{\Gamma}^\eta \tilde{\Gamma}^\beta\right]$.

Equations (4) and (5) are all that is needed to prove that 8 carefully chosen observables suffice in order to obtain a complete experiment ([4]). Among those should be the unpolarized cross section and the three single polarization observables. The remaining quantities have to be picked from at least two different classes of double polarization observables, with no more than two of them from the same class. The word 'prove' means in this case that for all cases mentioned in reference [4], equation (5) was used to express the missing 8 observables in terms of the measured ones.

In practical investigations of photoproduction data, the goal is not to determine the full reaction amplitudes, but rather the partial waves, in this case called multipoles.

3 Complete experiments in a truncated partial wave analysis

The expansions of the full amplitudes F_i into multipoles are known (cf. eg. [2]). In case these expansions are truncated at some finite angular momentum quantum number ℓ_{max}, an approximation that is justified for reactions with supressed background contributions (eg. π^0 photoproduction), then the profile functions defined in equation (2) can be arranged as a finite expansion into associated Legendre polynomials

$$\check{\Omega}^\alpha(W,\theta) = \frac{q}{k} \sum_{k=\beta_\alpha}^{2\ell_{max}+\beta_\alpha+\gamma_\alpha} (a_L)_k^\alpha(W)\, P_k^{\beta_\alpha}(\cos\theta), \tag{6}$$

$$(a_L)_k^\alpha(W) = \langle \mathcal{M}_{\ell_{max}}(W)|\,(\mathcal{C}_L)_k^\alpha\,|\mathcal{M}_{\ell_{max}}(W)\rangle. \tag{7}$$

The parameters β_α and γ_α defining this expansion are given in Table 2 (the whole notation is according to [6]).

The real Legendre coefficients $(a_L)^\alpha_k$ are given as bilinear hermitean forms in terms of the $4\ell_{max}$ multipoles, which are gathered in the vector $|\mathcal{M}_{\ell_{max}}\rangle$. Therefore, the problem of multipole-extraction from a set of fitted coefficients $(a_L)^\alpha_k$ leads to a similar mathematical structure compared to the equation (2) encountered in the investigation of complete experiments in section 2. The question for such complete sets can now be asked again, but in the context of a truncated partial wave analysis (TPWA).

Table 2. The parameters defining the TPWA problem, equations (6) and (7).

Type	$\check{O}^\alpha$	α	β_α	γ_α	Type	$\check{O}^\alpha$	α	β_α	γ_α
	$I(\theta)$	1	0	0		$\check{O}_{x'}$	14	1	0
S	$\check{\Sigma}$	4	2	-2	BR	$\check{O}_{z'}$	7	2	-1
	$\check{T}$	10	1	-1		$\check{C}_{x'}$	16	1	0
	$\check{P}$	12	1	-1		$\check{C}_{z'}$	2	0	$+1$
	$\check{G}$	3	2	-2		$\check{T}_{x'}$	6	2	-1
BT	$\check{H}$	5	1	-1	TR	$\check{T}_{z'}$	13	1	0
	$\check{E}$	9	0	0		$\check{L}_{x'}$	8	1	0
	$\check{F}$	11	1	-1		$\check{L}_{z'}$	15	0	$+1$

It is a very interesting fact that in this case, the number of observables that is needed for completeness reduces as compared to the case with full production amplitudes. This is true at least in the mathematically precise situation, without measurement uncertainty. The algebra that is needed to prove this result was first worked out by Omelaenko [7] (for a recent and more detailed account, cf. [8]).

It is sufficient to investigate the discrete ambiguities allowed by the group S observables, i.e. $\{\sigma_0, \Sigma, T, P\}$. It is then seen that the latter are invariant under one mathematical ambiguity transformation, called the 'double ambiguity', which is present in principle for all energies. There may also be additional pairs of solutions, called accidential ambiguities, depending on the numerical confguration of the Legendre coefficients. It can however be shown that those play no role for the mathematically exact case. The above mentioned double ambiguity on the other hand can be resolved by either the F or G observable, as well as every observable from the BR and TR classes. Therefore one is lead to mathematically complete sets containing just 5 observables, for example

$$\{\sigma_0, \Sigma, T, P, F\}. \tag{8}$$

4 TPWA fits using the bootstrapping method

Here we will describe preliminary results of a TPWA fit to actual data comprising the set of observables (8). The observables σ_0 and Σ are taken from the works [9]

and [10]. Recent measurements of T and F were performed at MAMI [11]. For P we take the Kharkov data [12].

The fit procedure proceeds as follows, using a truncation at $\ell_{max} = 1$ (S- and P-waves). First, Legendre coefficients are determined by fitting the angular distributions (6) to the data. The index set for the fitted observables is $\alpha_F \in \{1, 4, 10, 12, 11\}$ (cf. Table 2) in this particular case here. In the next step, we minimize the functional (up to now omitting correlations)

$$\Phi_{\mathcal{M}}\left(\mathcal{M}_{\ell_{max}}\right) = \sum_{\alpha_F, k} \left(\frac{\left(a_L^{Fit}\right)_k^{\alpha_F} - \langle \mathcal{M}_{\ell_{max}} | \left(\mathcal{C}_L\right)_k^{\alpha_F} | \mathcal{M}_{\ell_{max}} \rangle}{\Delta\left(a_L^{Fit}\right)_k^{\alpha_F}} \right)^2, \tag{9}$$

using the results from the angular fit and varying the real and imaginary parts of the multipoles (the FindMinimum routine of MATHEMATICA is employed). The overall phase of the multipoles is constrained to $\mathrm{Re}\left[E_{0+}\right] \geq 0$ and $\mathrm{Im}\left[E_{0+}\right] = 0$, since this phase can never be obtained from a truncated fit to the data alone.

In order to exclude any kind of model dependencies, the start parameters for the fit are not taken from a prediction, but are determined randomly by using a Monte Carlo sampling of the relevant, $(8\ell_{max} - 1) = 7$ dimensional multipole space (the space spanned by the real and imaginary parts). This sampling is simplified by the fact that the total cross section $\hat{\sigma}$, being a sum of moduli-squared of multipoles, already constrains the relevant part of the multipole space to a 6 dimensional ellipsoid.

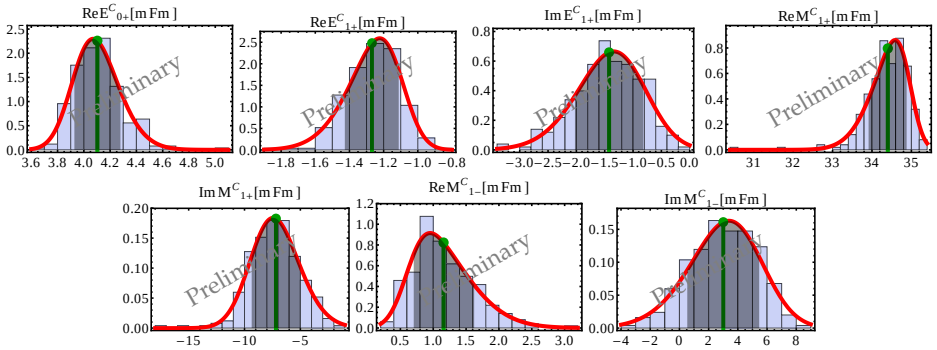

Fig. 1. Histograms resulting from the bootstrapping at $E_\gamma^{LAB} \approx 338\,\mathrm{MeV}$.

The amount of $N_{MC} = 1000$ Monte Carlo start configurations was chosen. It has to be reported that using this procedure, it was possible to find a pronounced best minimum for the dataset under investigation.

In addition one would wish to have an estimate for the errors of the resulting multipoles, as well as a check whether the data allow any ambiguities caused by their finite precision. To achieve both tasks, a method known as 'bootstrapping' was chosen ([13]). In this approach, the data are resampled using a gaussian distribution function centered at $\mu = \check{\Omega}^\alpha$ having a width $\sigma = \Delta\check{\Omega}^\alpha$ for each datapoint. In this way, an ensemble of 250 additional datasets was generated, each

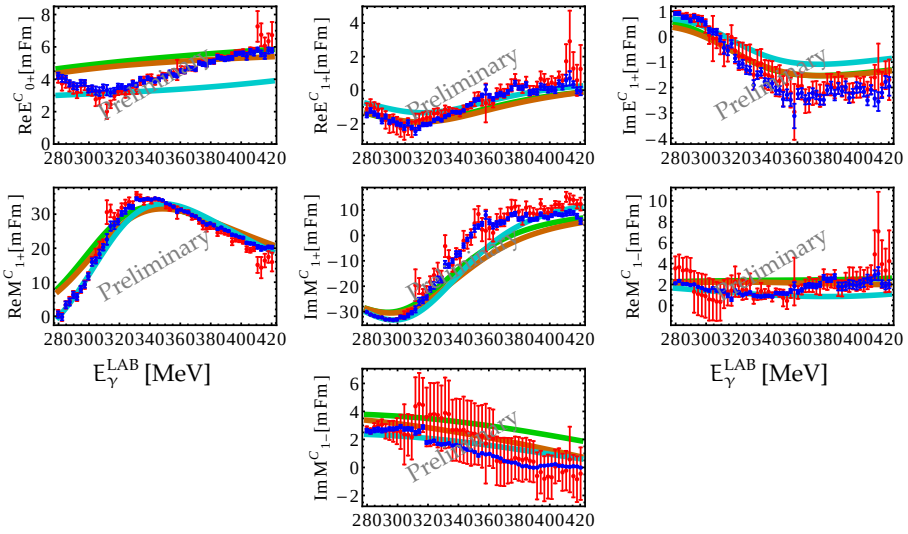

Fig. 2. Results of the bootstrapping procedure for S- and P-wave multipoles (red: Kharkov P data; blue: SAID-predictions for P). The colored model curves are for comparison taken from MAID [14] (green), SAID [15] (brown) and Bonn-Gatchina [16] (cyan).

time starting at the original datapoints. The above mentioned TPWA fit procedure was then applied to each ensemble member. If a good minimum is found in each case, one can histogram the results and extract mean and width for each parameter (cf. Figure 1).

The bootstrap did not show any indications of ambiguities allowed by the data. Therefore, the results for mean and width of the single solution found can be plotted against energy, the result of which is shown in Figure 2.

Because the errors of the Kharkov dataset are very large, additional fits were performed replacing these data by a SAID-prediction for P which has been endowed with a 5%-error at each datapoint. The results indicate that the uncertainty of the multipoles, especially for M_{1-}, is quite sensitive to this replacement (Figure 2).

5 Summary and outlook

Mathematically complete sets of observables contain a minimum number of 8 in the case of spin amplitude extraction and 5 for a TPWA. First investigations of a particularly simple fit in the Δ-region confirm the latter result.

Bootstrapping methods were proposed in order to get a good estimate for the error of the fitted multipoles. This error is seen to shrink in case more precise pseudodata for the recoil polarization observable P are introduced.

Acknowledgments

The author wishes to thank the organizers for the hospitality, as well as for providing a very relaxed and friendly atmosphere during the workshop. This work was supported by the *Deutsche Forschungsgemeinschaft* within SFB/TR16.

References

1. G. F. Chew, M. L. Goldberger, F. E. Low, and Y. Nambu, Phys. Rev. **106**, 1345 (1957).
2. A. M. Sandorfi, S. Hoblit, H. Kamano, T. -S. H. Lee, J. Phys. G **38**, 053001 (2011).
3. I. S. Barker, A. Donnachie, and J. K. Storrow, Nucl. Phys. B **95**, 347 (1975).
4. W.-T. Chiang and F. Tabakin, Phys. Rev. C **55**, 2054 (1997).
5. Y. Wunderlich, Diploma Thesis, University of Bonn (2012).
6. L. Tiator, AIP Conf. Proc. **1432**, 162 (2012).
7. A.S. Omelaenko, "Ambiguities of the multipole analysis of neutral-pion photoproduction from nucleons", YaF, Vol. **34**, 730 (1981).
8. Y. Wunderlich, R. Beck and L. Tiator, Phys. Rev. C **89**, 055203 (2014).
9. D. Hornidge et al., Phys. Rev. Lett. **111**, 062004 (2013).
10. R. Leukel and R. Beck, "Pion photoproduction results from MAMI", Proceedings of the NSTAR 2000 Conference, p. 14-21 (2001).
11. S. Schumann, P.B. Otte et al., Phys. Lett. B **750**, 252 (2015).
12. A.A. Belyaev et al., Nucl. Phys. B **213**, 201 (1983).
13. B. Efron, "Bootstrap methods: Another look at the jackknife", The Annals of Statistics, Vol. **7**, 1 (1979).
14. (MAID Partial Wave Analysis) http://www.kph.uni-mainz.de/MAID/
15. (SAID Partial Wave Analysis) http://gwdac.phys.gwu.edu/
16. (Bonn Gatchina Partial Wave Analysis) http://pwa.hiskp.uni-bonn.de/

BLED WORKSHOPS
IN PHYSICS
VOL. 16, NO. 1
p. 75

Proceedings of the Mini-Workshop
Exploring Hadron Resonances
Bled, Slovenia, July 5 - 11, 2015

Recent Spectroscopy Results from Belle

M. Bračko

University of Maribor, Smetanova ulica 17, SI-2000 Maribor, Slovenia and Jožef Stefan Institute, Jamova cesta 39, SI-1000 Ljubljana, Slovenia

Abstract. In this paper we present selected spectroscopy results based on measurements performed with the experimental data collected by the Belle detector, which has been operating at the KEKB asymmetric-energy e^+e^- collider in the KEK laboratory in Tsukuba, Japan. The selection of results is based on the interest, expressed at the workshop.

1 Introduction

The Belle detector [1] at the asymmetric-energy e^+e^- collider KEKB [2] was in operation between 1999 and 2010, and during this time it has accumulated about 1 ab^{-1} of data. The KEKB collider, often called a *B Factory*, was mostly operating around the $\Upsilon(4S)$ resonance, and as a result the Belle experiment was able to collect an impressive sample of about 772 million pairs of $B\overline{B}$ mesons. However, the experiment has also accumulated substantial data samples at other Υ resonances, like $\Upsilon(1S)$, $\Upsilon(2S)$ $\Upsilon(5S)$ and $\Upsilon(6S)$, as well as in the nearby continuum. In particular, the data samples collected at both, the $\Upsilon(4S)$ and $\Upsilon(5S)$ resonances, are the largest available in the world, corresponding to integrated luminosities of 800 fb^{-1} and 123 fb^{-1}, respectively [3]. Large amount of collected experimental data and excellent detector performance enabled many interesting spectroscopic results, including discoveries of new charmonium(-like) and bottomonium(-like) hadronic states and studies of their properties. This report focuses on some of the results, which were discussed at the workshop.

2 Charmonium and Charmonium-like States

At the start of the operation of the B Factories [4] the charmonium spectroscopy was a well established field: the experimental spectrum of $c\bar{c}$ states below the $D\overline{D}$ threshold were in good agreement with the theoretical prediction (see e.g. [5]), with the last remaining $c\bar{c}$ states below the open-charm threshold soon to be discovered [6], and no states outside of the conventional charmonium picture. However, the situation was drastically changed with the discoveries of new charmonium-like states (so called "XYZ" states).

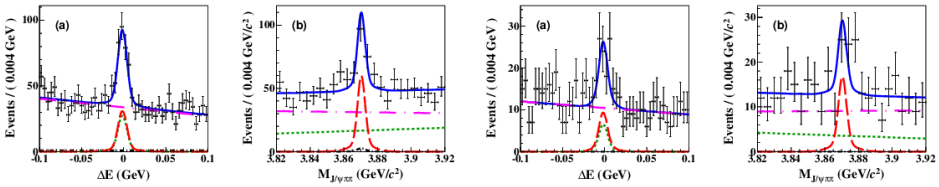

Fig. 1. Projections of the (ΔE, $M_{J/\psi\pi\pi}$) fit for the $B^0 \to X(3872)K^+\pi^-$ decay mode ((a),(b) left) and the $B^\pm \to X(3872)K^0_S\pi^\pm$ decay mode ((a),(b) right), with $X(3872) \to J/\psi\pi^+\pi^-$. The curves show the signal (red long-dashed curve), the background components (black dash-dotted line for the component peaking in $M_{J/\psi\pi\pi}$ but nonpeaking in ΔE, green dashed line for the one peaking in ΔE but nonpeaking in $M_{J/\psi\pi\pi}$, and magenta long dash-dotted line for combinatorial background), and the overall fit (blue solid curve).

2.1 The X(3872)-related news

The story about the "XYZ" states began in 2003, when Belle collaboration reported on $B^+ \to K^+J/\psi\pi^+\pi^-$ analysis, where a new state decaying to $J/\psi\pi^+\pi^-$ was discovered [7]. The new state, called X(3872), was soon confirmed by the CDF, DØ, *BABAR* collaborations [8], and recently also by the LHC experiments [9]. The properties of this narrow state ($\Gamma = (3.0^{+1.9}_{-1.4} \pm 0.9)$ MeV) with a mass of (3872.2 ± 0.8) MeV, which is very close to the $D^0\overline{D}^{*0}$ threshold [10], have been intensively studied by Belle and other experiments [11]. These studies determined the $J^{PC} = 1^{++}$ assignment, and suggested that the X(3872) state is a mixture of the conventional 2^3P_1 $c\bar{c}$ state and a loosely bound $D^0\overline{D}^{*0}$ molecular state.

In spite of the theoretical and experimental progress in understanding of the X(3872), studies of several X(3872) production modes, as well as search for new decay modes are still needed to fully understand the internal structure of this state. Recently, the Belle collaboration has presented the results of searches for X(3872) production via the $B^0 \to X(3872)K^+\pi^-$ and $B^+ \to X(3872)K^0_S\pi^+$ decay modes, where the X(3872) decays to $J/\psi\pi^+\pi^-$ on a data sample containing 772×10^6 $B\bar{B}$ events [12]. The same selection criteria as for the $B \to X(3872)K\pi$ signal events was also used to isolate the sample of $B \to \psi(2S)K\pi$ events for the calibration. The analysis (see Fig. 1 for results of the (ΔE, $M_{J/\psi\pi\pi}$) fit) yielded the first observation of the X(3872) in the decay $B^0 \to X(3872)K^+\pi^-$, with the measured branching ratio of $\mathcal{B}(B^0 \to X(3872)(K^+\pi^-)) \times \mathcal{B}(X(3872) \to J/\psi\pi^+\pi^-) = (7.9 \pm 1.3(\text{stat}) \pm 0.4(\text{syst})) \times 10^{-6}$. The result for the $\mathcal{B}(B^+ \to X(3872)K^0\pi^+) \times \mathcal{B}(X(3872) \to J/\psi\pi^+\pi^-) = (10.6 \pm 3.0(\text{stat}) \pm 0.9(\text{syst})) \times 10^{-6}$ shows that $B^0 \to X(3872)K^*(892)^0$ does not dominate the $B^0 \to X(3872)(K^+\pi^-)$ decay, which is in clear contrast to the $\psi(2S)$ case. No evident peaks were found in distributions of the $X(3872)\pi$ and $X(3872)K$ invariant masses.

If X(3872) is indeed a $D^0\bar{D}^{*0}$ molecule, other "X(3872)-like" molecular states with different quantum numbers can exist. Some may be revealed in the decays to final states containing the η_c meson. For example, a $D^0\bar{D}^{*0} - \bar{D}^0D^{*0}$ combination (denoted by $X_1(3872)$) with quantum numbers $J^{PC} = 1^{+-}$ would have a mass around 3.872 GeV/c^2 and would decay to $\eta_c\rho$ and $\eta_c\omega$. Combina-

Table 1. Results of branching fraction measurements for the B decays containing an intermediate exotic resonance. For $Z(3900)^0$ and $Z(4020)^0$ resonances the assumed masses are close to those of their charged partners.

Resonance	Decay mode	Upper limit (90% C.L.)
$X_1(3872)$	$\eta_c\pi^+\pi^-$	3.0×10^{-5}
	$\eta_c\omega$	6.9×10^{-5}
$X(3730)$	$\eta_c\eta$	4.6×10^{-5}
	$\eta_c\pi^0$	5.7×10^{-6}
$X(4014)$	$\eta_c\eta$	3.9×10^{-5}
	$\eta_c\pi^0$	1.2×10^{-5}
$Z(3900)^0$	$\eta_c\pi^+\pi^-$	4.7×10^{-5}
$Z(4020)^0$		1.6×10^{-5}
$X(3915)$	$\eta_c\eta$	3.3×10^{-5}
	$\eta_c\pi^0$	1.8×10^{-5}

tions of $D^0\bar{D}^0 + \bar{D}^0D^0$, denoted by $X(3730)$, and $D^{*0}\bar{D}^{*0} + \bar{D}^{*0}D^{*0}$, denoted by $X(4014)$, with quantum numbers $J^{PC} = 0^{++}$ would decay to $\eta_c\eta$ and $\eta_c\pi^0$. The mass of the $X(3730)$ state would be around $2m_{D^0} = 3.730$ GeV/c^2 while that of the $X(4014)$ state would be near $2m_{D^{*0}} = 4.014$ GeV/c^2. These molecular-state candidates were searched for in the recent Belle analysis [13]. In addition, neutral partners of the $Z(3900)^\pm$ [14] and $Z(4020)^\pm$ [15], and a poorly understood state $X(3915)$ were also searched for. The analysis was performed on the complete Belle data sample, searching for B decays to selected final states with the η_c meson. The η_c mesons were reconstructed via the $K^0_S K^\pm\pi^\mp$ mode and then four decays of charged B mesons were studied: 1.) $B^\pm \to K^\pm X \to K^\pm(\eta_c\pi^+\pi^-)$, where $X_1(3872)$, $Z(3900)^0$ and $Z(4020)^0$ were looked for; 2.) $B^\pm \to K^\pm X \to K^\pm(\eta_c\omega)$, where $X_1(3872)$ was looked for; 3.) $B^\pm \to K^\pm X \to K^\pm(\eta_c\eta)$, where $X(3730)$, $X(4014)$ and $X(3915)$ were looked for; 4.) $B^\pm \to K^\pm X \to K^\pm(\eta_c\pi^0)$, where $X(3730)$, $X(4014)$ and $X(3915)$ were looked for. No signal was observed and therefore only 90% confidence level upper limits were set on the product of branching fractions to the above mentioned intermediate states and decay branching fractions of these states in the range $(0.6 - 6.9) \times 10^{-5}$ (see table 1). Since the obtained upper limits for these exotic states are based on the full Belle data sample and are roughly of the same order as analogous quantities for their presumed partners (compare $\mathcal{B}(B^\pm \to K^\pm X_1(3872)) \times \mathcal{B}(X_1(3872) \to \eta_c\pi^+\pi^-)$ and $\mathcal{B}(B^\pm \to K^\pm X(3872)) \times \mathcal{B}(X(3872) \to J/\psi\pi^+\pi^-)$ from ref. [11]), more information about the nature of these states could only be extracted from the larger data sample, collected for example by the Belle II experiment [16].

2.2 Charged $c\bar{c}$-like states

In 2008 an exciting discovery of a new charmonium-like state was reported [17] by Belle in the $B^{+,0} \to K^{0,-}\pi^+\psi(2S)$ analysis[1], where a strong enhancement was

[1] Throughout the document, charge-conjugated modes are included in all decays, unless explicitly stated otherwise.

obtained in the $\pi^+\psi(2S)$ invariant mass distribution. The observed charged resonance, named $Z^+(4430)$, was characterised by a product branching fraction of $\mathcal{B}(\overline{B}^0 \to K^- Z^+(4430)) \times \mathcal{B}(Z^+(4430) \to \pi^+\psi(2S)) = (4.1 \pm 1.0 \pm 1.4) \cdot 10^{-5}$, which is typical for a charmonium state. The $Z^+(4430)$ is thus seen as the first charmonium-like charged meson with a minimal quark content of $c\bar{c}u\bar{d}$ – a serious tetraquark candidate. The signature of this exotic state was also searched for by the *BABAR* collaboration [18]. The performed analysis of the $B^{-,0} \to \psi\pi^- K^{0,+}$ (ψ = J/ψ or $\psi(2S)$) decays focused on a detailed study of the $K\pi^-$ system, and used the final *BABAR* data sample of 413 fb^{-1}, but found no significant evidence for this new state.

Soon afterwards, the Belle collaboration reported the update of the previous analysis [17], reanalysing the same data set as used previously, but performing a full Dalitz plot analysis, in order to check for the possible $\psi(2S)\pi^-$ mass reflections from the $K\pi$ system [19]. Results confirmed the existence of $Z^+(4430)$ and their experimental properties. Later on, another update of this measurement was reported by Belle, performing the full four-dimensional amplitude analysis on the entire Belle data sample [20]. The parameters of the $Z^+(4430)$ were further confirmed, and at the same time the measurement constrained $Z^+(4430)$ quantum numbers to preferred $J^P = 1^+$ hypothesis.

Already the observation of the $Z^+(4430)$ state suggested that studies of $B \to K\pi(c\bar{c})$ decays could reveal other similar neutral and charged partners. Belle thus reported also on a Dalitz plot analysis of $\overline{B}^0 \to K^-\pi^+\chi_{c1}$ decays with $657 \cdot 10^6$ $B\overline{B}$ pairs. [21] The fit model for $K\pi$ resonances is the same as in the $Z^+(4430)$ Dalitz analysis, but here it includes also the $K_3^*(1780)$ meson, and the fit results suggested that a broad doubly peaked structure in the $\pi^+\chi_{c1}$ invariant mass distribution should be interpreted by two new states, called $Z^+(4050)$ and $Z^+(4250)$.

More intereseting results on charged charmonium-like states followed initial discoveries. As already mentioned above, a few years ago the BESIII and Belle collaborations reported the observation of another charged charmonium-like state, $Z^+(3900)$, which decays into $J/\psi\pi^+$ [14]. Both experiments observed the new charged state in the production process $e^+e^- \to Y(4260)$, with $Y(4260)$ decaying into the $J/\psi\pi^+\pi^-$ final state. One of the most important experimental meassages came last year from the LHCb collaboration, which reported the observation of $Z^+(4430)$ [22] in B decays. The measured parameters including the spin-parity were found to be in good agreement with the results obtained in the updated Belle analysis on $Z^+(4430)$. So finally, after several years, the existence of a new type of hadrons, charged charmonium-like states with their quark content being different from mesonic or baryonic, is confirmed.

The Belle collaboration continues the research, consistent with the rich tradition in this field: Last year the Belle reported on a new measurement with a full four-dimensional amplitude analysis of the 3-body decay $B \to J/\psi\pi^+K$ [23], where another charged charmonium-like state was observed. The state, called $Z^+(4200)$, with a preferred spin-parity 1^+ was observed in the $J/\psi\pi^+$ decay mode. Within this analysis, the first evidence for the decay $Z^+(4430) \to J/\psi\pi^+$ was found, which is the second decay mode of the $Z^+(4430)$ state. Fig. 2 shows the

$M^2(J/\psi\pi^+)$ projections of the Dalitz plot. The curves indicate the fit results with and without the new $Z(4200)+$ state.

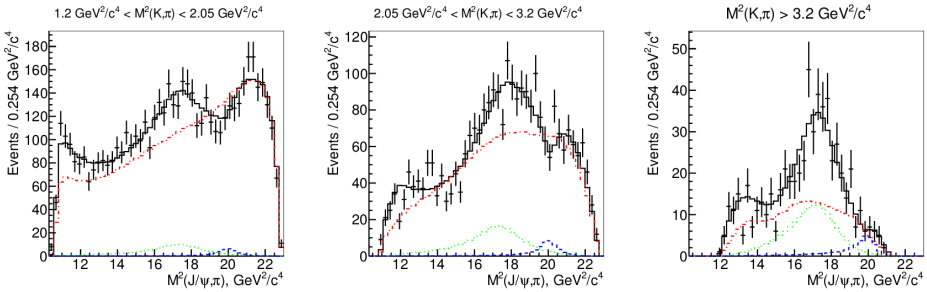

Fig. 2. The fit results with the $Z^+(4200)$ ($J^P = 1^+$) in the default model. The points with error bars are data; the solid histograms are fit results, the dashed histograms are the $Z^+(4430)$ contributions, the dotted histograms are the $Z^+(4200)$ contributions and the dash-dotted histograms are contributions of all K^* resonances.

3 Summary and Conclusions

Many new particles have already been discovered during the operation of the Belle experiment at the KEKB collider, and some of them are mentioned in this report. Although the operation of the experiment has finished, data analyses are still ongoing and therefore more interesting results on charmonium(-like) and bottomonium(-like) spectroscopy can still be expected from Belle in the near future. These results are eagerly awaited by the community and will be widely discussed at various occassions, in particular at workshops and conferences.

Even more progress in the spectroscopy field is expected from the huge available data sample, which will come from the Belle II experiment [16].

References

1. Belle Collaboration, *Nucl. Instrum. Methods* A **479**, 117 (2002).
2. S. Kurokawa and E. Kikutani, *Nucl. Instrum. Methods* A **499**, 1 (2003), and other papers included in this Volume.
3. J. Brodzicka *et al.*, *Prog. Theor. Exp. Phys.* , 04D001 (2012).
4. A. J. Bevan *et al.*, *Eur. Phys. J.* C **74**, 3026 (2014).
5. M. B. Voloshin, *Prog. Part. Nucl. Phys.* **61**, 455 (2008).
6. Belle Collaboration, *Phys. Rev. Lett.* **89**, 102001 (2002); Cleo Collaboration, *Phys. Rev. Lett.* **95**, 102003 (2005).
7. Belle Collaboration, *Phys. Rev. Lett.* **91**, 262001 (2003).
8. CDF Collaboration, *Phys. Rev. Lett.* **93**, 072001 (2004); DØ Collaboration, *Phys. Rev. Lett.* **93**, 162002 (2004); *BABAR* Collaboration, *Phys. Rev.* D **71**, 071103 (2005).

9. LHCb Collaboration, *Eur. Phys. J.* C **72**, 1972 (2012); CMS Collaboration, *J. High Energy Phys.* **04**, 154 (2013).
10. K.A. Olive *et al.* (Particle Data Group), *Chin. Phys. C* **38**, 090001 (2014).
11. Belle Collaboration, *Phys. Rev.* D **84**, 052004(R) (2011); CDF Collaboration, *Phys. Rev. Lett.* **103**, 152001 (2009); LHCb Collaboration, *Phys. Rev. Lett.* **110**, 222001 (2013).
12. Belle Collaboration, *Phys. Rev.* D **91**, 051101(R) (2015).
13. Belle Collaboration, *J. High Energy Phys.* **06**, 132 (2015).
14. Belle Collaboration, *Phys. Rev. Lett.* **110**, 252002 (2013); BESIII Collaboration, *Phys. Rev. Lett.* **110**, 252001 (2013); BESIII Collaboration, *Phys. Rev. Lett.* **112**, 022001 (2014); T. Xiao, S. Dobbs, A. Tomaradze and K. K. Seth, *Phys. Lett.* B **727**, 366 (2013).
15. BESIII Collaboration, *Phys. Rev. Lett.* **111**, 242001 (2013); *Phys. Rev. Lett.* **112**, 132001 (2014).
16. Belle II Collaboration, Belle II Technical design report, [arXiv:1011.0352 [physics.ins-det]].
17. Belle Collaboration, *Phys. Rev. Lett.* **100**, 142001 (2008).
18. *BABAR* Collaboration), *Phys. Rev.* D **79**, 112001 (2009).
19. Belle Collaboration, *Phys. Rev.* D **80**, 031104 (2009).
20. Belle Collaboration, *Phys. Rev.* D **88**, 074026 (2013).
21. Belle Collaboration), *Phys. Rev.* D **78**, 072004 (2008).
22. LHCb Collaboration, *Phys. Rev. Lett.* **112**, 222002 (2014).
23. Belle Collaboration), *Phys. Rev.* D **90**, 112009 (2014).

BLED WORKSHOPS
IN PHYSICS
VOL. 16, NO. 1
p. 81

Proceedings of the Mini-Workshop
Exploring Hadron Resonances
Bled, Slovenia, July 5 - 11, 2015

Eta and kaon production in a chiral quark model

B. Golli

Faculty of Education, University of Ljubljana, 1000 Ljubljana, Slovenia and Jožef Stefan Institute, 1000 Ljubljana, Slovenia

Abstract. We apply a coupled channel formalism incorporating quasi-bound quark-model states to calculate the pion- and photo-production amplitudes of η mesons and kaons. The meson-baryon and photon-baryon vertices are determined in the Cloudy Bag Model. Our model predicts sizable amplitudes in the P13, P33 and S11 partial waves in agreement with the recent partial-wave analyses of the MAID and the Bonn-Gatchina groups.

1 The model

This work is a continuation of a joint project on the description of baryon resonances by the Coimbra group (Manuel Fiolhais and Pedro Alberto) and the Ljubljana group (Simon Širca and B. G.) [1–8]. In the present work we extend our method which incorporates excited baryons represented as quasi-bound quark-model states into a coupled channel formalism using the K-matrix approach to calculate the scattering and photo-production amplitudes of strange mesons.

In our approach the T matrix for inelastic meson scattering is obtained by solving the Heitler's equation

$$T_{MB\,M'B'} = K_{MB\,M'B'} + i \sum_{M''B''} T_{MB\,M''B''} K_{M''B''\,M'B'}\,, \tag{1}$$

and similarly for the process $\gamma N \to MB$:

$$T_{MB\,\gamma N} = K_{MB\,\gamma N} + i \sum_{M'B'} T_{MB\,M'B'} K_{M'B'\,\gamma N}\,. \tag{2}$$

The K-matrix is split in the resonant and the background contribution

$$K_{M'B'\,MB} = -\sum_{\mathcal{R}} \frac{\mathcal{V}^{M}_{B\mathcal{R}} \mathcal{V}^{M'}_{B'\mathcal{R}}}{Z_{\mathcal{R}}(W)(W - W_{\mathcal{R}})} + K^{bkg}_{M'B'\,MB}\,; \tag{3}$$

in the case of photoproduction, the meson-baryon vertex is replaced by the corresponding electro-magnetic vertex $\mathcal{V}^{\gamma}_{B\mathcal{R}}$.

The vertices are calculated in a version of the Cloudy Bag Model extended to the pseudo-scalar SU(3) meson octet [9] and the ρ meson:

$$H_{int} = -\int d\mathbf{r} \left[\frac{i}{2f}\, \bar{q}\lambda_a(\gamma_5\phi_a + \boldsymbol{\gamma}\cdot\mathbf{A}_a)q\; \delta_S + \frac{1}{4f^2}\, \bar{q}\lambda_a\gamma^{\mu} q(\phi \times \partial_{\mu}\phi)_a \theta_V \right], \quad a = 1, 2, \ldots, 8\,. \tag{4}$$

The model provides a consistent parameterization of the baryon-meson and baryon-photon coupling constants and form factors in terms of f (equivalent to f_π) and the bag radius R_{bag}. We use the following values $R_{bag} = 0.83$ fm and $f = 76$ MeV (consistent with the ground state calculations), while f for η and K can be increased in accordance with the phenomenological relations $f_K = 1.2\, f_\pi$, $f_\eta = 1.2\, f_\pi$. In addition, the bare masses of the resonances are also free parameters.

2 Pion scattering into the ηN, KΛ and KΣ channels

The ηN, KΛ and KΣ channels contribute significantly in the P11, P13 and S11 partial waves and less in the D13 partial wave; we have not included the latter partial wave in the present contribution. The KΣ channel is dominated by the S11, P13 and P33 partial waves; its contribution in the P31, S31 and D33 waves turns out to be less important.

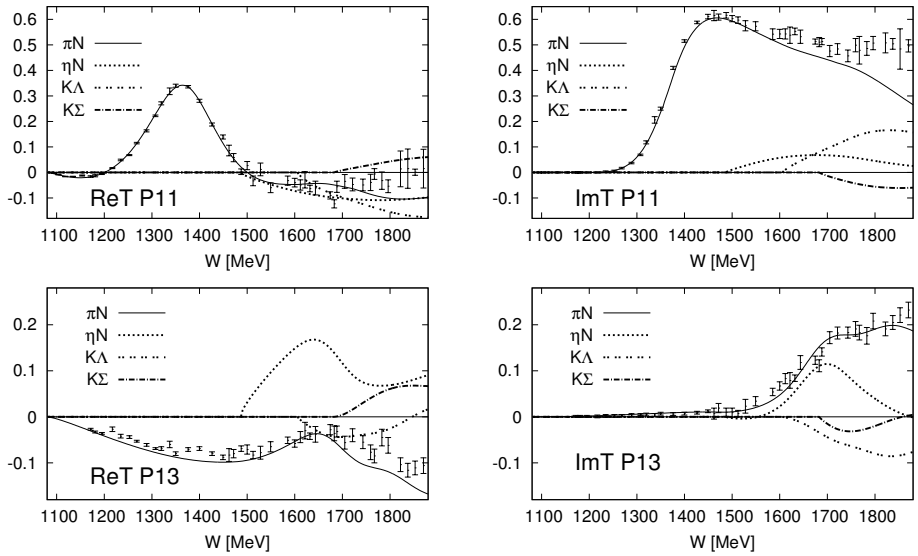

Fig. 1. The real and the imaginary part of the scattering T matrix for the elastic and the ηN, KΛ and KΣ channels. The data points are from the SAID partial-wave analysis [14].

Fig. 1 shows the results for positive parity $I = \frac{1}{2}$ partial waves. The P13 partial wave has not been considered in our previous calculations. In the present calculation we have included both resonances, the N(1720) and the N(1900), assuming one quark is excited to the d-state. The spin 1/2 (3/2) configuration turns out to dominate the lower (upper) resonance; the mixing angle of 10° provides the best agreement with experiment. Furthermore, in order to reproduce the experimental behaviour of ReT it has been necessary to include the second (volume) term in (4). Here a value of f closer to 93 MeV yields a better agreement with experiment. This term turns out to be important also in the P31 partial wave but is less significant in other partial waves discussed here.

In the P33 partial wave (see Fig. 2) η production in the ηΔ channel turns out to be almost negligible, but the KΣ channel yields rather important contribution which is also reflected in the photoproduction amplitudes, discussed in the following.

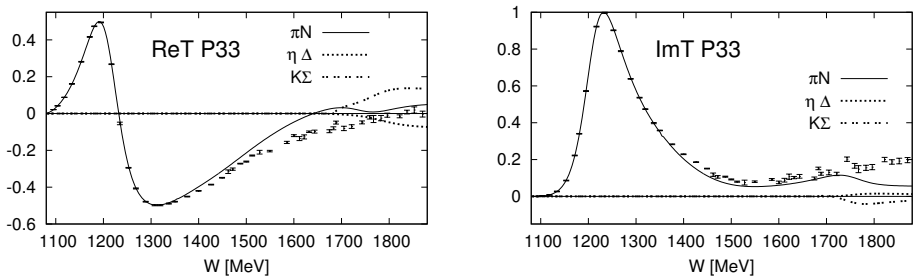

Fig. 2. The T matrix for the elastic and the ηΔ and KΣ P33 channels. Notation as in Fig. 1.

The important contribution of the ηN and KΛ channels in the S11 partial wave has already been discussed in our previous paper [7]. In the present approach we have not assumed a fixed mixing angle ($\vartheta \approx 30°$) between the spin $\frac{1}{2}$ and $\frac{3}{2}$ three-quark configuration but have rather generated the configuration mixing through pion and kaon loops. This improves the behaviour of the T matrix at lower *W* but somewhat weakens the photoproduction amplitudes.

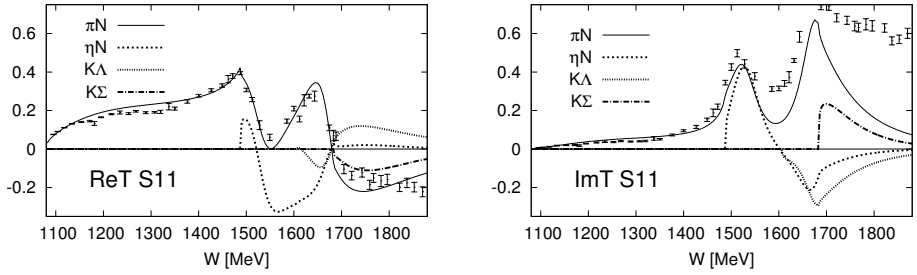

Fig. 3. The T matrix in the S11 partial wave. Notation as in Fig. 1.

3 Photoproduction of η mesons on the proton

Our model predicts that the N(1535) S11 resonance dominates η production, in accordance with the most recent MAID analysis [11] and the two analyses of the Bonn-Gatchina group [13] (disregarding the overall sign) (see Fig. 4).

In the P11 partial wave the η photoproduction amplitude is small; in addition, the contribution from the Roper resonance is almost negligible. On the other hand, the resonant contribution from the two resonances in the P13 partial wave dominates the M_{1+} and E_{1+} photoproduction amplitudes (see Fig. 5). While the

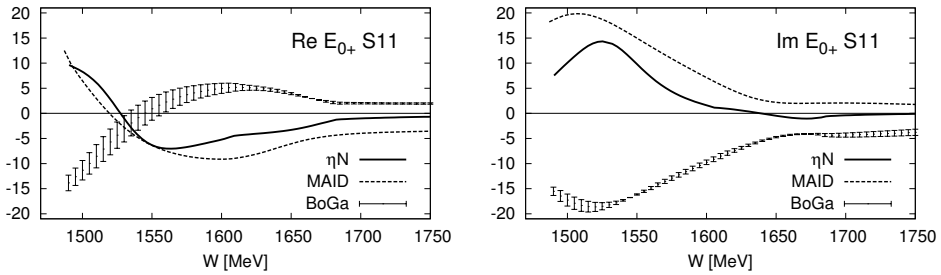

Fig. 4. The E_{0+} photoproduction amplitude (in units mfm^{-1}) compared to the recent MAID analysis [11] and the BG2014-01 and BG2014-02 solutions of the Bonn-Gatchina group [13].

M_{1+} amplitude remains close to the values obtained in the recent MAID and the Bonn-Gatchina analyses, the value of the E_{1+} multipole seems to give a too strong value in the region of the lower N(1720) resonance – but is in agreement with our result for the $\pi N \to \eta N$ channel.

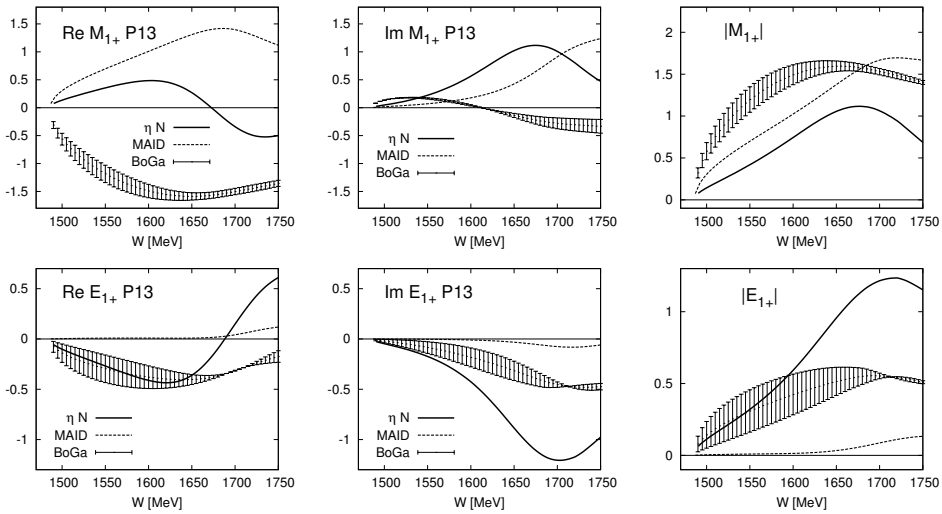

Fig. 5. As Fig. 4 for the M_{1+} and E_{1+} multipoles.

4 $K^+\Lambda$ photoproduction

The situation is similar to η production; the dominant contribution is the E_{0+} and arises through the excitation of the S11 resonances (see Fig. 6). The contribution of the P11 resonances is negligible. The strengths of the E_{1+} and M_{1+} multipoles in the P13 partial wave are almost equal, in agreement with the multipole analyses (see Fig. 7).

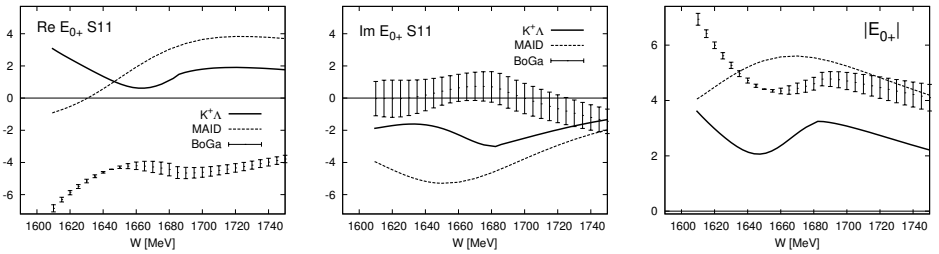

Fig. 6. The E_{0+} amplitude for the $K^+\Lambda$ channel. Notation as in Fig. 4; KAON-MAID taken from [12].

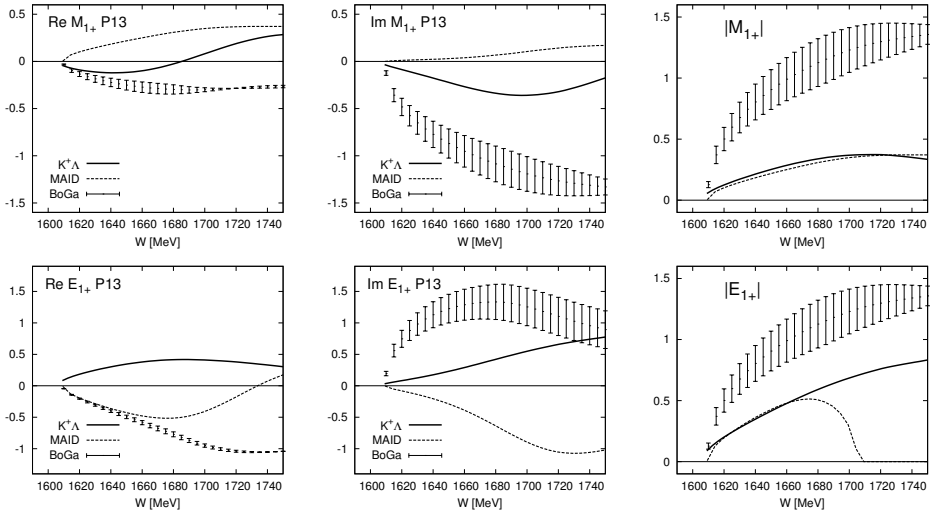

Fig. 7. As in Fig. 6 for the M_{1+} and E_{1+} multipoles.

5 KΣ photoproduction

We present only the results for the $K^0\Sigma^+$ channel since the background contribution here is considerably smaller than in the $K^+\Sigma^-$ channel in which the behaviour close to the threshold is governed by the kaon pole term absent in the former channel. The $K^0\Sigma^+$ amplitudes consist of the isospin singlet and isospin triplet part, i.e. $A(\gamma + p \to K^0\Sigma^+) = \sqrt{2}\, A_p^{(1/2)} - \frac{1}{3} A^{(3/2)}$.

The E_{0+} multipole is dominated by the S11 resonances (see Fig. 8) while the contribution from the S31 resonance is negligible. The experimental situation here is rather unclear since even the two recent analyses of the Bonn-Gatchina group considerably differ from each other. Nontheless, the strength predicted by our model is in agreement with the multipole analysis.

The M_{1+} amplitude (see Fig. 9) is well described by the $\Delta(1600)$ resonance and the tail of the dominating $\Delta(1232)$ resonance. Let us notice that the same resonant mechanism governs the $K^+\Sigma^0$ channel (the P33 resonant contribution is a factor of -2 larger than the one shown in Fig. 9). The contribution from the P13 resonances is small. The situation is reversed in the case of the E_{1+} multipole;

there is no quark contribution in the P33 partial wave (similarly as in the πN channel), the main contribution arises from the quark s to d transition in the two P13 resonances.

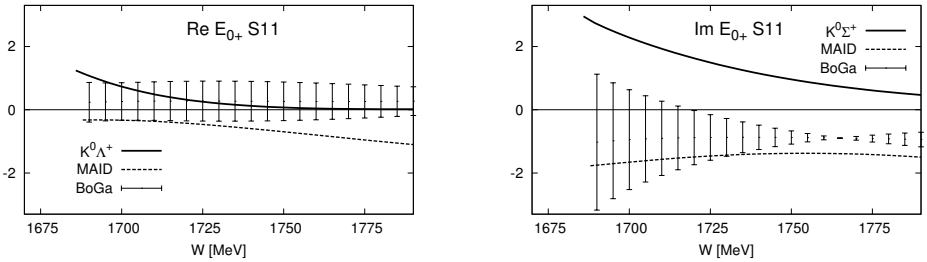

Fig. 8. The E_{0+} photoproduction amplitude for the $K^0\Sigma^+$ channel. Notation as in Fig. 6.

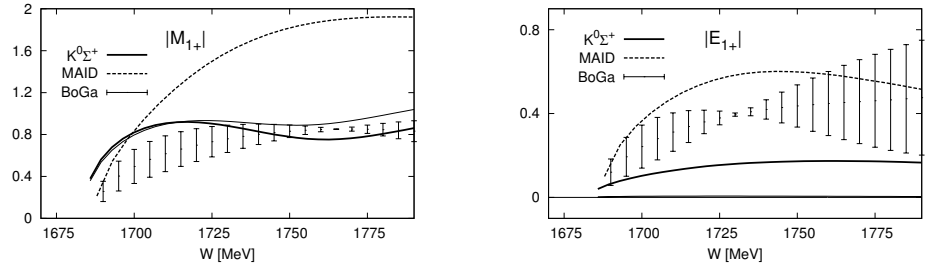

Fig. 9. The absolute values of the photoproduction amplitude for $\gamma N \to K^0\Sigma^+$. The thin solid line is the P33 contribution. Notation as in Fig. 6.

Acknowledgment. We would like to thank Lotar Tiator for sending us the preliminary results of the etaMAID analysis; see also the contribution of Jugoslav Stahov to these Proceedings.

References

1. M. Fiolhais, B. Golli, S. Širca, Phys. Lett. B **373**, 229 (1996).
2. P. Alberto, M. Fiolhais, B. Golli, and J. Marques, Phys. Lett. B **523**, 273 (2001).
3. B. Golli, S. Sirca, L. Amoreira, M. Fiolhais Phys.Lett. B553, 51-60 (2003).
4. P. Alberto, L. Amoreira, M. Fiolhais, B. Golli, and S. Širca, Eur. Phys. J. A **26**, 99 (2005).
5. B. Golli and S. Širca, Eur. Phys. J. A **38**, 271 (2008).
6. B. Golli, S. Širca, and M. Fiolhais, Eur. Phys. J. A **42**, 185 (2009).
7. B. Golli, S. Širca, Eur. Phys. J. A **47**, 61 (2011).
8. B. Golli, S. Širca, Eur. Phys. J. A **49**, 111 (2013).
9. E. A. Veit, B. K. Jennings, A. W. Thomas, R. C. Barret, Phys. Rev. D **31**, 1033 (1985).
10. D. Drechsel, S.S. Kamalov, L. Tiator, Eur. Phys. J. A **34**, 69 (2007).
11. J. Stahov et al., contribution to these Proceedings.
12. (Kaon MAID Partial Wave Analysis) http://www.kph.uni-mainz.de/MAID/kaon/
13. (Bonn Gatchina Partial Wave Analysis) http://pwa.hiskp.uni-bonn.de/
14. (SAID Partial Wave Analysis) http://gwdac.phys.gwu.edu/

BLED WORKSHOPS
IN PHYSICS
VOL. 16, NO. 1
p. 87

Proceedings of the Mini-Workshop
Exploring Hadron Resonances
Bled, Slovenia, July 5 - 11, 2015

Vector and scalar charmonium resonances with lattice QCD*

Luka Leskovec[a], C.B. Lang[b], Daniel Mohler[c], Saša Prelovsek[a,d]

[a]Jozef Stefan Institute, Ljubljana, Slovenia
[b]Institute of Physics, University of Graz, Graz, Austria
[c]Fermi National Accelerator Laboratory, Batavia, Illinois, USA
[d]University of Ljubljana, Ljubljana, Slovenia

Abstract. We study $\bar{D}D$ scattering with lattice QCD in order to determine the masses and decay widths of vector and scalar charmonium resonances above the open charm threshold. In the vector channel, the resulting elastic phase shift yields the familiar vector resonance $\psi(3770)$. At $m_\pi = 156$ MeV the simulated resonance mass and decay width agree with experimental data within the large statistical uncertainty. In the scalar channel we study the first excitation of the $\chi_{c0}(1P)$, as there is presently no commonly accepted candidate for it. We simulate $\bar{D}D$ scattering in s-wave with lattice QCD and investigate several different scenarios. The simulated data suggests an unobserved narrow resonance with the mass slightly below 4 GeV. Further studies are needed to shed light on the puzzle of the excited scalar charmonia.

Charmonium states below the open-charm threshold $\bar{D}D$ are well understood theoretically and experimentally, as their masses, decay widths and selected transition matrix elements are experimentally among the most precisely known quantities of the Standard Model. Theoretically these states are described either by models motivated by QCD or by lattice QCD. Recent lattice QCD studies have calculated the charmonium mass splittings taking into account both the continuum limit and extrapolating the results down to the physical point [1, 2], while radiative transition rates between low-lying charmonia have been determined for example in Refs. [3, 4].

In this work we use lattice QCD to study the charmonium and charmonium-like states near or above the open-charm thresholds. Our focus lies in the effects of strong decay of near threshold charmonium or charmonium-like states to a pair of charmed mesons $\bar{D}D$. Our assumptions of elastic $\bar{D}D$ scattering seem well justified from a phenomenological point of view as any possible open-charm threshold effects would arise from coupling of the resonances to the $\bar{D}D$ decay channel.

In our calculations we use two ensembles of gauge configurations with the parameters listed in [5]. Ensemble (1) has $N_f = 2$ and $m_\pi = 266$ MeV, while ensemble (2) has $N_f = 2 + 1$ and $m_\pi = 156$ MeV. Further details on the gauge ensembles and our implementation of charm quarks may be found in [6–8] for

* Talk delivered by Luka Leskovec

ensemble (1) and in [9, 10] for ensemble (2). We treat the charm quark with the Fermilab method [11, 12] to minimize the heavy-quark discretization effects. In our implementation, the heavy mesons obey the dispersion relation:

$$E_M(p) = M_1 + \frac{\mathbf{p}^2}{2M_2} - \frac{(\mathbf{p}^2)^2}{8M_4^3} + \dots , \tag{1}$$

where $\mathbf{p} = \frac{2\pi}{L}\mathbf{q}$, $\mathbf{q} \in N^3$ and M_1, M_2 and M_4 are the parameters of the dispersion relation.

To investigate the charmonium resonance in elastic $\bar{D}D$ scattering we require also the dispersion relation for D mesons, $E_D(p)$. As D mesons include the charm quark their dispersion relation is also given by Eq. (1) with parameters M_1, M_2 and M_4 for D mesons listed in [5].

We study two specific channels, the vector charmonium channel with $J^{PC} = 1^{--}$, where the J/ψ, $\psi(2S)$, $\psi(3770)$ and other resonances are present, and the scalar charmonium channel with $J^{PC} = 0^{++}$, where the $\chi_{c0}(1P)$ is present.

In the vector channel we focus on the near open-charm threshold states $\psi(3770)$ and $\psi(2S)$ and the effect of the $\bar{D}D$ threshold on them. The $\psi(3770)$ with $M = 3773.15 \pm 0.33$ MeV and $\Gamma = 27.2 \pm 1.0$ MeV is located only $\simeq 45$ MeV above $\bar{D}D$ threshold [13, 14]. The $\psi(3770)$ dominant decay mode is $\psi(3770) \to \bar{D}D$ in p-wave with a branching fraction of 0.93^{+8}_{-9} [13]. It is a well-established experimental resonance and is generally accepted to be predominantly the conventional $^{2s+1}nL_J = {}^3 1D_1$ $\bar{c}c$ state [15].

In the scalar channel the only established scalar charmonium state is the $\chi_{c0}(1P)$, interpreted as the ${}^3P_0$ $\bar{c}c$ and it is located well below the open charm threshold. A further known resonance, the $X(3915)$ with a decay width of 20 ± 5 MeV is seen only in the $J/\psi\,\omega$ and $\gamma\gamma$ decay channels [13]. While BaBar has determined its J^P quantum numbers to be 0^+ [16], their determination assumes that a $J^P = 2^+$ resonance would be produced in the helicity 2 state, which does not necessarily hold for exotic mesons[1] [18]. Consequently the PDG recently assigned the $X(3915)$ to the $\chi_{c0}(2P)$ [13], however certain convincing reasons given by Guo & Meissner [19] and Olsen [20] raise doubts about this assignment:

- The dominant decay mode is expected to be a "fall-apart" mode into $\bar{D}D$, which would to a broad resonance. $m_{D\bar{D}}$ invariant mass spectra of various experiments show no evidence for $X(3915) \to D\bar{D}$.
- The partial decay width for the OZI suppressed $X(3915) \to \omega J/\psi$ seems large as detailed in Ref. [19], which in turn results in contradicting limits for this decay in Ref. [20].

To study the vector and scalar charmonium resonance we performed a lattice QCD calculation of elastic $\bar{D}D$ scattering in p-wave and s-wave. Several $\bar{c}c$ and $D\bar{D}$ interpolating fields were used in both channels, where the (stochastic) distillation method [21, 22] was used to evaluate the Wick contractions.

In the vector channel, the well known $\psi(3770)$ resonance is present just above $\bar{D}D$ threshold. We performed two scattering analyses [23]: in the first case (a) taking into account the $\psi(3770)$ and $\bar{D}D$ and in the second case (b) also the $\psi(2S)$ to

[1] See Ref. [17] on why the $X(3915)$ could be a $J = 2$ resonance.

investigate its effects on the $\bar{D}D$ threshold on the $\psi(2S)$ [24]. The results for both cases are presented in Table 1. Our determination of the $\psi(3770)$ decay width

	Ensemble (1)		Ensemble (2)		exp
	case (a)	case (b)	case (a)	case (b)	$D^+D^-/D^0\bar{D}^0$
$\psi(3770)$					
m_R [GeV]	3.784(7)(10)	3.774(6)(10)	3.786(56)(10)	3.789(68)(10)	3.77315(33)
g (no unit)	13.2(1.2)	19.7(1.4)	24(19)	28(21)	18.7(1.4)
$\psi(2S)$					
m_B [GeV]		3.676(6)(9)		3.682(13)(9)	3.686109^{+12}_{-14}

Table 1. Parameters of the various Breit-Wigner fits for the vector resonance $\psi(3770)$ and bound state $\psi(2S)$. The $\psi(3770) \to D\bar{D}$ width $\Gamma = g^2p^3/(6\pi s)$ is parametrized in terms of the coupling g and compared the value of the coupling derived from experiment [13]. The first errors are statistical and the second errors (where present) are from the scale setting uncertainty. The experimental data and errors are based on PDG values.

might be affected by the $\Psi(4040)$ on Ensemble (1), however Ensemble (2) does not suffer from this issue and the determination of the resonance parameters is more reliable on Ensemble (2).

In the scalar channel the scattering analysis was performed only on Ensemble (1), as the resulting scattering data on Ensemble (2) (with $m_\pi = 156$ MeV) is too noisy. The calculation on Ensemble (1) (with $m_\pi = 266$ MeV) renders the scattering phase shift only at a few values of the $\bar{D}D$ invariant mass, which does not allow for a clear answer to the puzzles in the scalar channel. We investigated several different models for the scattering phase shift and have found that our data supports the existence of single narrow resonance slightly below 4 GeV with a decay width $\Gamma[\chi'_{c0} \to D\bar{D}] \leq 100$ MeV if the $\chi_{c0}(1P)$ is treated as a $\bar{D}D$ bound state. The other scenarios with only one narrow resonance state, a broad resonance or two nearby resonances are not supported by our data, however we cannot exclude these possibilities with statistical certainty.

The full results of this study presented at the Bled workshop and highlighted here can be found in Ref. [5]. The current situation at least in the scalar charmonium is not clear. To clarify the higher lying scalar states further experimental and lattice QCD efforts are required to map out the *s*-wave $D\bar{D}$ scattering in more detail. In the vector channel most issues seem clear, however small discrepancies appear due to different assumptions in the analyses. Future lattice studies of these states should be able to illuminate whether the assumptions are justified.

We are grateful to Anna Hasenfratz and the PACS-CS collaboration for providing the gauge configurations. The calculations were performed on computing clusters at Jozef Stefan Institute and the University of Graz.

References

1. Fermilab Lattice, MILC, D. Mohler *et al.*, PoS **LATTICE2014**, 085 (2015), [arXiv:1412.1057].

2. B. A. Galloway, P. Knecht, J. Koponen, C. T. H. Davies and G. P. Lepage, PoS **LATTICE2014**, 092 (2014), [arXiv:1411.1318].
3. D. Beirevi, M. Kruse and F. Sanfilippo, JHEP **05**, 014 (2015), [arXiv:1411.6426].
4. G. C. Donald *et al.*, Phys. Rev. **D86**, 094501 (2012), [arXiv:1208.2855].
5. C. B. Lang, L. Leskovec, D. Mohler and S. Prelovsek, JHEP **09**, 089 (2015), [arXiv:1503.05363].
6. A. Hasenfratz, R. Hoffmann and S. Schaefer, Phys. Rev. **D78**, 014515 (2008), [arXiv:0805.2369].
7. A. Hasenfratz, R. Hoffmann and S. Schaefer, Phys. Rev. **D78**, 054511 (2008), [arXiv:0806.4586].
8. D. Mohler, S. Prelovsek and R. M. Woloshyn, Phys. Rev. **D87**, 034501 (2013), [arXiv:1208.4059].
9. PACS-CS, S. Aoki *et al.*, Phys. Rev. **D79**, 034503 (2009), [arXiv:0807.1661].
10. C. B. Lang, L. Leskovec, D. Mohler, S. Prelovsek and R. M. Woloshyn, Phys. Rev. **D90**, 034510 (2014), [arXiv:1403.8103].
11. A. X. El-Khadra, A. S. Kronfeld and P. B. Mackenzie, Phys. Rev. **D55**, 3933 (1997), [arXiv:hep-lat/9604004].
12. M. B. Oktay and A. S. Kronfeld, Phys. Rev. **D78**, 014504 (2008), [arXiv:0803.0523].
13. Particle Data Group, K. Olive *et al.*, Chin.Phys. **C38**, 090001 (2014).
14. V. V. Anashin *et al.*, Phys. Lett. **B711**, 292 (2012), [arXiv:1109.4205].
15. E. Eichten, S. Godfrey, H. Mahlke and J. L. Rosner, Rev. Mod. Phys. **80**, 1161 (2008), [arXiv:hep-ph/0701208].
16. BaBar, J. P. Lees *et al.*, Phys. Rev. **D86**, 072002 (2012), [arXiv:1207.2651].
17. Z.-Y. Zhou, Z. Xiao and H.-Q. Zhou, Phys. Rev. Lett. **115**, 022001 (2015), [arXiv:1501.00879].
18. N. Brambilla *et al.*, Eur. Phys. J. **C74**, 2981 (2014), [arXiv:1404.3723].
19. F.-K. Guo and U.-G. Meissner, Phys. Rev. **D86**, 091501 (2012), [arXiv:1208.1134].
20. S. L. Olsen, Phys. Rev. **D91**, 057501 (2015), [arXiv:1410.6534].
21. Hadron Spectrum, M. Peardon *et al.*, Phys. Rev. **D80**, 054506 (2009), [arXiv:0905.2160].
22. C. Morningstar *et al.*, Phys. Rev. **D83**, 114505 (2011), [arXiv:1104.3870].
23. Lüscher, Martin, Nucl. Phys. **B354**, 531 (1991).
24. C. DeTar *et al.*, PoS **LATTICE2012**, 257 (2012), [arXiv:1211.2253].

BLED WORKSHOPS
IN PHYSICS
VOL. 16, NO. 1
p. 91

Proceedings of the Mini-Workshop
Exploring Hadron Resonances
Bled, Slovenia, July 5 - 11, 2015

Resonances in the Nambu–Jona-Lasinio model

Mitja Rosina[a,b]

[a]Faculty of Mathematics and Physics, University of Ljubljana, Jadranska 19, P.O. Box 2964, 1001 Ljubljana, Slovenia
[b]J. Stefan Institute, 1000 Ljubljana, Slovenia

Abstract. We have designed a soluble model similar to the Nambu–Jona-Lasino model, regularized in a box with periodic boundary conditions, in order to explore the properties of resonances when only discrete eigenvalues are available. The study might give a lesson to similar problems in Lattice QCD.

1 The quasispin NJL-like model

It is very instructive to understand the key features of a simplified model containing the spontaneous chiral symmetry breaking. Some time ago we have constructed a soluble version of the Nambu–Jona-Lasino model [1, 2]. Now we explore what it tells about the sigma meson.

We make the following simplifications:

1. We assume a sharp 3-momentum cutoff $0 \leq |\mathbf{p}_i| \leq \Lambda$;
2. The space is restricted to a box of volume $\mathcal{V}$ with periodic boundary conditions. This gives a finite number of discrete momentum states, $\mathcal{N} = N_h N_c N_f \mathcal{V}\Lambda^3/6\pi^2$ occupied by N quarks. (N_h, N_c and N_f are the number of quark helicities, colours and flavours.)
3. We take an average value of kinetic energy for all momentum states: $|\mathbf{p}_i| \to P = \frac{3}{4}\Lambda$.
4. While in the NJL model the interaction conserves the sum of momenta of both quarks we assume that each quark conserves its momentum and only switches from the Dirac level to Fermi level.
5. Temporarily, we restrict to one flavour of quarks, $N_f = 1$.

Let us repeat the "Quasispin Hamiltonian" [1, 2].

$$H = \sum_{k=1}^{N} \left(\gamma_5(k) h(k) P + m_0 \beta(k) \right) + \\ - \frac{g}{2} \left(\sum_{k=1}^{N} \beta(k) \sum_{l=1}^{N} \beta(l) + \sum_{k=1}^{N} i\beta(k)\gamma_5(k) \sum_{l=1}^{N} i\beta(l)\gamma_5(l) \right) \quad .$$

Here γ_5 and β are Dirac matrices, m_0 is the bare quark mass and $g = 4G/\mathcal{V}$ where G is the interaction strength in the original (continuum) NJL.

We introduce the quasispin operators which obey the spin commutation relations

$$j_x = \frac{1}{2}\beta\ , \quad j_y = \frac{1}{2}i\beta\gamma_5\ , \quad j_z = \frac{1}{2}\gamma_5\ ,$$

$$R_\alpha = \sum_{k=1}^{N} \frac{1+h(k)}{2} j_\alpha(k)\ ,\ L_\alpha = \sum_{k=1}^{N} \frac{1-h(k)}{2} j_\alpha(k)\ ,\ J_\alpha = R_\alpha + L_\alpha = \sum_{k=1}^{N} j_\alpha(k)\,.$$

The model Hamiltonian can then be written as

$$H = 2P(R_z - L_z) + 2m_0 J_x - 2g(J_x^2 + J_y^2) \quad .$$

The three model parameters

$$\Lambda = 648\,\mathrm{MeV}, \quad G = 40.6\,\mathrm{MeV\,fm}^3, \quad m_0 = 4.58\,\mathrm{MeV}$$

have been fitted (in a Hartree-Fock + RPA approximation) to the observables

$$M = \sqrt{\Big(E_g(N) - E_g(N-1)\Big)^2 - P^2} = 335\,\mathrm{MeV}$$
$$Q = \langle\, g|\bar{\psi}\psi|g\rangle = \frac{1}{\mathcal{V}}\langle\, g|\sum_i \beta(i)|g\,\rangle = \frac{1}{\mathcal{V}}\langle\, g|J_x|g\,\rangle = 250^3\ \mathrm{MeV}^3$$
$$m_\pi = E_1(N) - E_g(N) = 138\,\mathrm{MeV}\,.$$

The values of our model parameters are very close to those of the full Nambu-Jona Lasinio model used by the Coimbra group [3] and by Buballa [4].

2 The spectrum of 0^- and 0^+ excitations – Emergence of the σ meson

It is easy to evaluate the matrix elements of the quasispin Hamiltonian using the angular momentum algebra. If N is not too large the corresponding sparse matrix can be diagonalized using *Mathematica*.

Excited levels of the ground state band (R=L=N/4) in Fig. 1 are almost equidistant and are suggestive of n-pion states (in s-state). The level spacings ΔE are slightly decreasing with the assumed number of pions n_π due to the attractive interaction between pions. Inbetween appear also "intruder states" which can be interpreted as sigma excitations. The interpretation as σ meson is further supported by the large value of the matrix element of J_x between the ground state and the "intruder state". (Odd "multipion states" have zero value and even ones have a rather small value.)

n_π	parity	E [MeV]	ΔE [MeV]	Intruder
8	+	866	63	
	-	816		$\sigma(667)+\pi(136)+13$ MeV
7	-	803	93	
6	+	710	99	
	+	667		$\sigma(667)$
5	-	611	108	
4	+	503	115	
3	-	388	123	
2	+	265	129	
1	-	136	136	
0	+	0	0	

Fig. 1. Levels of the ground state band (R=L=N/4), level spacing between opposite parity states, and the assumed number of pions n_π pions

3 The width of the σ meson

In the attempt to describe resonances when only discrete eigenvalues are available we get a discrete sigma resonance energy, but not its width. We are trying to get the complex pole. For that purpose, we explore the method of analytic continuation from the bound state [5]. For this purpose, we vary one of the model parameters, the bare quark mass m from the region where the σ meson would be bound ($E_\sigma < E_{2\pi}$) down to the physical value of $m \to m_0$ (where $E_\sigma \gg E_{2\pi}$).

At $m > 64$ MeV there are two positive parity states between the first and second negative parity states (the one-pion and three-pion excitations); the lower one is the intruder (σ meson) and the upper one is the correlated two-pion state. At $m = 64$ MeV both positive parity states coincide – the threshold for $\sigma \to 2\pi$. When we decrease m further, the energy of the σ meson decreases slower than the 2π energy and it appears at higher multipion states. For the physical value $m = m_0 = 4.58$ MeV σ is already the sixth excited state, next to the six-pion state. It is obviously in the continuum, prompt to decay into 2π, in a more complete choice of interaction.

The method consists of the following steps:

- Determine the threshold value m_{th} and calculate $\epsilon = E_\sigma - E_{2\pi}$ as a function of m for $m > m_{th}$.
- Introduce a variable $x = \sqrt{m - m_{th}}$; calculate $k(x) = i\sqrt{-\epsilon}$ in the bound state region (Fig. 2).
- Fit $k(x)$ by a polynomial $k(x) = i(c_0 + c_1 x + c_2 x^2 + \ldots + c_{2M} x^{2M})$.

- Construct a Padé approximant:

$$k(x) = i\,\frac{a_0 + a_1 x + \ldots + a_M x^M}{1 + b_1 x + \ldots + b_M x^M}\ .$$

- Analytically continue $k(x)$ to the region $m < m_{th}$ (i.e. to imaginary x) where $k(x)$ becomes complex.
- Determine the position and the width of the resonance as analytic continuation in m (Fig. 3 and Fig. 4):

$$E_{res} = \mathrm{Re}\,(\mathrm{cont}_{m\to m_0} k^2)\,, \qquad \Gamma = -2\,\mathrm{Im}\,(\mathrm{cont}_{m\to m_0} k^2)\ .$$

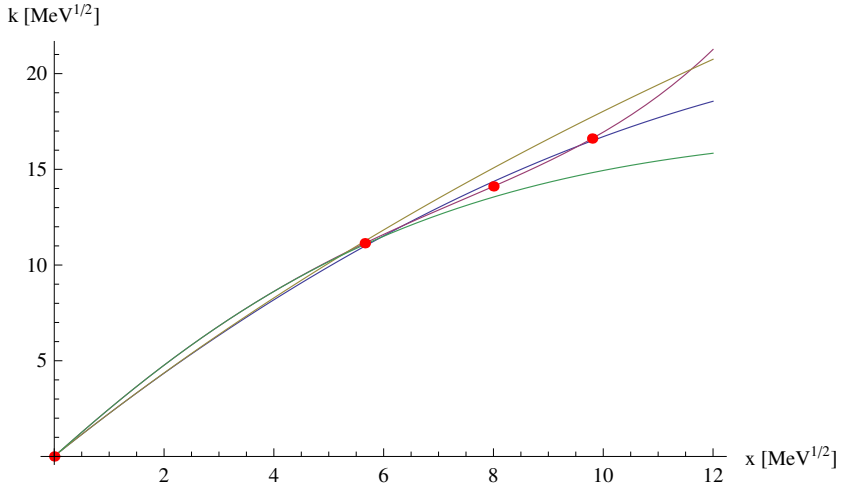

Fig. 2. The fit of $k(x)$ with quadratic(lower middle) and quartic polynomial (upper middle) and with Padé approximants of order 1 (below) and 2 (above)

We notice that the results for E_{res} and Γ in Fig. 3 and 4 deviate strongly for first and second order Padé approximants. This is due to the large stretch for the analytic continuation so that convergence at higher orders cannot be expected. Nevertheless, it is rewarding that the physical values for E_{res} and Γ lie somewhere in the middle between both curves.

To conclude, the method of analytic continuation in this case is just a game, but it is instructive. Intentionally, we have plotted the energy and width of the σ meson as a function of the corresponding pion mass rather than as a function of the model parameter m. This is reminiscent of the extrapolation of pion mass from about 500 Mev towards its physical value the way tha lattice people have to struggle.

References

1. B. T. Oblak and M. Rosina, Bled Workshops in Physics **7**, No. 1 (2006) 92; **8**, No. 1 (2007) 66; **9**, No. 1 (2008) 98 ; also available at http://www-f1.ijs.si/BledPub.

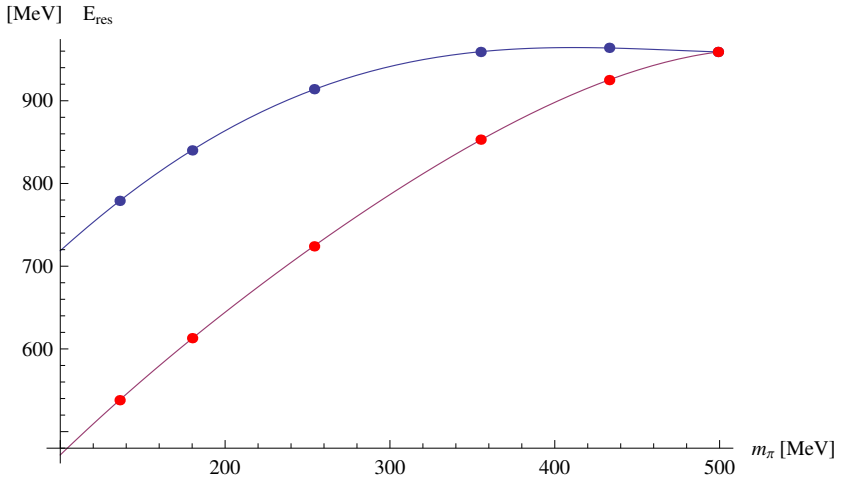

Fig. 3. The resonance energy E_{res} of the σ meson as a function of the pion mass – extrapolation using Padé approximants of order 1 (below) and 2 (above)

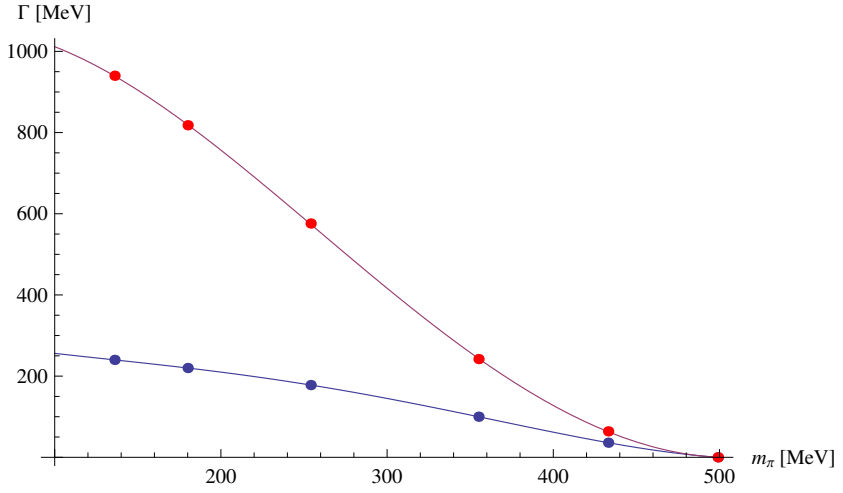

Fig. 4. The width Γ of the σ meson as a function of the pion mass – extrapolation using Padé approximants of order 1 (below) and 2 (above)

2. M.Rosina and B.T.Oblak, Few-Body Syst. **47** (2010) 117-123.
3. M. Fiolhais, J. da Providência, M. Rosina and C. A. de Sousa, Phys. Rev. C **56** (1997) 3311.
4. M. Buballa, M.: Phys. Reports **407** (2005) 205.
5. V.M. Krasnopolsky and V.I.Kukulin, *Phys. Lett*, **69A** (1978) 251, V.M. Krasnopolsky and V.I.Kukulin, *Phys. Lett*, **96B** (1980) 4, N. Tanaka et al. *Phys. Rev.* **C59** (1999) 1391.

Bled Workshops
in Physics
Vol. 16, No. 1
p. 96

Proceedings of the Mini-Workshop
Exploring Hadron Resonances
Bled, Slovenia, July 5 - 11, 2015

The Roper resonance — Ignoramus ignorabimus?

S. Širca[a,b]

[a] Faculty of Mathematics and Physics, University of Ljubljana, Jadranska 19, 1000 Ljubljana, Slovenia
[b] Jožef Stefan Institute, Jamova 39, 1000 Ljubljana, Slovenia

Abstract. In this talk we present a brief review of some of the recent developments on the Roper resonance front. We name some of the most exciting experimental results from MAMI, Jefferson Lab and other laboratories; elucidate several attempts at explaining the nature of this elusive structure within models involving quark+meson and baryon+meson degrees of freedom; and offer a glimpse into the remarkable progress made in the past few years by Lattice QCD.

1 Introduction

Compared to the familiar $\Delta(1232)$ excitation, the nature of the Roper resonance, $N^*(1440)$, which is the first excited state of the nucleon with equal quantum numbers, remains a puzzle — in spite of it being discovered in πN scattering about 50 years ago [1] and in spite of it long since being awarded four-star PDG status. In particular, it appears to be virtually impossible to observe it directly in any kind of spectra or in "simple" observables like partial cross-sections; it has a very large width (extracted from partial-wave analyses) ranging from as low as 135 MeV to as high as 605 MeV in the most recent analysis, with an uncertainty of more than 100 MeV; the scattering amplitude, $T_{\pi N}$, has a very peculiar behavior with not much more as a hint of the characteristic maximum of the imaginary part and zero-crossing of the real part at the resonace energy. The theoretical picture is just as unclear: for example, the mechanism in Lattice QCD that would cause the positive-parity $N^*(1440)$ resonance to drift below the negative parity $N^*(1535)$ excitation when approaching the chiral limit, remains elusive.

Studies of the Roper resonance within dynamical coupled-channels models based on baryon-meson degrees of freedom (see, for example, [2,3]) further complicate this picture by identifying multiple resonance poles originating in what is assumed to be the same bare state. Typically one sees three P_{11} poles below 2 GeV, two of which are associated with the $N^*(1440)$ and one with $N^*(1710)$. In the most recent analysis of [3], the poles belonging to the $N^*(1440)$ are at $(1353-i\,106)$ MeV and $(1357-i\,114)$ MeV.

It is natural to ask whether the two poles can in any way be associated with features seen in individual measurements. Indeed there is a whole series of experiments in which it can be argued that *two* mechanisms or a particular interference

involving the Roper are needed in order to explain the observed quantities. For example, it has been shown in [4] and [5] that the data on αp and πN scattering from Saturne can be explained by assuming two structures, the lower of which ($M \approx 1.39\,\mathrm{GeV}$, $\Gamma \approx 0.19\,\mathrm{GeV}$) is only seen in α-p scattering in addition to πN elastic and $\pi N \to N(\pi\pi)_S$, while the upper one ($M \approx 1.39\,\mathrm{GeV}$, $\Gamma \approx 0.19\,\mathrm{GeV}$) is seen only in πN elastic and $\pi N \to \pi\Delta$. Similarly, it has been found in [6] that a strong interference of $N^*(1440) \to N(\pi\pi)^{T=0}_{S-\mathrm{wave}}$ and $N^*(1440) \to \pi\Delta$ is needed in order to reproduce the $\pi\pi \to \pi\pi N$ data close to threshold as measured by the Crystal Ball collaboration. As yet another example, one could name the analysis of data acquired with the Wasa/Promice setup [7] where the properties of the Roper excitation have been studied by the $pp \to pp\pi\pi$ process. It has been shown that the $N^*(1440) \to N(\pi\pi)^{T=0}_{S-\mathrm{wave}}$ process is dominant for $T_p \lesssim 1\,\mathrm{GeV}$, but in the $T_p \gtrsim 1\,\mathrm{GeV}$, the $NN \to \Delta\Delta \to NN\pi\pi$ process alone can explain neither the angular nor the energy distributions: rather, an inclusion of the interference between the $N^*(1440) \to N\sigma$ and $N^*(1440) \to \Delta\pi \to N\sigma$ processes is needed in order to describe the data.

2 The Roper resonance in pion electro-production

Following the successes in studying the nature of the $\Delta(1232)$ excitation, the $N^*(1440)$ resonance has also been the subject of recent investigation at both leading electron-scattering facilities, MAMI and JLab. The first, "easy" experiments have accessed the Roper excitation without polarization or with polarized beam only. Typical results of such investigations were the Legendre coefficients of individual partial cross-sections σ_L, σ_T, σ_{LT}, σ_{TT} and σ'_{LT} with large signatures of the Roper seen in the D_0 coefficient of σ'_{LT} (see, for example, [8]). In a combined study of one-pion and two-pion electro-production [9] based on the JM05 model (JLab-MSU Collaboration) it has been shown that apart from the major non-resonant contribution to the integrated cross-section, practically only the s-channel resonant contributions from $N^*(1440)$ and $N^*(1520)$ are needed in order to reproduce the data almost perfectly.

It is well known that, generally speaking, adding another polarization degree of freedom amplifies the sensitivity of observables to specific resonant or non-resonant amplitudes. For example, by measuring the recoil polarization components P_n, P_l and P_t of the proton in the $p(\vec{e}, e'\vec{p})\pi^0$ process, one probes the Roper-relevant multipoles M_{1-} and L_{1-} in a rather selective manner, as in

$$(P_n)R_T^n = -\mathrm{Im}\, E_{0+}^* \,(3E_{1+} + M_{1+} + 2M_{1-}) \ ,$$

where the leading M_{1-} multipole interferes with the non-resonant E_{0+} multipole, or

$$(P_l)R_{TT'}^l \propto \mathrm{Re}\, E_{0+}^* \,(3E_{1+} + M_{1+} + 2M_{1-})$$

that measures the real part of the same interference, or

$$(P_n)R_{TL}^n \text{ that contains } \mathrm{Im}\, L_{1-}^* M_{1-} \ ,$$
$$(P_l)R_{TL'}^l \text{ that contains } \mathrm{Re}\, L_{1-}^* M_{1-} \ ,$$

i. e. the real and imaginary parts of the interferences of both resonant multipoles (although they are small) or, finally, combinations like

$$(P_n)R_L^n \propto -2\,\mathrm{Im}\,L_{0+}^*\,(2L_{1+}-L_{1-})\ ,$$
$$(P_t)R_{TL'}^t \propto \mathrm{Re}\,\left\{L_{0+}^*\,(2M_{1+}+M_{1-})+E_{0+}\left(2L_{1+}^*-L_{1-}^*\right)+\cdots\right\}\ .$$

An experiment of this type has been recently performed at MAMI [10]. The limited kinematic capability of the instrumental setup does not allow for a full multipole decomposition as performed, for example, by [11, 12] in the case of the $\Delta(1232)$ where the full angular coverage could be achieved. Nevertheless it has been possible to extract the recoil polarization components P_x', P_y and P_z' (related to P_l, P_t and P_n just by simple rotations) in the energy region of the Roper resonance at $Q^2 \approx 0.1\,(\mathrm{GeV}/c)^2$ at $\theta = 90^\circ$. The preliminary results, averaged over the acceptance, are [13]

$$P_x' = (11.2 \pm 1.7)\,\%\,,$$
$$P_y = (-5.4 \pm 1.5)\,\%\,,$$
$$P_z' = (88.5 \pm 1.9)\,\%\,.$$

(The errors are statistical only.) A detailed analysis of the data and its interpretation in the sense of their sensitivity to variations in $A_{1/2}$ and $S_{1/2}$ — as predicted by a variety of models — is underway.

3 The Roper resonance in quark models

For quite some time, the transverse ($A_{1/2}$) and scalar ($S_{1/2}$) helicity amplitudes have represented benchmark observables for quark models applied to the Roper electro-excitation, with various levels of success. If the Roper were a purely radial excitation ("breathing mode" of the nucleon), corresponding to the $(1s)^3 \to (1s)^2(2s)^1$ quark transition, this should correpond to a sizeable scalar (monopole) strength, together with a non-zero transverse (dipole) amplitude. On the other hand, if the Roper were a q^3g hybrid, the monopole amplitude should be suppressed and the transverse part should dominate. The data clearly rule out the hybrid picture since the scalar helicity amplitude is clearly different from zero and comparable in magnitude to the transverse amplitude [14]. Virtually all modern relativistic quark models reproduce this behavior, including the zero-crossing of $A_{1/2}$ at $Q^2 \approx 0.5\,(\mathrm{GeV}/c)^2$; see, for example [15–18]. This all boils down to overwhelming evidence of the Roper resonance being a first radial excitation of the q^3 ground state, although all models fail to describe the low-Q^2 behavior of $A_{1/2}$; see [20] for a possible remedy within a "χPT-inspired" effective theory. It is also evident that meson cloud effects are large below $Q^2 \approx 1\,(\mathrm{GeV}/c)^2$, both in $A_{1/2}$ and $S_{1/2}$; see, for example, [21].

The issue of meson dressing of the quark core opens the whole avenue of exploration by means of chiral quark models (optionally incorporated into coupled-channels models). This approach with respect to all nucleon resonances, not only the Roper, is discussed in the contribution by B. Golli [19].

4 Lattice studies

The correct level ordering of the positive-parity $N^*(1440)$ with respect to the negative-parity $N^*(1535)$ on the Lattice when approaching the physical limit remains an unsolved problem even in the most recent lattice calculations. At most, one observes "evidence" of the physical level ordering; see, for example, the study of [22]. Still, there has been significant progress in identifying the wave-function of the Roper excitation by exploiting new interpolators and by using different levels of smearing to expand the operator basis, resulting in the transition from a scattering state to a resonance when the quark mass drops, as well as in a significant curvature in the chiral regime, which is indicative of the Roper mesonic dressing [23]. The wave-function — more precisely, the probability distribution of the d-quark about the two u-quarks fixed at the origin — has been determined at pion masses as low as 156 MeV [24]. A node in the wave-function when the d-quark is excited to the $2s$ state is clearly seen (or two nodes for a $3s$ excitation), in complete analogy to the nodes in the wave-function of the hydrogen atom. Although still plagued by strong finite-volume effects, the first explicit construction of the $N^*(1440)$ wave-function is a very exciting result, pointing to the possibility further developments like the exploration of the $N \to N^*(1440)$ electro-magnetic transition form-factors.

References

1. D. Roper et al., Phys. Rev. Lett. **12** (1964) 137.
2. N. Suzuki et al., Phys. Rev. Lett. **104** (2010) 042302.
3. D. Rönchen et al., Eur. Phys. J. A **49** (2013) 44.
4. H. P. Morsch, P. Zupranski, Phys. Rev. C **61** (1999) 024002.
5. H. P. Morsch, P. Zupranski, Phys. Rev. C **71** (2005) 065203.
6. H. Kamano, M. Arima, Phys. Rev. C **73** (2006) 055203.
7. J. Pätzold et al., Phys. Rev. C **67** (2003) 052202(R).
8. K. Joo et al. (CLAS Collaboration), Phys. Rev. C **72** (2005) 058202.
9. G. V. Fedotov et al. (CLAS Collaboration), Phys. Rev. C **79** (2009) 015204.
10. H. Merkel (spokesperson), *Study of the Roper resonance in the* $p(\vec{e}, e'\vec{p})\pi^0$ *process*, MAMI Proposal A1–2/09.
11. J. Kelly et al. (Hall A Collaboration), Phys. Rev. Lett. **95** (2005) 102001.
12. J. Kelly et al. (Hall A Collaboration), Phys. Rev. C **75** (2007) 025201.
13. S. Štajner, private communication.
14. I. G. Aznauryan, V. D. Burkert, *Electroexcitation of nucleon resonances*, Prog. Part. Nucl. Phys. **67** (2012) 1.
15. H. J. Weber, Phys. Rev. C **41** (1990) 2783.
16. S. Kapstick, B. D. Keister, Phys. Rev. D **51** (1995) 3598.
17. F. Cardarelli et al., Phys. Lett. B **397** (1997) 13.
18. I. G. Aznauryan, Phys. Rev. C **76** (2008) 025212.
19. B. Golli, contribution to these Proceedings.
20. T. Bauer, S. Scherer, L. Tiator, Phys. Rev. C **90** (2014) 015201.
21. S. Mokeev et al., Phys. Rev. C **86** (2012) 035203.
22. M. S. Mahbub et al., Phys. Lett. B **693** (2010) 351.
23. M. S. Mahbub et al., Phys. Lett. B **707** (2012) 389.
24. D. S. Roberts, W. Kamleh, D. B. Leinweber, Phys. Lett. B **725** (2013) 164.

Povzetki v slovenščini

Resonance in njihova razvejitvena razmerja iz perspektive časovnega razvoj

Ido Gilary

Shulich Faculty of Chemistry, Technion, Haifa, 3200003, Israel

Časovni razvoj metastabilnih stanj kaže značinosti vezanih stanj in sipanih stanj. Dinamiko teh stanj lahko opišemo s kompleksno energijo, ki ponazarja lego in širino resonance. Opisani in pojasneni so razni pristopi k temu problemu.

Lastnosti nukleona v snovi, v modelu z mezoni π, ρ in ω

Ju-Hyun Jung[a], Ulugbek Yakhshiev[b] in Hyun-Chul Kim[b]

[a] Theoretical Physics, Institute of Physics, University of Graz, Universitaetsplatz 5, A-8010 Graz, Austria
[b] Department of Physics, Inha University, Incheon 402-751, Republic of Korea

Poročamo o svežih raziskavah transverzalne gostote naboja in energije/gibalne količine pri nukleonu v jedrski snovi, osnovanih na solitonskem modelu $\pi-\rho-\omega$, prilagojenem za sistem v snovi. Rezultati nam pomagajo ugotoviti splošne lastosti takšne prilagoditve zgradbe nukleonov, vezanih v jedrsko snov. Na kratko predstavimo rezultate za transverzalno gostoto naboja in energije/gibalne količine.

ηMAID-2015: posodobitev z novimi podatki in novimi resonancami

V.L. Kashevarov, L. Tiator, M. Ostrick

Institut fuer Kernphysik, Johannes Gutenberg-Universitaet D-55099 Mainz, Germany

Predstavimo sveže podatke o fotoprodukciji η in η' na protonih, ki jih je izmerila Kolaboracija A2 na pospeševalniku MAMI. Celotni presek za fotoprodukcijo η kaže ost pri energiji praga za η'. Analizirali smo nove podatke in stare podatke (od kolaboracij GRAAL, CBELSA/TAPS in CLAS) z razvojem po pridruženih Legendreovih polinomih. Za reproduciranje novih podatkov smo uporabili izobarni model ηMAID, posodobljen s kanalom η' in novimi resonancami. Nova verzija, η MAID-2015, razmeroma dobro opiše podatke, pridobljene s fotonskimi žarki z energijami do 3.7 GeV.

Analitična zgradba neperturbativnih kvarkovih propagatorjev in mezonskih procesov

Dalibor Kekez[a] in Dubravko Klabučar[b]

[a] Rugjer Bošković Institute, Bijenička c. 54, 10000 Zagreb, Croatia
[b] Physics Department, Faculty of Science, Zagreb University, Bijenička c. 32, Zagreb 10000, Croatia

Raziskujemo analitično zgradbo nekaterih nastavkov za kvarkove propagatorje v neperturbativnem področju kromodinamike. Če izberemo fizikalno motivirano parametrizacijo masne funkcije $M(p^2)$ oblečenih kvarkov, odvisne od gibalne količine in z določeno analitično zgradbo, je skrajno težavno napovedati in obvladati analitično zgradbo ustreznega neperturbativnega kvarkovega propagatorja. Tudi problem Wickove rotacije, ki povezuje izražavo v prostoru Minkowskega in Evklida, je skrajno težaven v neperturbativnem območju. Izpeljemo obliko propagatorja, ki omogoča Wickovo rotacijo in dopušča enakovredne račune v prostoru Minkowskega in Evklida. Kljub preprostosti nudi ta model dober kvalitativen in semikvantitativen opis nekaterih procesov z psevdoskalarnimi mezoni.

Primerjava med mezoni in resonancami $W_L W_L$ pri energijah več TeV

Antonio Dobado[a], Rafael L. Delgado[a], Felipe J. Llanes-Estrada[a] and Domenec Espriu[b]

[a] Dept. Fisica Teorica I, Univ. Complutense, 28040 Madrid
[b] Institut de Ciencies del Cosmos (ICCUB), Marti Franques 1, 08028 Barcelona, Spain.

Mikavni signali z Velikega hadronskega trkalnika (LHC) namigujejo, da morda obstajajo v področju zloma elektro-šibke simetrije resonance v območju več TeV. Spomnimo na nekaj ključnih resonanc mezon-mezon v območju GeV, ki bi utegnile imeti analogne resonance pri visokih energijah in nam služijo za primerjavo, hkrati z odgovarjujočo unitarizirano efektivno teorijo. Čeprav je podrobna dinamika lahko različna, pa zahteve po unitarnosti, kavzalnosti in globalnem zlomu simetrije (z uporabo metode inverzne amplitude) dovoljujejo prenos intuicije v večinoma neizmerjeno območje visokih energij. Če bo povečano število dogodkov na ATLASU okrog 2 TeV podprlo tako novo resonanco, to lahko pomeni anomalno sklopitev $q\bar{q}W$.

Resonance v konstituentnem kvarkovem modelu.

R. Kleinhappel and W. Plessas

Theoretical Physics, Institute of Physics, University of Graz, A-8010 Graz, Austria

Na kratko poročamo o današnjem opisu barionskih resonanc v realističnem modelu s konstituentnimi kvarki, v katerem običajno obravnavamo resonance kot

vzbujena vezana stanja, in pokažemo pot do bolj realistične teorije, v kateri nastopijo resonance kot kompleksni poli v ravnini gibalna količina/energija, torej z realno maso in končno širino.

Račun vzbujenih resonanc mezona ρ in faznih premikov ππ v P-valu z razširjenim kvarkovim modelom

Susana Coito[a], George Rupp[b] in Eef van Beveren[c]

[a] Institute of Modern Physics, CAS, Lanzhou 730000, China
[b] CeFEMA, Instituto Superior Técnico, Universidade de Lisboa, 1049-001 Lisboa, Portugal
[c] Centro de F´isica Computacional, Departamento de F´isica, Universidade de Coimbra, 3004-516 Coimbra, Portugal

Raziskujemo vektorsko resonanco $\rho(770)$, njene radialne ponovitve ter ustrezne fazne premike ππ v P-valu z razširjenim kvarkovim modelom, ki vsebuje tudi pare mezonov in pare $q\bar{q}$. Pri tem upoštevamo vse važne razpadne kanale: psevdoskalar-psevdoskalar, vektor- psevdoskalar, vektor-vektor, vektor-skalar, aksialni vektor-psevdoskalar in aksialni vektor-vektor, skupaj 26 kanalov. Dva modelska parametra sta določena s prejšnjimi vrednostmi, trije pa iz resonance ρ in nizkoenergijskih faznih premikov ππ v P-valu. Začasni rezultati že nakazujejo sposobnost modela, da reproducira te fazne premike ter maso in širino mezona ρ. Vendar rastejo fazni premiki pri višjih energijah prestrmo. Možno zdravilo je vključitev resonanc v končnih stanjih v večini kanalov. Raziskava se nadaljuje.

Prispevek pionskega oblaka k elektromagnetni strukturi nukleona

D. Kupelwieser and W. Schweiger

Institute of Physics, University of Graz, A-8010 Graz, Austria

V tem prispevku nadaljujemo in razširimo prejšnje račune elektro-šibkih oblikovnih faktorjev hadronov z uporabo točkovne oblike relativistične kvantne mehanike. Posebej se zanimamo za pionske učinke na elektromagnetno zgradbo nukleona. V ta namen uporabimo hibridni model s konstituentnimi kvarki, ki vsebuje poleg trojice valenčnih kvarkov še komponento $3q+\pi$. S preprosto valovno funkcijo za konfiguracijo 3q dobimo smiselne rezultate za oblikovne faktorje nukleona. V skladu z drugimim avtorji ugotovimo, da je učinek pionov znaten le pod $Q^2 \leq 0.5\ \mathrm{GeV}^2$.

Analiza delnih valov za podatke pri fotoprodukciji mezona η z upoštevanjem omejitev zaradi analitičnosti

M. Hadžimehmedović[a], V. Kashevarov[c], K. Nikonov[c], R. Omerović[a], H. Osmanović[a], M. Ostrick[c], J. Stahov[a], A. Svarc[b] in L. Tiator[c]

[a] University of Tuzla, Faculty of Science, Bosnia and Herzegovina
[b] Rudjer Bošković Institute, Zagreb, Croatia
[a] Institut fuer Kernphysik, Johannes Gutenberg Universtaet Mainz, Germany

Izvedemo analizo delnih valov za podatke pri fotoprodukciji η. Dobljeni multipoli so v skladu z analitičnostjo pri fiksnem t in pri fiksnem s. Analitičnost pri fiksnem t zagotovimo s Pietarinenovo metodo. Invariantne amplitude ubogajo zahtevano navzkrižno simetrijo.

Napredek pri poznavanju sklopitev nevtrona

W. J. Briscoe in I. Strakovsky

The George Washington University, Washington, DC 20052, USA

Podajamo pregled prizadevanj skupine GW SAID za analizo fotoprodukcije pionov na nevtronski tarči. Razločitev izoskalarnih in izovektorskih elektromagnetnih sklopitev resonanc N^* in Δ^* zahteva primerljive in skladne podatke na protonski in na nevtronski tarči. Interakcija v končnem stanju igra kritično vlogo pri najsodobnejši analizi in izvrednotenju podatkov za proces $\gamma n \to \pi N$ pri eksperimentih z devteronsko tarčo. Ta je pomemben sestavni del tekočih programov v laboratorijih JLab, MAMI-C, SPring-8, CBELSA in ELPH.

Vzbujanje barionskih resonanc s fotoprodukcijo mezonov

Lothar Tiator[a] in Alfred Svarc[b]

[a] Institut fuer Kernphysik, Johannes Gutenberg Universtaet Mainz, Germany
[b] Rudjer Bošković Institute, Zagreb, Croatia

Spektroskopija lahkih hadronov je še vedno živahno področje v fiziki jedra in delcev. Celo 50 let po odkritju Roperjeve resonance in več kot 30 let po pionirskem delu Hoehlerja and Cutkoskyja je še veliko odprtih vprašanj glede barionskih resonanc. Danes je glavni vzbujevalni mehanizem fotoprodukcija in elektroprodukcija mezonov, merjena na elektronskih pospeševalnikih kot so MAMI, ELSA in JLab. V združenem prizadevanju izvrednotimo lege in jakosti polov iz parcialnih valov, dobljenih z analizo parcialnih valov pri nedavnih meritvah polarizacij ob uporabi analitičnih omejitev iz disperzijskih relacij pri fiksnem t. Poseben poudarek pri barionskih resonancah je na strukturi pola na različnih Riemannovih ploskvah.

Popolni eksperimenti pri fotoprodukciji psevdoskalarnih mezonov

Yannick Wunderlich

Helmholtz-Institut fuer Strahlen- und Kernphysik, Universitaet Bonn, Nussallee 14-16, 53115 Bonn, Germany

Predstavim problem, kako enolično izvrednotiti amplitude za fotoprodukcijo iz tako imenovanih popolnih eksperimentov. Pri tem smo lahko pozorni na določanje amplitude za celotno tvorbo ali pa na določanje multipolov. Na kratko obravnavam oba primera. Podrobneje opišem preliminarne rezultate prilagajanja multipolov kakor tudi določanja njihovih napak pri nedavnih meritvah polarizacije v področju resonance Δ.

Novi spektroskopski rezultati iz laboratorija Belle

Marko Bračko

Univerza v Mariboru, Smetanova ulica 17, SI-2000 Maribor, in Institut J. Stefan, Jamova cesta 39, SI-1000 Ljubljana

V prispevku predstavimo izbrane rezultate spektroskopskih meritev, opravljenih na izmerjenih podatkih, pridobljenih z detektorjem Belle, ki je stal ob trkalniku KEKB v laboratoriju KEK v Cukubi, na Japonskem. Trkalnik je obratoval med letoma 1999 in 2010, v tem času pa je s stabilnim delovanjem pri trkih elektronov in pozitronov različnih energij postal prava "tovarna" parov mezonov B, mezonov D in še leptonov tau. Ogromne količine kakovostnih podatkov so omogočile tudi številne spektroskopske meritve. Izbor tukaj predstavljenih rezultatov ustreza zanimanju in razpravam na delavnici.

Produkcija mezonov eta in kaonov v kiralnem kvarkovem modelu

Bojan Golli

Pedagoška fakulteta, Univerza v Ljubljani in Institut J. Stefan, Ljubljana, Slovenija

Formalizem sklopljenih kanalov, ki vključuje kvazi vezana večkvarkovska stanja, uporabimo za izračun sipalnih in fotoprodukcijskih amplitud mezonov eta in kaonov. Sklopitvene konstante in oblikovne faktorje določimo v modelu oblačne vreče. Model napove znatne amplitude v parcialnih valovih P13, P33 in S11, v skladu z najnovejšimi analizami parcialnih valov skupine iz Mainza in skupine iz Bonna in Peterburga.

Vektorske in skalarne resonance čarmonija v kromodinamiki na mreži

Luka Leskovec[a], C. B. Lang[c], Daniel Mohler[d] in Saša Prelovšek[a,b]

[a] Institut Jožef Stefan, Ljubljana, Slovenija
[b] Univerza v Ljubljani, Ljubljana, Slovenija
[c] Institute of Physics, University of Graz, Graz, Austria
[d] Fermi National Accelerator Laboratory, Batavia, Illinois, USA

Proučujemo sipanje mezonov $\bar{D}$ na D s kromodinamiko na mreži, da bi določili mase in razpadne širine vektorskih in skalarnih resonanc čarmonija nad pragom za razpad v čarobne mezone. V vektorskem kanalu dobimo znano resonanco $\psi(3770)$. Simulacija pri vrednosti pionove mase $m_\pi = 156$ MeV da maso in razpadno širino resonance, ki se ujema z eksperimentalnimi podatki znotraj velike statistične negotovosti. V skalarnem kanalu proučujemo prvo vzbujeno stanje $\chi_{c0}(1P)$, za katero ni zaenkrat nobenega sprejetega kandidata. Za sipanje $\bar{D}$ na D v s-valu raziskujemo razne scenarije. Simulacija nakazuje še neopaženo ozko resonanco z maso malo pod 4 GeV. Potrebne so nadaljnje raziskave, da bi osvetlili uganke pri skalarnih vzbujenih stanjih čarmonija.

Resonance v modelu Nambuja in Jona-Lasinia

Mitja Rosina

Fakulteta za matematiko in fiziko, Univerza v Ljubljani, Jadranska 19, p.p.2964, 1001 Ljubljana, Slovenija in Institut J. Stefan, 1000 Ljubljana, Slovenija

Pred leti smo sestavili rešljivo verzijo modela Nambuja in Jona-Lasinia, ki še vedno ustrezno opiše spontani zlom kiralne simetrije in pojav mezonov pi. Njeni značilnosti sta regularizacija polja v škatli s periodičnimi robnimi pogoji ter poenostavljena kinetična energija in interakcija. Sedaj nas pa zanima opis resonanc, kadar so na voljo le diskretne laste vrednosti energije. Kot zgled navajamo mezon σ. Raziskava je lahko poučna za podobne probleme pri kromodinamiki na mreži.

Roperjeva resonanca — ignoramus ignorabimus?

S. Širca

Fakulteta za matematiko in fiziko, Univerza v Ljubljani, Jadranska 19, p.p.2964, 1001 Ljubljana, Slovenija in Institut J. Stefan, 1000 Ljubljana, Slovenija

V tem prispevku ponudimo kratek pregled nekaterih zadnjih dosežkov na področju raziskav Roperjeve resonance. Naštejemo nekaj najbolj razburljivih eksperimentalnih rezultatov iz centrov MAMI in Jefferson Lab ter drugih laboratorijev; osvetlimo nekaj poskusov, da bi razložili naravo te zagonetne strukture v okviru modelov s kvarkovskimi in mezonskimi ali barionskimi in mezonskimi prostostnimi stopnjami; in odpremo vpogled v znaten napredek, ki so ga v zadnjih letih naredili kromodinamski računi na mreži.

BLEJSKE DELAVNICE IZ FIZIKE, LETNIK 16, ŠT. 1, ISSN 1580-4992

BLED WORKSHOPS IN PHYSICS, VOL. 16, NO. 1

Zbornik delavnice 'Raziskave hadronskih resonanc',
Bled, 5. – 11. julij 2015

Proceedings of the Mini-Workshop 'Exploring Hadron Resonances',
Bled, July 5 – 11, 2015

Uredili in oblikovali Bojan Golli, Mitja Rosina, Simon Širca

Članki so recenzirani. Recenzijo je opravil uredniški odbor.

Izid publikacije je finančno podprla Javna agencija za raziskovalno dejavnost RS iz sredstev državnega proračuna iz naslova razpisa za sofinanciranje domačih znanstvenih periodičnih publikacij.

Tehnični urednik Matjaž Zaveršnik

Založilo: DMFA – založništvo, Jadranska 19, 1000 Ljubljana, Slovenija

Natisnila tiskarna Birografika Bori v nakladi 80 izvodov

Publikacija DMFA številka 1974

Brezplačni izvod za udeležence delavnice